SIMULTANEOUS REAL-TIME VISCOELASTICITY, MASS AND CELL CYCLE MONITORING FOR SINGLE ADHERENT CANCER CELLS

BY

OLAOLUWA OLUFEMI ADENIBA

DISSERTATION

Submitted in partial fulfillment of the requirements
for the degree of Doctor of Philosophy in Mechanical Engineering
in the Graduate College of the
University of Illinois at Urbana-Champaign, 2019

Urbana, Illinois

Doctoral Committee:

Professor Rashid Bashir, Director of Research
Professor Taher Saif, Chair
Associate Professor Dipanjan Pan
Associate Professor Seok Kim

Abstract

Cancer is a complex disease caused by the combined effects of genetic and environmental factors. Evidently, there exists a correlation between the surrounding environment of a cell, its biophysical properties and health. Information gained from biomechanics has led to an improved understanding of the way diseases evolve and their progression cycle, providing methods targeted towards curing these diseases.

Countless studies have been carried out on the mechanisms underlying cell cycle progression. More particularly, these studies on the mechanics of individual cells have pointed to their coordination, which helps us understand cellular metabolic and physiological process better. Development of more precise, versatile and reliable measurement tools and techniques will provide a greater understanding of cellular behavior and biophysical properties. Micromechanical systems (MEMS) technology can provide these tools – for analyzing single cells and providing important and useful information of their biophysical properties.

In modern research, the ability to reliably investigate and understand these cellular properties requires measurement devices that provide high sensitivity, high throughput, and adaptability to include multiple on-chip functionalities. Many MEMS-based resonant sensors have been extensively studied and used as biological and chemical sensors. However, previous works have shown that there are several technology limitations that inhibit application of various MEMS-sensors to mechanical measurement and analysis, including insufficient cell capture efficiency, media perfusion for long term growth, cell adhesion and cell movement/spreading and cell-sensor modelling. Cellular mechanics and viscoelastic properties are known to play a role in biological processes such as cell growth, stem cell differentiation, cell crawling, wound healing, protein

regulation, cell malignancy and even apoptosis (programmed cell death). Thus, an accurate measurement of stiffness and growth is fundamental to understanding cellular proliferation in cancer.

Capturing these biophysical properties of cancer cells over the duration of their growth cycle through MEMS devices can help provide a better insight into the mechanics of the metastasis of cancer cells. Meanwhile, many MEMS sensing devices still require further development and characterization to reliably investigate long-term cell behaviors. This dissertation focuses on characterization of our MEMS resonant sensors to address current challenges in the measurement of long-term biophysical behaviors of cells across its cell cycle. The amplitude and frequency of MEMS resonant pedestal sensors were used in conjunction with a vibration induced and optically-sensed phase shift of target light incident on an adhering sample to extract the loss tangent - a measure of the relative viscoelasticity of soft materials. This observed phase shift, combined with a representative two-degree-of-freedom Kelvin-Voigt model, is used to simultaneously obtain the elasticity (stiffness), viscosity and mass associated with individual adherent cancer cells. The research is unique as it decouples the heterogeneity of individual cells in our population and further refines our viscoelastic solution space. This novel development enables long-term simultaneous measurement of changes in stiffness and mass of normal and cancerous cells over time. This is the first investigation of the time-varying simultaneous measurement of viscoelasticity and mass for individual adherent cells using our MEMS resonant sensors.

to my family and friends,

with love

Acknowledgement

I would like to acknowledge the inspirational guidance of my PhD advisor, Professor Rashid Bashir whose drive for excellence is totally enviable. I could not have walked this graduate school journey without your patience and kind support. Your person and spirit is rare. Through you, I have gleaned a lot of life's lessons I will love to keep till I grow old. Immense thanks goes to my committee members, Professor Taher Saif, Associate Professor Dipanjan Pan, Associate Professor Seok Kim and Associate Professor Sungwoo Nam for their unflinching support and guidance through my study at the University of Illinois. I am thankful to Emeritus Professor Ilesanmi Adesida for his continued advice and help. I would also like to special thank Dr. Elise Corbin for being there to provide valuable insights when it was needed the most. I am also thankful to Kathy Smith for her sincere and heartfelt advice through my down moments.

I will not forget my biological parents, Dr. Stephen Babatunde and Mrs Josephine Mojisola Adeniba for their prayers and for providing shoulders to cry on when things went south. You are a solid rock and I owe you all the appreciation for this. Special thanks to Kings Assembly Campus Outreach family and my LIBNA Group Lab mates and friends within the Urbana-Champaign community that created a support system for me to thrive through difficult times; despite being far away from home. In conclusion, I am deeply grateful to my heartthrob and sweetheart, Tanitoluwa who has made all this effort meaningful and has believed in me. I cannot thank you enough. I am sincerely grateful for the broken path that brought us together - you are the best decision I have ever made.

Thank you.

Table of Contents

List of Tables

List of Figures

Chapter 1 : Introduction

Recent insights in the fields of cell cycle regulation and cancer would each along have provided prime examples of research at the 'Frontiers of Science'. However, some of the most revealing information about both topics has been derived from the intersection of the two fields. The intent of this chapter is to introduce the basics of cells; cell cycle, cancer and their overlap. It has been established that cell cycle machinery controls cell proliferation and cancer is a disease of inappropriate cell proliferation. Understanding the molecular mechanisms of the deregulation of cell cycle progression in cancer can provide important insights into how normal cells become tumorigenic.

1.1 Cancer

Cancer is a complicated disease that stems from several mutations in a cell. These occurrences often affect and controls cell growth, and results in numerous biophysical properties. Cancer cells grow and divide at an unregulated, quickened pace and can invade other tissues. Cancer is not just one disease but many diseases. Its types can be grouped into broader categories. The main categories include:

- **Carcinoma** - cancer that begins in the skin or in tissues that line or cover internal organs
- **Sarcoma** - cancer that begins in bone, cartilage, fat, muscle, blood vessels, or other connective or supportive tissues.
- **Leukemia** - cancer that starts in blood-forming tissue such as the bone marrow and causes large numbers of abnormal blood cells to be produced and enter the blood.
- **Lymphoma and myeloma** - cancers that begin in the cells of the immune system.

- **Central nervous system cancers** - cancers that begin in the tissues of the brain and spinal cord.

As cancer spreads it makes it even harder to treat, and the survival rate decreases dramatically. It is therefore better diagnosed early while a greater understanding of cellular properties will aid in the future of cancer diagnoses. Among other causes of death, cancer ranks second in the United States of America (USA), and is becoming more widespread with 1.52 million new diagnoses made in 2010 alone[1]. Figure 1.1 depicts the causes of death in the USA.

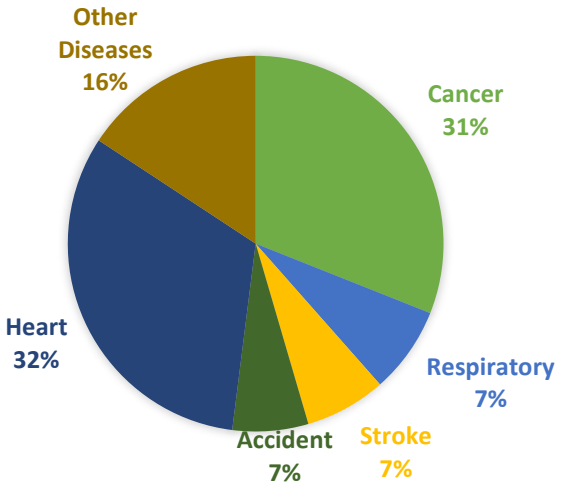

Fig 1:1 Causes of Death in the USA, Cancer ranks second[16]

1.2 Cell Biomechanics

1.2.1 Cellular Architecture

Cells can be subdivided into the following subcategories:

1. Prokaryotes: Prokaryotes are relatively small cells surrounded by the plasma membrane, with a characteristic cell wall that may differ in composition depending on the particular organism. Prokaryotes lack a nucleus (although they do have circular or linear DNA) and other membrane-bound organelles (though they do contain ribosomes).

2. Eukaryotes: Eukaryotic cells are also surrounded by the plasma membrane, but on the other

hand, they have distinct nuclei bound by a nuclear membrane or envelope. Eukaryotic cells also contain membrane-bound organelles, such as (mitochondria, chloroplasts, lysosomes, rough and smooth endoplasmic reticulum, vacuoles). In addition, they possess organized chromosomes which store genetic material[17]. Human cells are eukaryotic. They are far more complex involving a more well-defined internal structure with multiple sub-cellular components, including separate membrane bound nucleus and organelles, seen in Figure 1.2 (b). The nucleus is a major component containing the chromosomes and DNA that drive major metabolic activity such as gene transcription and replication.

Growth and progression through the cell cycle are regulated by the nucleus. The cytoskeleton, which is the material structure of the cell acts as a cellular scaffolding to prevent the plasma membrane from collapsing to its lowest energy system. Its functionality includes cellular locomotion, cell-cell linkages, and cell-ECM linkages. The cytoskeleton is made up of three major types of filaments: actin microfilaments, microtubules, and intermediate filaments that play a significant role in the mechanical properties of a cell. Substrate stiffness and other environmental factors affect the cell structure, and in turn changing the functionality of the cell.

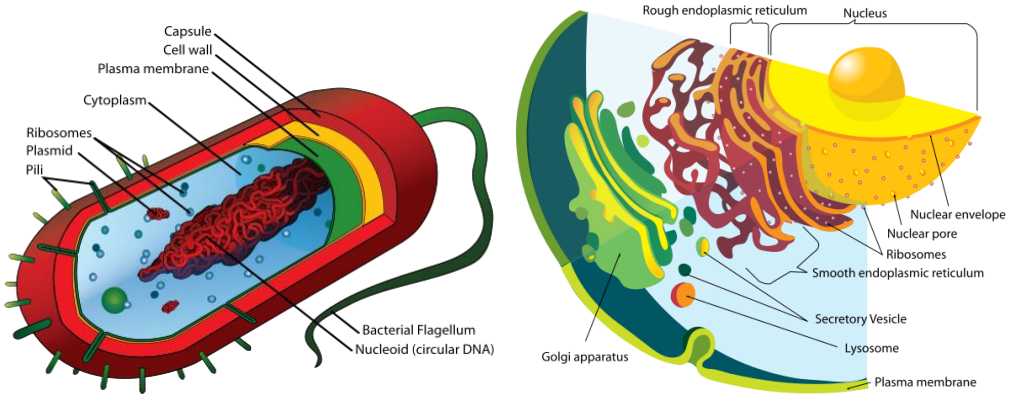

Fig 1:2 Schematic Left: prokaryotic, Right: eukaryotic cell cross-section showing the membrane bound organelles [17]

1.2.2 Mechanical Properties of Cells

Biological matter often behaves both as an elastic solid and as a viscous fluid and is therefore considered to be viscoelastic. Living cells and tissues, despite great biological complexity, can be characterized as viscoelastic matter. Cells behave in an elastic manner over short time scales to withstand sudden forces from surrounding cells, while over longer time scales they behave in a viscous manner. This property allows cells, for example, to squeeze inside narrow blood vessels or between other cells by undergoing large deformations in response to forces applied over long time scales.

Cellular viscoelasticity arises due to the co-existence of solid and liquid phases. Cells and tissues have high water content as well as a structural matrix consisting of polymers. These biopolymers can support cell shape and provide cells with a structural rigidity. However, they are also highly dynamic and can undergo large scale rearrangements. A living cell is a complex dynamical system, which constantly undergoes remodeling to adapt to changing environmental conditions. Cells adapt their mechanical properties in order to match that of their surroundings. The mechanical changes in cells under normal conditions and in response to external forces may be highly complex and difficult to measure. However, recent advances in rheological techniques have enabled the measurement of the mechanical properties of living matter. Cellular mechanical properties can be measured by several advanced techniques such as atomic force microscopy (AFM)[26-28], magnetic twisting cytometry[29], micropipette aspiration[30-32], optomechanical measures[33], and quartz crystal microbalance (QCM)[34], micro-cantilevers[4,9,10,23,24]

The mechanical properties of cells and their surroundings are important for regulating many

biological functions such as cell growth, cell movement, wound healing, cancer metastases and cell differentiation or the determination of cell fate. In a landmark experiment a few years ago, it was discovered that stem cells (cells that have not specialized into particular types) grown on soft matrices differentiate into different cell types depending on the elastic material of the matrix. For example, stem cells grown on soft surfaces with low values of elastic modulus become brain cells, while cells grown on stiff surfaces with high elastic modulus become bone cells. These findings showed that cellular biochemical and genetic response are linked to the physical properties of cells and their surroundings [18].

1.2.3 Cell Cycle and Cancer

Cancer is frequently considered to be disease of the cell cycle. Cancer cells differ from normal cells in many important characteristics. These includes the loss of differentiation, self-sufficiency in growth signals, limitless replicative potential, increased invasiveness, and decreased drug sensitivity[25]. These differences do not arise simply from uncontrolled cellular growth, but rather from a cellular evolution. The increased incidence of cancer as a function of age has long been interpreted to suggest the progressive acquisition of mutations and epigenetic abnormalities in the expression of multiple genes that have diverse functions are required for tumorigenesis. An important group of these genes is involved in cell cycle checkpoints, which are positions of control that ensure the order of events in the cell cycle, and that integrate DNA replication with cell cycle progression.

Cell cycle transition is an ordered, tightly-regulated process that involves multiple checkpoints that assess extracellular growth signals, cell size, and DNA integrity. The somatic cell cycle is divided into four distinct phases (Fig. 1.3). During two of these phases, the cells execute the basic

events in cell division like generation of a single and faithful copy of its genetic material (synthetic or S phase) and partitioning of all the cellular components between the two identical daughter cells (mitosis or M phase). The two other phases of cell cycle represent gap periods (G1 and G2), during which the cells prepare themselves for the successful completion of the S and M phases, respectively. When the cells cease proliferation, due either to specific antimitogenic signals or to the absence of proper mitogenic signaling, then they exit the cycle and enter a non-dividing, quiescent state, known as G0. In addition, the cell cycle may be arrested at the G1 or G2 checkpoints that assess cell size, extracellular growth signals, and DNA integrity [19]. Related to these events are four factors that appear to control the entry into the M-phase:

1. The accumulation of a specific cellular mass is a factor for somatic cells. This is called the *mass factor*. Some cells need to obtain a specific growth rate for mitosis to begin. This is called the *growth rate factor*.
2. The time between successive M-phases appears to be controlled by timer or oscillator genes. This is the *time factor* and appears to be a factor in embryo cells.
3. The entry into the M-phase also requires completion of the S-phase. This insures that daughter cells receive complete DNA complements and is called the completion of chromosomal *replication factor*.

The process of replicating DNA and dividing a cell can be described as a series of coordinated events that compose a ‘‘cell division cycle,’’ illustrated for mammalian cells in Figure 1.3 (see legend for details). In this, at least two types of cell cycle control mechanisms are recognized: a cascade of protein phosphorylation that relay a cell from one stage to the next and a set of checkpoints that monitor completion of critical events and delay progression to the next stage if necessary[20].

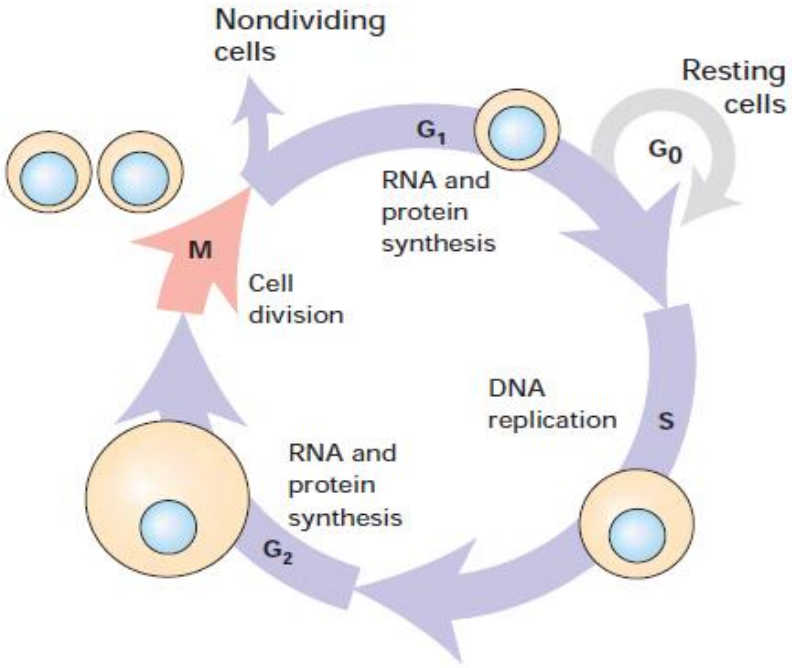

Fig 1:3 The mammalian cell cycle. In each cell division cycle, chromosomes are replicated once (DNA synthesis or S-phase) and segregated to create two genetically identical daughter cells (mitosis or M-phase). These events are spaced by intervals of growth reorganization (gap phases G1 and G2). Cells can stop cycling after division, entering a state of quiescence (G0). Commitment to traverse an entire cycle is made in late G1. Progress through the cycle is accomplished in part by the regulated activity of numerous CDK-cyclin complexes.[20]

The first type of control involves a highly regulated kinase family. A second type of cell regulation, checkpoint control is more supervisory. It is not an essential part of the cycle progression machinery. Cell cycle checkpoints sense flaws in critical events such as DNA replication and chromosome segregation. When checkpoints are activated, for example by under replicated or damaged DNA, signals are relayed to the cell cycle-progression machinery. These signals cause a delay in cycle progression machinery, until the danger of mutation has been averted. Because checkpoint function is not required in every cell cycle, the extent of checkpoint function is no as obvious as that of components integral to the process, such as CDKs-Cyclin-dependent Kinases.

Superficially, the connection between the cell cycle and cancer is obvious: cell cycle machinery

controls cell proliferation, and cancer is a disease of inappropriate cell proliferation. Fundamentally, all cancers permit the existence of too many cells. However, this cell number excess is linked in a vicious cycle with a reduction in sensitivity to signals that normally tell a cell to adhere, differentiate, or die. This combination of altered properties increases the difficulty of deciphering which changes are primarily responsible for causing cancer [20].

1.3 References

1) Park, K., Millet, L. J., Kim, N., Li, H., Jin, X., Popescu, G., Aluru, N. R., Hsia, K. J., & Bashir, R. Measurement of adherent cell mass and growth. *Proc Natl Acad Sci USA*, 107 (23), 20691–20696, (2010).
2) Park, K.., Jang, J., Irimia, D., Toner, M., Sturgis,J. Robinson, J.P., Lee, J. and Bashir, R. Living cantilever arrays' for characterization of mass of single live cells in fluids. *Lab on a Chip* 8 (7), 1034-1041 (2008)
3) Stephen M.H. A multi-modal continuous-systems model of a Novel High-Q Disk Resonator in a viscous liquid, *Proceedings of the 11th Nanomechanical Sensing Workshop, Madrid Spain,* (2014)
4) Cox, R., Josse, F, Heinrich, S. M., Brand, O. and Dufour, I. Characteristics of laterally vibrating resonant microcantilevers in viscous liquid media, *Journal of Applied Physics* 111 (1), 014907 (2012)
5) Corbin, E. A. Detection of Mass, Growth Rate, and Stiffness of Single Breast Cancer Cells using Micromechanical Sensors (2014)
6) Mitchison, J. M. Single Cell studies of the cell cycle and some models. *Theor Biol Med Model*, 2(4), (2005)
7) Tse, H. T. K., Weaver, W. M., & Carlo, D. Increased Asymmetric and Multi-Daughter Cell Division in Mechanically Confined Microenvironments. *PLoS One.* 7(6), (2012)
8) Popescu, G, et al. Optical imaging of cell mass and growth dynamics. *Am J Physiol Cell Physiol*. 295(2), C538-44 (2008)
9) Godin, M., Delgado, F.F., Son, S., Grover, W.H., Bryan, A.K., Tzur, A, Jorgensen, P, Payer, K, Grossman, A.D., Kirschner, M.W. and Manalis, S.R. Using buoyant mass to measure the growth of single cells, *Nat Methods.* 7(5):387-90 (2010)
10) Dohn, S., Sandberg, R., Svendsen, W., & Boisen, A. Enhanced functionality of cantilever based mass sensors using higher modes. *Applied Physics Letters*, 86(23), 1–3 (2005).
11) Park, K. and Bashir, R. MEMS-based resonant sensor with uniform mass sensitivity. *15th International Conference on Solid-State Sensors, Actuators and Microsystems.* 2010
12) Sader, J.E, Sanelli, J.A, Adamson, B.D., Wei, X, Mulvaney, P., Bieske, E.J., Monty, J.P., Marusic, I., Crawford, S.A., and Friend, J.R. Spring constant calibration of atomic force microscope cantilevers of arbitrary shape. *Review of Scientific Instruments*, 83(10). (2012)
13) Wolfe, S.L. (1972). Biology of the cell. Wadsworth Pub. Co. ISBN 978-0-534-00106-3.
14) Arpita Upadhyaya: *Article on Soft Matter* Mechanical Properties of Cells. 2013
15) Park, M., and Lee S, Cell Cycle and Cancer. *Journal of Biochemistry and Molecular Biology* 36(1), 60-65 (2003)
16) Collins K, Jacks T, and Pavletich N.P., The Cell Cycle and Cancer, *P Natl Acad Sci USA* 94 (7) 2776-2778 (1997)
17) Tzur A., Kafri R., LeBleu V. S., Lahav G., and Kirschner M. W. Cell growth and size homeostasis in proliferating animal cells. *Science*, 325(5937):167–171 (2009)
18) H. Lodish, A. Berk, P. Matsudaira, C. A. Kaiser, M. Krieger, M. P. Scott, L. Zipursky, and J. Darnell, *Molecular Cell Biology*, Fifth. Macmillan, (2004), p. 17.
19) Hogg W.R, Coulter W.H. Apparatus and Method for Measuring a Dividing Particle Size of a Particulate System. U.S. Patent 3,557,352. (1971)

20) Tzur A., Kafri R., LeBleu V. S., Lahav G., and Kirschner M. W. Cell growth and size homeostasis in proliferating animal cells. *Science*, 325(5937):167–171 (2009)
21) Di-Carlo D., Lee L.P. Dynamic single-cell analysis for quantitative biology. *Analytical Chemistry*. 78(23):7918-7925 (2006)
22) Gere, J. M. and Timoshenko, S.P., Mechanics of Materials, PWS Publishing Company. (1997)
23) Cox R., Josse F., Heinrich S.M., Dufour I., Brand O. Resonant microcantilevers vibrating laterally in viscous liquid media. *IEEE International Frequency Control Symposium, FCS*, (2010)
24) Cox R., Josse F. Jinjin Z., Heinrich S.M., Dufour I., Beardslee, L.A., Brand O. Damping and mass sensitivity of laterally vibrating resonant microcantilevers in viscous liquid media. *Joint Conference of the IEEE International Frequency Control and the European Frequency and Time Forum (FCS) Proceedings,* (2011)
25) Hanahan, D., & Weinberg, R. A. The Hallmark of Cancer: **T**he Next Generation. *Cell* 144(5), 646–674 (2000)
26) Kuznetsova, T. G., Starodubtseva, M. N., Yegorenkov, N. I., Chizhik, S. A. & Zhdanov, R. I. Atomic force microscopy probing of cell elasticity. *Micron* 38, 824–833 (2007)
27) Cross, S. E., Jin, Y.-S., Rao, J. and Gimzewski, J. K. Nanomechanical analysis of cells from cancer patients. *Nature Nano* 2, 780–783 (2007).
28) Plodinec, M. *et al.* The nanomechanical signature of breast cancer. *Nature Nano* 7, 757–765 (2012).
29) Wang, N., Butler, J. P. and Ingber, D. E. Mechanotransduction across the cell surface and through the cytoskeleton. *Science* 260, 1124–1127 (1993).
30) Hochmuth, R. M. Micropipette aspiration of living cells. *J Biomech* 33, 15–22 (2000).
31) Sato, M., Ohshima, N. and Nerem, R. M. Viscoelastic properties of cultured porcine aortic endothelial cells exposed to shear stress. *J Biomech* 29, 461–467 (1996).
32) Evans E., Yeung, A. Apparent viscosity and cortical tension of blood granulocytes determined by micropipet aspiration. *Biophys J* 56, 151–160 (1989).
33) Park, K., Mehrnezhad, A., Corbin, E. A. & Bashir, R. Optomechanical measurement of the stiffness of single adherent cells. *Lab Chip* 15, 3460–3464 (2015).
34) Li, J., Thielemann, C., Reuning, U. & Johannsmann, D. Monitoring of integrin-mediated adhesion of human ovarian cancer cells to model protein surfaces by quartz crystal resonators: evaluation in the impedance analysis mode. *Biosens Bioelectron* 20, 1333–1340 (2005).

Chapter 2 : Cell Micromechanics: Background, Properties and Methods

Stiffness and mass, and other biophysical properties are fundamental physiological properties that are regulated by environmental and genetic factors, which have implications in cell biology, tissue engineering, and the research of cancers and diseases. Specifically, the mechanics of cellular growth and division are important for diagnostics and drug development, with the purpose of investigating and identifying drug targets to stiffen/soften cancer cells or even slow/stop the growth of these cells. However, the utilization of mechanical properties requires understanding of the cellular processes that drive them. For example, stiffness has been shown to be a biomarker for metastatic potential of cancer cells[1]; suggesting that there exists cellular mechanism that compensate for changes in contractile forces to maintain a relatively stable internal environment. Furthermore, it was shown that cell growth rate is a function of cell mass[2]. The cell mass homeostasis therefore ensures that the cell mass and cell cycle transitions are coordinately linked[2]. Any change in this homeostasis can lead to uncontrolled proliferation, a hallmark of cancer. This chapter provides a background on cell viscoelasticity(stiffness) and mass and the current techniques used in measuring of these biophysical properties of cells. Some of the limitations of these technique are highlighted.

2.1 Cell Viscoelasticity

The structural and physical properties of cells allow the cell to withstand the physiological environment in which they live. Deviations from these properties will influence biological functionality and behavior, such as growth, differentiation, spreading, and migration as well as the structural health of the cell. Given these wide-ranging implications, quantification of these

mechanical properties has been an active area of research. Continuum mechanics provides the basis of these measurements; therefore, the properties of the cell are expressed in terms of classical mechanics terms such as elastic modulus and shear modulus. There are various classical models to describe the properties of the cells; however, most models reflect that cells exhibit both fluid-like and solid-like behavior. When both behaviors are exhibited, this is described as viscoelasticity and includes a non-zero viscosity and a complex elastic modulus. Therefore, when a constant force or deformation is applied, the cell will either creep or relax over time. These properties affect the mechanical interactions. Measuring the elastic modulus of the cell has been proven to be extremely challenging since the reported values vary over a few orders of magnitude. There are multiple factors that have to be considered to account for the cell being soft, thin, and submerged in fluid.

Traditionally, mechanical models of materials are constructed by combining idealized springs and dashpot elements. These constitutive models can be experimentally used to describe the response of the cell based on experimental data. The basic models of viscoelasticity used to describe a cell are Maxwell, Kelvin-Voigt, and standard linear solid[3]. All of the models are defined by the response they give when a stress or strain is applied. The Maxwell model consists of a spring and dashpot in series, shown in figure 2.1A. If the body is placed under a constant strain, the stress will gradually relax. However, if the body is placed under a constant stress, the strain has multiple components: (i) the instantaneous elastic component (referring to the spring) and (ii) the time-dependent viscous component that grows as long as the stress is applied. A limitation of the model is that it gives an inaccurate creep prediction[3.]

Rearranging the Maxwell model generates the Kelvin-Voigt model, which consists of a spring and

dashpot in parallel, shown in figure 2.1B. A Kelvin-Voigt body placed under a constant stress will deform at a decreasing rate approaching the steady-state strain. Once the constant stress is removed the material will gradually relax to the original shape. This model provides an accurate creep prediction of the strain, though it is much less accurate with relaxation[3]. The standard linear solid combines the concepts of both Maxwell and Kelvin-Voigt materials. In this model, a spring and one dashpot in series with a second spring in parallel, shown in figure 2.1C. Although the standard linear solid model is considered more accurate in predicting the proper response, it is more complicated to estimate all parameters[3].

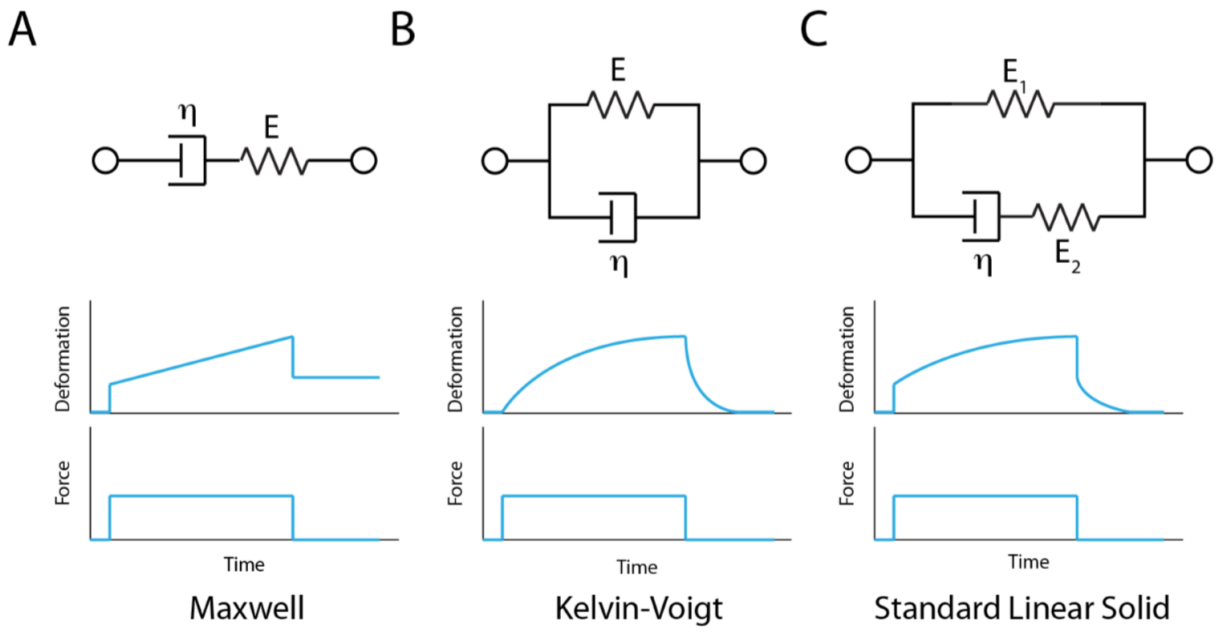

Fig 2:1 Schematic of generalized model analogies of linear viscoelastic behavior: (A) Maxwell, (B) Kelvin – Voigt, and (C) Standard Linear Solid[3]

2.2 Cell Mass

Cell growth is the process of building mass to increase size. A relevant study of interest in this field is the highlighting of factors that regulates overall cell growth and coordination of growth with cell cycle progression. A cell must maintain homeostasis, or equilibrium state, over the cell

cycle to function properly. This is the regulation of the internal system of the cell for proper function. Many diseases occur as a result of an imbalance of cell size homeostasis, which is linked to the coordination of the cell cycle. Growth is a normal part of life; however, growth rate is dependent on species. Although there is significant variation between individuals, the internal workings and organs of a person are proportional to the body. As organisms grow their size is maintained. In an experiment[2], some individual cells were grown on a mass sensor and measured their mass for 50 hours. The results demonstrate that adherent human colon epithelial cells have increased growth rates with a larger cell mass, and the average growth rate increases linearly with the cell mass, at 3.25%/hr.

As explained in figure 1.2, the cell cycle is the period of time for cellular reproduction, including growth of the parent cell and its division into two daughter cells. Two distinct phases divide the cell cycle: interphase, the time period where the cell grows and acquires mass, and mitosis, the process where the cell divides. Interphase itself comprises three distinct segments: a gap, G1, where the cell grows in size, synthesis where DNA is replicated, and another gap, G2, for additional cell growth. Checkpoints exist after each gap to ensure the cell is prepared to enter either synthesis or mitosis.

2.3 Growth Models

There are two major models used to analyze the cell cycle: one based on an exponential increase and another based on a linear increase. Variations in growth rate over the cell cycle may elucidate mechanisms underlying cell growth better than the magnitude of growth rate alone.

Exponential growth rate for an individual cell is proportional to cell size mass, volume, or density during the cell cycle. Linear growth rate for an individual cell is constant meaning the cell increases size by the same amount regardless of its current size or state. The exponential growth rate is derived from the increasing amount of ribosomal machinery present in the cell that doubles along with size during the cell cycle. Figure 2.2 presents examples of how cell mass would change in each of the two models. Since growth is dependent on the ribosomes, larger cells grow faster through more protein synthesis. However, cells should be in balanced growth where the bulk properties of cells remain unchanged for several generations, thus requiring additional cell size control mechanisms for cell size homeostasis over generations. If larger cells grow more rapidly than smaller ones, as in the exponential model, cell size variation in the population would increase in each generation. Because this does not occur, we know that if growth is exponential or, more generally, if it increases with cell size some mechanism must limit size variation in cells. In Mitchison.et.al[3], two approaches to understanding growth during the cell cycle are single-cell studies, where growth during the cell cycle of a single cell is measured, and cell-culture studies, where growth during the cell cycle of a large number of cells as an aggregate is analyzed. Mitchison has proposed that single-cell studies, because they show variations in cell growth patterns, are more suitable for understanding cell growth during the cell cycle, and should be preferred over culture studies. Specifically, Mitchison argues that one can glean the cellular growth pattern by microscopically observing single cells during the division cycle. In contrast to Mitchison's viewpoint, it is argued here that the biological laws underlying cell growth are not to be found in single-cell studies. The cellular growth law can and should be understood by studying cells as an aggregate.

These ideas are applied to the controversy between proponents of linear growth as a possible growth pattern during the cell cycle and the proponents of exponential growth during the cell cycle. Differential (pulse) and integral (single cell) experiments are compared with regard to cell cycle analysis and it is concluded that pulse-labeling approaches are preferred over microscopic examination of cell growth for distinguishing between linear and exponential growth patterns. Even more to the point, aggregate experiments are to be preferred to single-cell studies. The logical consistency of exponential growth – integrating and accounting for biochemistry, cell biology, and rigorous experimental analysis – leads to the conclusion that proposals of linear growth are the result of experimental perturbations and measurement limitations. It is proposed by Mitchison that the universal pattern of cell growth during the cell cycle is exponential.

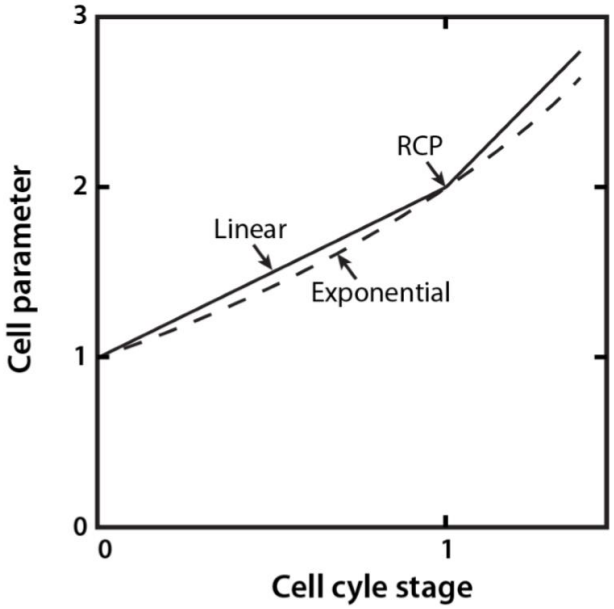

Fig 2:2 Exponential and linear models of growth. One daughter cell grows through the cell cycle and then divides to form two new daughter cells. As part of the linear growth curve there is a discontinuity in the curve called a rate change point (RCP) [4]

2.3.1 Bulk Analysis Limitations

Populations of cells or bulk dynamics can produce to misleading results especially when measuring

time dependent measurements. Early growth studies that could only study populations of cells have established a baseline for modern analysis techniques. Cellular heterogeneity within a population is a fundamental principle of cell biology and should be a key consideration when investigating cells. However, as advanced tools are developed, and we are able to capture growth on the single cell level, we need to rethink our analysis to reflect our new capabilities. There has been several works that focused on the understanding and analysis of individual cells and a review of single cell data using new techniques to determine cell growth rate on a cell-by-cell basis.

2.3.2 Mechanical Interaction with the Cellular Environment

As discussed earlier the cellular architecture of a cell plays a vital role in the "balance of forces"[5]. Studies have revealed that all living cells are in controlled mechanical tension through cytoskeletal filaments that both generate and resist mechanical loads or deformations. The cytoskeletal filaments will orient enzymes and substrates involved in biochemical reactions that mediate critical cellular functions. Thus, as a cell responds to a mechanical load its cytoskeletal structure is deformed, ultimately altering the chemical activity that modulates the cell behavior such as cell growth, differentiation, motility, and apoptosis. Therefore, cell stiffness, or how it responds physically to an external force is an indicator of cellular function. A change in cell stiffness has been recently identified as a characteristic of cancer cells and an important parameter that affects the way they metastasize[6]. Cross et al. show that cancerous cells can be distinguished from normal ones even when they show similar shapes[6], since cancer cells are 1.4 to 1.8 times softer than the normal counterpart. Another study comparing different breast cell lines found similar results[38], and it has been shown that cell stiffness is a biomarker of the degree of metastatic potential[1]. Discher et al. have investigated how cell stiffness is influenced by the properties of the anchorage

substrate[7]. Due to the large variability in solid stiffness, the behavior of cells on soft materials is a characteristic of phenotypes, specifically how cells grow on soft agar is a tool for cancer identification. Molecular pathways are influenced by adhesion and the feedback of the matrix stiffness on the cell state has important implications on growth, differentiation, and disease[7]. Tilghman et al. showed how cancer cell lines respond to polyacrylamide gels ranging in various stiffnesses[8]. They classified the findings into two categories: “rigidity dependent” and “rigidity independent,” and measured the growth of these cells lines on stiffnesses ranging from 150 Pa to 4.8 kPa. This study begins to show that the stiffer matrices were more conducive to proliferation of cells, while showing overall that cancer proliferation is highly rigidity dependent[8]. In an interesting review[39], it is shown that research findings over the past century provides reasonable, and at times unequivocal, evidence that many people do have ‘occult’ tumors – one that exists within the organ and unnoticed by the host. It is suggested in this paper that the microenvironment surrounding the tumor in this case provides tumor – suppressive signals as long as the architecture of the tissue homeostasis is essentially controlled. However, once tissue homeostasis is lost, the altered microenvironment can itself become a potent tumor promoter resulting in cancer. It is therefore inferred that initiation of tumors is unavoidable, but their progression to malignancy can and should be controlled[39].

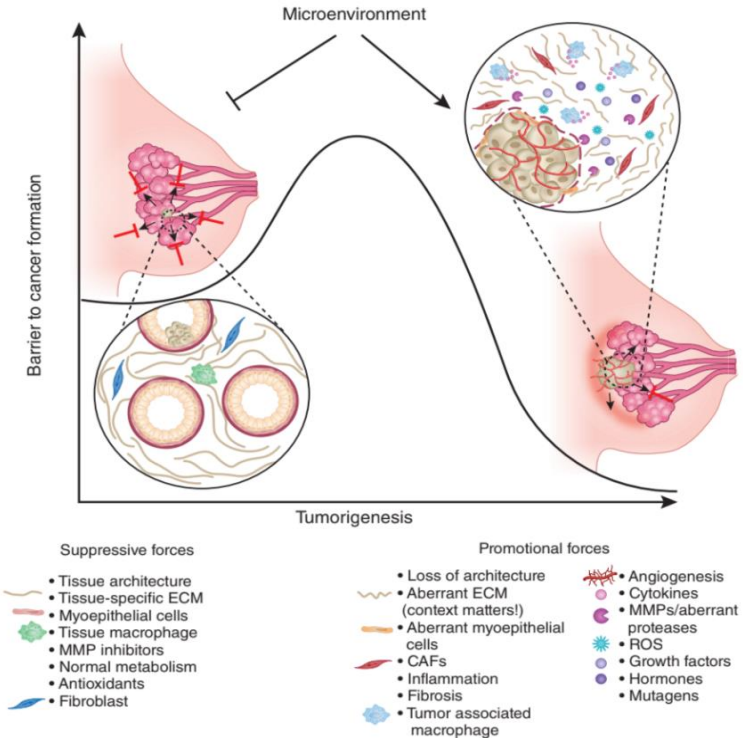

Fig 2:2b The normal tissue microenvironment acts as a barrier to tumorigenesis. Under conditions of normal tissue homeostasis, the microenvironment exerts suppressive forces to keep occult tumors in check (bottom left in graph). But the microenvironment can also be permissive to tumor growth, and the combination of mutagens, inflammation, growth factors and other tissue-associated promotional forces shown in this figure can breach the barrier to tumor formation, resulting in full-blown cancer (top right)[39].

2.4 Cell Mechanical Measurement Methods

In order to measure the mechanical properties of the cell, either a known force or a stress must be applied to the cell and the resulting deformation has to be accurately measured. Many methods have been developed for measuring cell mechanics, and there are a handful of methods that have been widely adopted. Figure 2.4 shows the most common techniques that have been used to probe cells, including micropipette aspiration, optical tweezers, magnetic twisting cytometry, and atomic force microscopy (AFM).

Micropipette aspiration works by applying a suction pressure to a cell in suspension by means of a glass micropipette, causing the cell to be slightly aspirated into the pipette (figure 2.4A). By

measuring the length of aspiration, and comparing with the known suction force, cellular elastic properties can be determined. There have been many studies using micropipette aspiration performed on neutrophils, chondrocytes, endothelial cells and fibroblasts in suspension[9-19].

The optical tweezer device uses a focus laser beam to apply attractive or repulsive forces to microscopic objects through the refractive index mismatch of the object and surrounding medium. This method traps and moves organelles or microbeads attached to or internalized by the cell at the focal point of the laser beam (figure 2.4B). By monitoring the deformation and applied force, the cell properties are calculated. Optical tweezers have been used extensively on many cell types, including human erythrocytes and red blood cell[20, 21].

Magnetic twisting cytometry uses ligand coated ferromagnetic microbeads to apply small twisting forces to an adherent cell bound to the cell surface. Once the beads are attached to the cell, an oscillating magnetic field is applied causing the bead to twist or torque on the cell. By using a model of cell deformation, you can estimate the cell elastic modulus of the cell through relationship between the applied torque and resulting bead rotation and translation (figure 2.4C) [22]. While this is a commonly used technology it is most appropriate for probing the cell membrane.

AFM has become one of the most frequently used tools for sensing and actuating on the nanometer scale and is a prominent tool in biological sciences for probing cells. The elastic modulus of cells and biological tissues are extracted through force-distance curves, where a microcantilever probe is pushed into the surface to a set force then is retracted (figure 2.4D).

Typically, AFM techniques use a sharp tip; however, for soft materials or cells, a spherical tip is more commonly used because it allows for greater indentation without puncturing the cell membrane. Then a material model for tissue stiffness is used with Hertzian mechanics to fit the curve and extract the elastic modulus of the cell. There have been many studies using AFM to probe the stiffness of a wide variety of cells, biomolecules, and biomaterials[1, 6, 23-26.] They can be used to measure elastic component of a whole and subcellular component of a cell.

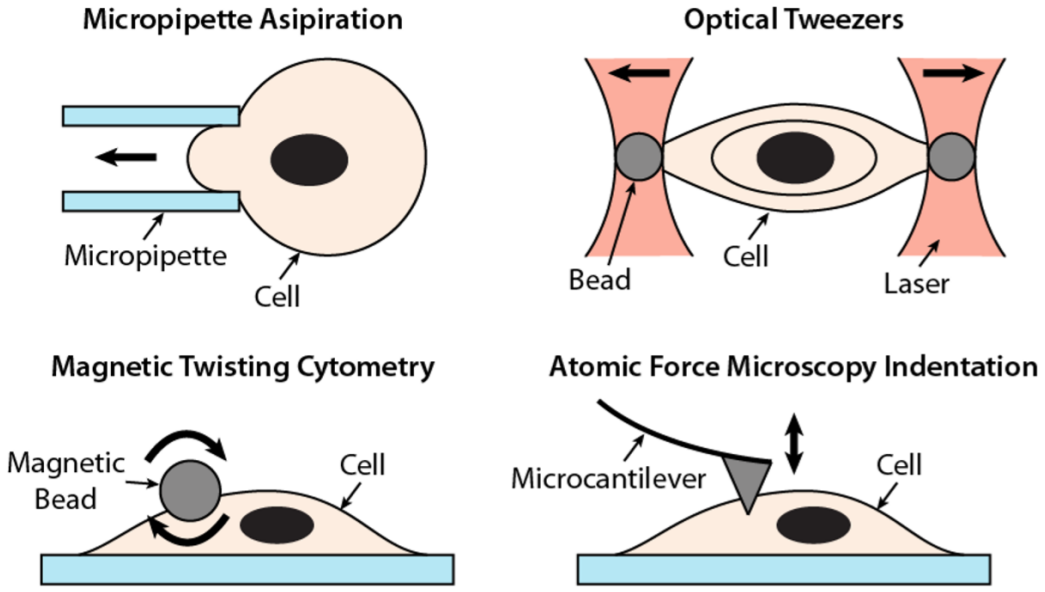

Fig 2:3 Experimental mechanical measurement techniques for measuring mechanical properties on the cellular level (A) micropipette aspiration (B) optical tweezers (C) magnetic twisting cytometry (D) atomic force microscopy indentation

Table T1 shows compares several measurement techniques; their advantages and ability to measure these properties (stiffness and mass) over time.

2.4.1 MEMS Resonant Mass Sensors

Microcantilevers are one of the most common forms of resonant sensors. They were first developed for atomic force microscopy (AFM) in 1986, but they have been used for many different types of measurements, including chemical and biological sensing. Fast response time, high

sensitivity, and scalability are some of its advantages. Since microcantilevers are the simplest form of a resonant sensor, it also has a simple geometry it makes it easy to determine the effective spring constant. Their use for mass sensing has developed based on the idea of resonant frequency shift, since the resonant frequency is greatly affected by addition of mass at the free end of the cantilever. These devices are also advantageous as they can be operated in air or submerged in a liquid, which is necessary for studying biologics. These can further be fabricated in an array, as seen in Figure 2.5, to provide high measurement throughout. The principles of resonant frequency shift, characteristics of the specific device used in this dissertation and the method for estimating an adhering mass is explained in the following sections.

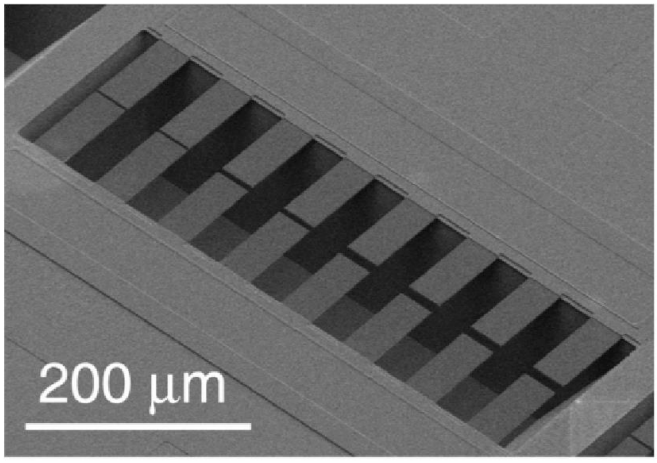

Fig 2:4 SEM image of cantilever arrays showing 120 µm × 100 µm cantilevers [29]

2.4.2 Frequency Shift Operation

The simple geometries of a cantilever make it easy to calculate the effective spring constant and device resonant frequency. In mass sensing, where an object of interest is adhered to the end of the device, the shift in the resonant frequency is used to extract the adhered mass. In other words, if the mass is placed directly on the free end of the cantilever the mass may be directly calculated from resonance frequency shift and the known spring constant of the device. Figure 2.6 presents

an example of measured resonant frequency and the shift when a mass is added. Scaling of the cantilever is an extremely desirable trait for easy manipulation of the sensitivity based on the object's size and mass. This has made them a very attractive solution for various applications such as the detection of DNA, viruses, bacteria, spores, etc. One limitation of the microcantilever is the non-uniform mass sensitivity over the cantilever surface. This means that the mass reading is directly linked to the position of the cell on the cantilever and must be considered. Microcantilevers were first developed for atomic force microscopy (AFM) but have been used for many different types of measurements, everything from chemical and biological sensing. This is an especially attractive option due to fast response time, high sensitivity, and ability to upscale to an array. Microcantilevers are easy to fabricate, in a cleanroom facility. They allow for label-free, non-invasive long-term sensing of cells over long periods of time. This is ideal for studying growth trends of cells. The measurement equipment can be automated to take readings every few minutes to get good temporal resolution. These MEMS resonant method allows for biophysical studies of individual cells and will be used throughout this dissertation.

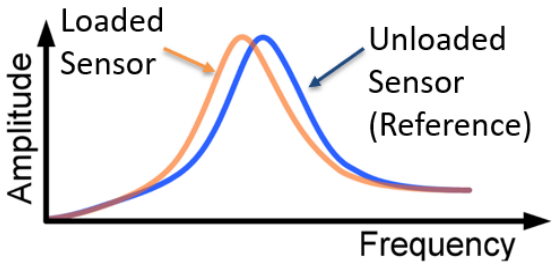

Fig 2:5 An example of the frequency response of a sensor. The peak on the right (blue) is the frequency data for the cantilever without a cell. After a cell is captured, the resonant frequency shifts to a lower frequency resulting in the peak on the left (orange). Comparing the frequency shift a mass can be extracted.

2.4.3 Dynamics of Resonant Sensors (Cantilever)

If the cantilever is represented through a lumped model with a mass, and is subjected to a harmonic excitation force, $Fe^{i\omega t}$, we can write the differential equation describing the cantilever

deflection:

$$m\frac{d^2z}{dt} + c\frac{dz}{dt} + kz = Fe^{i\omega t} \quad (2.1)$$

Where m is the mass, c is the damping coefficient, k is the spring constant, F is the amplitude of excitation, and ω is the angular frequency. The resonant frequency of the system is described by Equation 2.1.

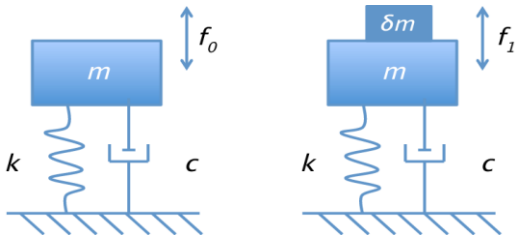

Fig 2:6 It is assumed that δm is a point mass on m and that the measurement is being taken in air, so the effect damping, c, is very minimal. Unloaded (left) and loaded (right) resonant frequency diagrams.

$$\text{Unloaded Resonant Frequency: } f_0 = \frac{1}{2\pi}\sqrt{\frac{k}{m}} \quad (2.2)$$

Where f_0 is the resonant frequency, k is the spring constant and m is the mass of cantilever[2]. From Equation 2.2, Equation 2.3 takes into account the additional point mass from Equation 2.2, as shown in Figure 3.

$$\text{Loaded Resonant Frequency: } f_1 = \frac{1}{2\pi}\sqrt{\frac{k}{m+\delta m}} \quad (2.3)$$

Where f_1 is the loaded resonant frequency, k is the spring constant, and m+δm is the mass of the cantilever plus a change in mass. The change in mass (δm) is modeled as a point mass[3]. Combining Equations 2.2 and 2.3 and rearranging terms, Equation 2.4 describes the change in mass.

$$\delta m = \frac{k}{4\pi^2}\left(\frac{1}{f_1^2} - \frac{1}{f_0^2}\right) \quad (2.4)$$

Where δm is the change in mass, f_1 is the loaded resonant frequency and f_0 is the unloaded resonant frequency. Presented in the sections below are methods that help in collecting cell mass

information based on resonant behavior and data provided by the devices. Microcantilevers can have extremely high mass sensitivity, which makes them desirable for mass sensing, and this sensitivity can be easily manipulated simply by scaling down cantilever dimensions. Small changes in cantilever length and thickness lead to large differences in stiffness, and thus spring constant, as shown in equation 2.5. For a rectangular cantilever with length L, width w, thickness t, and Young's modulus E, the spring constant k of the device is evaluated as:

$$k = \frac{3EI}{L^3} = \frac{Ew}{4}\left(\frac{t}{L}\right)^3 \qquad (2.5)$$

Where I = $wt^3/_{12}$ is the moment of inertia of the cross-section with respect to the bending axis. By combining and manipulating the above equations, it is possible to tune the response of the microcantilever for accurate sensing of cell mass of a single cell attached at the end of the cantilever.

Since the sensitivity of a microcantilever sensor is determined by minute changes in frequency, another important variable that needs to be considered is being able to resolve the frequency. This depends on the quality factor, Q, of the resonant peak. For mechanical systems the quality factor defines resonant peak and shape, and it is high influenced by the viscous damping. From equation 2.1, the quality factor is derived and shown below in equation 2.6

$$Q = \frac{\sqrt{km}}{c} \qquad (2.6).$$

If you consider the case where a cantilever is transitioned from air to water, Q decreases with increased damping. This causes the width of the resonant peak to increase and makes accurate measurement more challenging. Increasing quality factor by making the resonant peak becomes narrower and sharper leads to higher measurement sensitivity from the ability to resolve smaller

resonant frequency shifts. This can be achieved through modifications to device design, materials, and damping environment. However, this optimization often requires tradeoffs with other functionalities that must be appropriately considered.

2.5 Recent resonant Mass and Stiffness Sensors

2.5.1 Cantilever Structure Array: Mass

This technique provides information about single, adherent cells. The cantilever array is a multiplexed iteration in silicon (Figure 2.3) of the basic cantilever design described in the previous section. The array allows for more cells to be measured at one time. Similar to the basic cantilever design, the cantilever arrays are faced with the same challenges as the basic cantilever design. They experience non-uniform mass sensitivity over the surface of the sensor. This method is great because it takes the idea of a cantilever sensor and allows it to be multiplexed and run many different cell measurements in the same experiment.

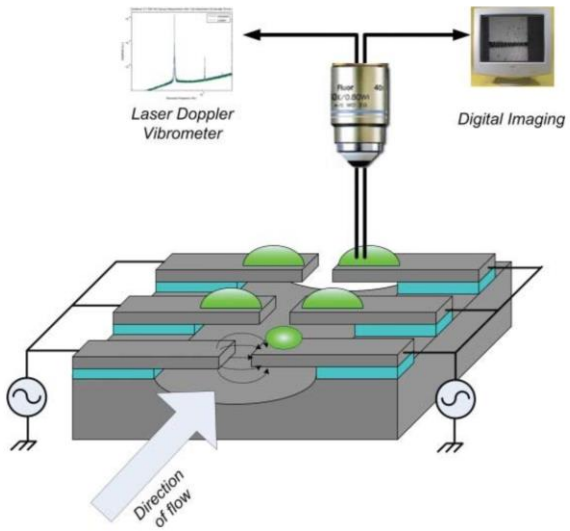

Fig 2:7 Cantilever Structure Arrays[3]

One of the unique aspects of cantilevers is that they can be scaled up to arrays for high throughput. The small size of the cantilever allows for high sensitivity. They are a favorable method for non-

invasively monitoring the mass of a single cell. These cantilever arrays are used to measure adherent cell mass. They consist of many silicon cantilevers arranged in parallel for the measurement of adherent cells.

As mentioned above, one downside to this method is the sensitivity dependence of the cell location on the cantilever. As the cell gets closer to the tip of the cantilever, the measurement gets more accurate. This is cumbersome and requires a lot many of calculations to overcome. Additionally, the sensors are highly damped when in a liquid environment, further decreasing the sensitivity. This damping can be overcome, however, by placing the liquid environment inside of the cantilever as demonstrated in the next method.

2.5.2 Suspended Microchannel Resonator

The hollow cantilever structures consist of a silicon cantilever with an embedded microfluidic channel. It cleverly decreases the effects of damping in liquid seen in the cantilever array sensors by creating a microfluidic channel inside the cantilever (Figure 2.4) and then performing the measurements in a vacuum environment. This reduction in damping allows mass to be measured with femtogram precision. These structures are used to measure the single cell mass of suspended cells.

This method is great because it cleverly decreases the effects of damping in liquid seen in the cantilever array sensors by creating a microfluidic channel inside the cantilever and then performing the measurements in a vacuum environment. Also, the dependence on the cell's location does not matter, since the cell is not adhered to the cantilever surface.

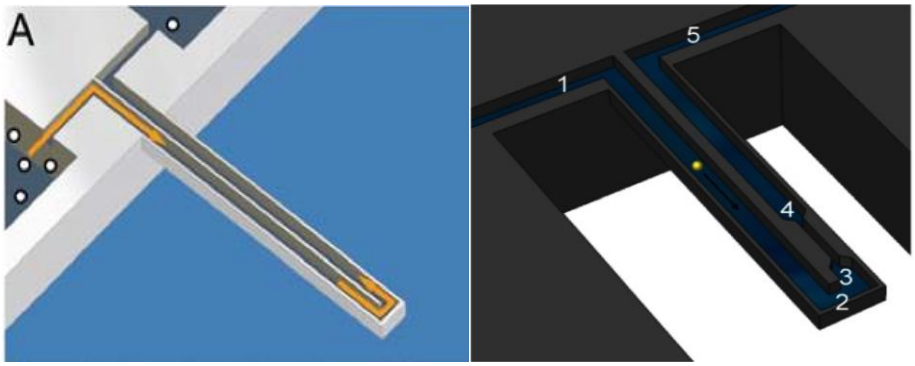

Fig 2:8 Suspended Microchannel Resonator (SMR) Left: Unmodified SMR to measure mass of suspended cells Right: A modified hollow microchannel to characterize the passage time and travel velocity and surface friction through points 2-3. This is used in estimating deformability of transiting cells [19,35]

Bryan et. al. in 2009[27] called the hollow cantilever design a suspended microchannel resonator (SMR) when it was used to measure mass, density and volume of yeast throughout the cell cycle. The device oscillates at a frequency proportional to its mass, like the general cantilever equation, but the mass of this cantilever changes as a cell is repeatedly flowed back and forth through the microfluidic chamber, creating a dynamic trap that allows for consecutive buoyant mass measurements of the same cell. Unfortunately, this method is only valid for cells that thrive in a suspended culture. Most cells, however, are adherent and grow best when they are attached to a surface similar in stiffness to their native tissue extracellular matrix. This suspended microchannel resonator (SMR) consists of a silicon cantilever with an embedded microfluidic channel that resonates at a frequency proportional to its mass, which changes as individual cells flow through the channel. The SMR measures mass with femtogram precision, allowing for rapid determination of the growth rate in a fraction of a complete cell cycle. The flow direction was continuously altered in the microfluidic channel to create a dynamic trap that allows for consecutive buoyant mass measurements of the same cell. Unfortunately, this setup does not allow for mass measurements of adherent cells because the cells must constantly be flowed back and forth through the channel. This setup does provide very little damping, therefore very high mass sensitivity. The

device is used in a vacuum and the fluid is located inside the cantilever. Furthermore, there is as shown in figure 2.9B, a later version of the device design incorporates a constriction that gives insight into the passage parameters of each cell. These parameters including travel time and entry velocity and surface friction through points 2-3 are used in estimating the deformability of each cell. When accounting for cell buoyant mass, it is observed that cells possessing higher metastatic potential exhibit faster entry velocities than cells with lower metastatic potential. Additionally, cells with higher metastatic potential exhibit greater than expected changes in transit velocities, suggesting that not only the increased deformability but reduced friction may be a factor in enabling invasive cancer cells to efficiently squeeze through tight spaces. While this method provides excellent sensitivity, it requires the cells to be in suspension, which is not the best environment to study adherent cells. Adherent cells grow and behave most normally when then can adhere to a surface similar in stiffness to their native tissue environment.

2.5.3 In-plane Mode: Quartz Crystal Microbalances: Mass

Gryte, et. al. in 1993 first used the Quartz Crystal Microbalances (QCM) to monitor the attachment and detachment of anchored mammalian cells in real time. QCM consists of an AT-cut piezoelectriz quartz crystal in between two electrodes. It functions by applying an alternating voltage potential across the quartz crystal by the two excitation electrodes on opposite sides of the quartz crystal. This causes the crystal to oscillate at a characteristic resonant frequency[36].

An advantage it offers is that the QCM allows the monitoring of adherent cells, unlike the hollow cantilevers, and the sensitivity of the measurement is not dependent on the location of the cell, unlike the traditional cantilever design. The benefit of this method when it was first developed was real-time measurements. They used this technique to study lysis and detachment of Vero cells in

real-time. Previous adhesion studies were tedious and the interpretation of the data was up to the user, very subjective.

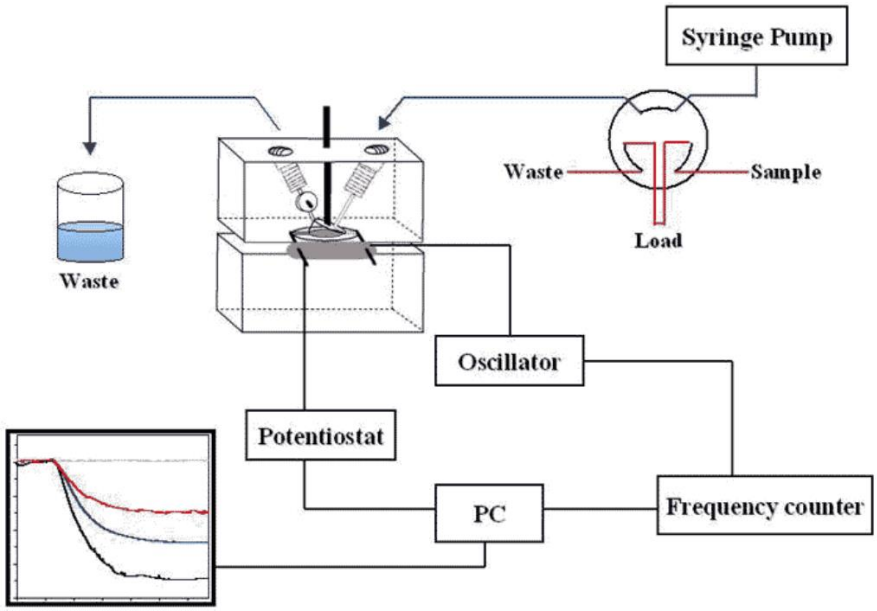

Fig 2:9 Setup of Quartz Crystal Microbalance (QCM) [37]

The QCM is governed by the following equation:

$$\Delta f = \frac{-2f_0^2 \Delta m}{A\sqrt{\rho_q \mu_q}} \qquad (2.7)$$

Where Δf is the resonant frequency decrease, f is the intrinsic frequency of the crystal, Δm is the change in elastic mass (grams), A is the electrode area, ρ_q is the density of the quartz, and μ_q is the shear modulus. This equation assumes rigid layer behavior, where the resonant QCM frequency depends on the mass, m, attached to the quartz crystal surface. This is called the Sauerbrey relationship. This relationship can be used to determine the change in mass at the surface of the quartz crystal. Any mass bound to the surface will oscillate with similar lateral displacement as the oscillating quartz crystal. If the body is very stiff, then no energy is lost and the oscillations are elastic. If the body is not stiff, then there is energy lost and the process is inelastic. The sensitivity

of this ‘quartz crystal nanobalance’ is 0.1μg, but it is valid only for very small elastic masses. It does not function for masses larger than 2% of the crystal mass. While this method is good at determining bulk, adherent cell information, it does not provide information about single cells due to its large substrate size requirement of 14mm.

2.5.4 Picobalance

The picoscopic cell balance [34], which thrives on the frequency shift operation, is used to non-invasively measure adherent cells at high mass and time resolution. The balance, which is based on an actively actuated silicon microcantilever, is mounted on an inverted optical microscope and operates under cell culture conditions (Fig. 2.11a). Attaching a cell to the microcantilever changes the effective mass and thus shifts the natural resonance frequency of the cantilever. However, accurately detecting the natural resonance frequency of a non-driven cantilever in liquid is difficult. To enhance the mass sensitivity of the cantilever, a low-power intensity-modulated blue laser (405 nm, ≤ 50 μ W) is focused at the base of the cantilever to generate very small cantilever oscillations in the range of approximately 1–15 Å (Fig. 2.11b). To avoid interference with the blue laser, the adhering cell is placed at the opposite end of the cantilever. The movement, amplitude and phase of the cantilever (Fig. 2.11b) are read out optically by an infrared laser (852 nm, ≤ 250 μ W). These values are perfectly fitted by a driven and damped harmonic oscillator model, making the mass analysis of the attached cell straightforward. it has not been possible to track individual adherent cells in physiological conditions at the mass and time resolutions required to observe fast cellular dynamics. This technique is compatible with fluorescence microscopy and is used to monitor single adherent cells over a time range (from milliseconds to days) and at a mass resolution (below 1% ~ 10pg) sufficient to characterize how cells regulate mass and volume.

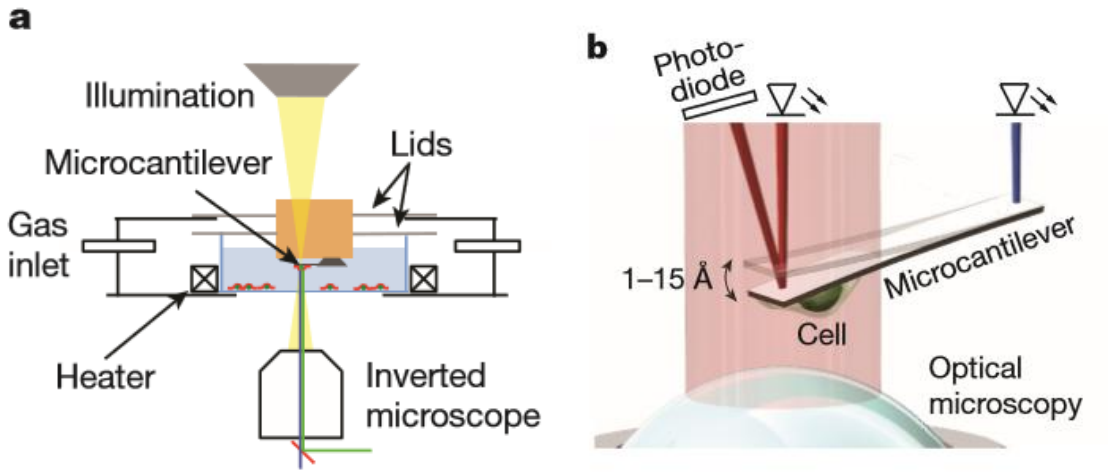

Fig 2:10 Working principle of the picoscopic cell balance in culture conditions. a, Design of the cell balance. The chamber surrounding the microcantilever used to pick up and measure the mass of an adherent cell controls temperature, gas atmosphere and humidity to prevent evaporation of the culture medium (Methods). Sliding lids allow the microcantilever holder to be moved relative to the Petri dish. The chamber is compatible with optical microscopy. b The mass of a cell adhering to the cantilever is measured by oscillating the cantilever at its natural resonance frequency and amplitudes of around 1–15 Å using an intensity-modulated blue laser at its base. Oscillation amplitude and frequency are read out by reflecting an infrared laser from the free end of the cantilever. Simultaneously, cell morphology and state are characterized by optical microscopy [34].

2.5.5 Pedestal Sensor Array

In general, microcantilevers are attractive for mass sensing because of the potential for measurements with high sensitivity and high throughput. However, it is well-known that the cantilever beam structure has a non-uniform mass sensitivity and that calculation of mass depends strongly on position and placement of the object on the sensor. This is challenging in mass sensing of biological targets that must first be captured on the devices. Difficulty in estimating mass placement ultimately limits the accuracy of mass measurements made with the cantilever structure [2, 29]. To overcome this limitation, a MEMS resonant platform sensor has been designed to eliminate spatially dependent and non-uniform mass sensitivity[2] and can be used to measure the mass and long-term growth rate of single adherent cells. A four beam-spring sensor structure, seen in Figure 2.3, was designed to minimize the variation of the displacement amplitude across the vibrating platform. The sensor is a square pedestal (60×60 μm^2) suspended over a 50 μm pit by four beams

acting as springs (l = 80 μm, w = 4 μm). This unique structure, through both modeling and experimental data, exhibited a maximum 4% difference in mass sensitivity at any position on the pedestal. Just like other cantilever sensors, it operates in a first resonance mode for mass sensing, which is a vertical displacement vibration with resonant frequencies of approximately 160 kHz in air and 60 kHz in liquid. One key concern when measuring cells is providing the proper micro environment, which, for cells, means that the sensor must remain in liquid. This can provide problems of its own, because as you scale down, damping by liquid can drastically affect the resonant frequency measurement. Actuation in liquid also requires a strong external force, and the sensor is actuated by passing an actuation current through the sensor in a static magnetic field to generate a Lorentz force [2, 29].

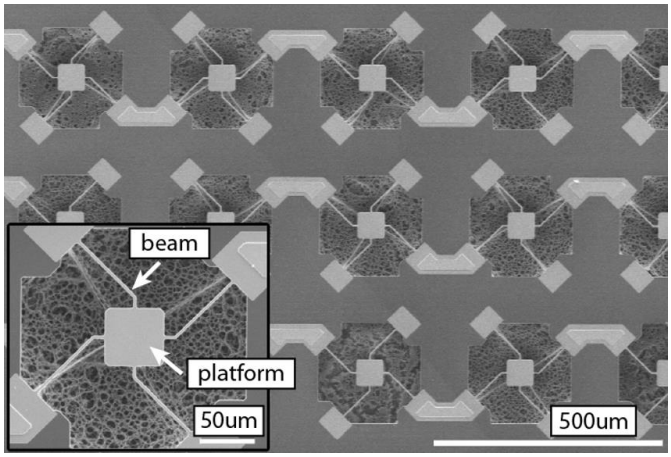

Fig 2:11 SEM images showing a sensor array, an individual sensor is shown in the inset. The beam springs and the platform area are also indicated. The uniform mass sensitivity area of the sensor is on the platform area, if a cell or mass is captured on one of the springs the mass measurement is no longer accurate[33].

2.5.5.1 Experimental Setup and Cell Mass Measurements

Figure 2.13 shows a Laser Doppler Vibrometer (LDV) system that, in conjunction with a feedback system and a lock-in amplifier, measures the velocity of the vibrating MEMS sensor platform to ultimately determine the resonant frequency of the device. This is achieved by monitoring the difference in phase between applied actuation current and sensor vibration.

The excitation frequency is updated based on this phase until converging upon the resonant frequency. This procedure is used to estimate the resonant frequency of the devices in a series of different states to extract the mass of the adhered cell. Specifically, three separate resonant frequency measurements are used in estimating the mass of an object: in air, in liquid, and in liquid with adhered load. The in-air measurement serves as a dry calibration of the empty resonator sensors to determine the effective spring constant of the device through the relationship in equation 2.8.

$$\omega = 2\pi f = \frac{1}{2\pi}\sqrt{\frac{k}{m}} \tag{2.8}$$

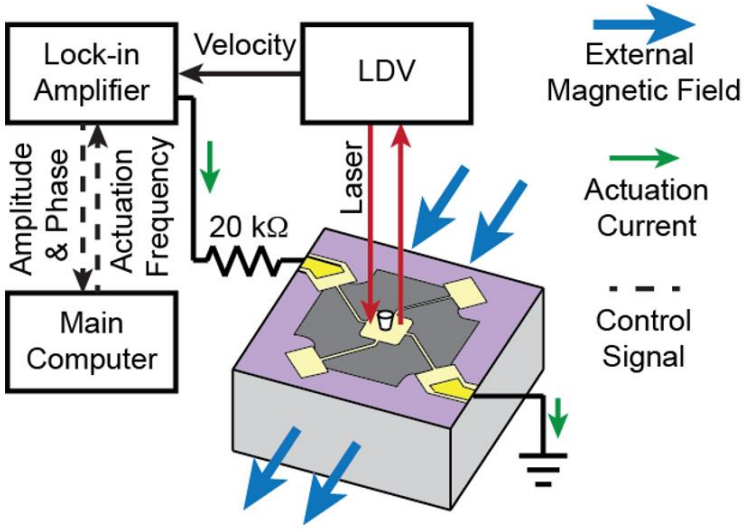

Fig 2:12 Overview of mass measurement with the sensor. Our measurement uses electromagnetic actuation and a Laser Doppler Vibrometer (LDV) system to measure the velocity of the vibrating platform in conjunction with a feedback loop and a lock-in amplifier to iteratively determine the resonant frequency.[31]

The mass of each device, m, is known to be 110 ng due to high precision fabrication process. This generally yields a spring constant, k, of approximately 19.4 N/m. The spring constant calculated in equation 2.7 holds for both gaseous and aqueous environments,

$$\omega = k_{wet} = k_{dry} = m(2\pi f)^2 \quad (2.9)$$

where k_{wet} is the spring constant of the device in fluid and k_{dry} is the spring constant of the device in air.

The second resonant frequency is measured with the empty devices submerged in the surrounding fluid necessary for maintaining cell viability during the experiment. While the spring constant is unchanged, the location of the resonant peak is shifted to approximately 60 kHz. This shift is due to increased hydrodynamic loading on the sensor. The viscosity of the surrounding fluid results in an additional force opposing the vibration of the sensor and appears as an added mass that decreases the resonant frequency. Since cell mass is also measured in liquid, this is the appropriate reference frequency

Finally, cells are added to the chip and allowed to settle and attach to the sensor platforms for at least two hours before measurement. This is so that the cells can properly adhere and reach the equilibrium temperature (37 °C). The resonant frequency the loaded sensor is now measured in the same fashion. The mass is the extracted from the shift in frequency relative to the in-liquid reference frequency. This extraction is described by equations 2.10, 2.11 and 2.12.

$$m_{platform} = \frac{k_{wet}}{(2\pi f_{wet_{empty}})^2} \quad (2.10)$$

$$m_{cell+platform} = \frac{k_{wet}}{(2\pi f_{wet})^2} \quad (2.11)$$

$$m_{cell+platform} - m_{platform} = \frac{k_{wet}}{4\pi^2}(f_{wet}^{-2} - f_{wet_{empty}}^{-2}) \quad (2.12)$$

where $m_{platform}$ is the mass of the empty device, $m_{cell+platform}$ is the device mass and the cell mass together, m_{cell} is the mass of the cell, f_{wet} is the frequency of the platform and cell in fluid,

$f_{wet_{empty}}$ is the reference frequency of the platform in fluid. Mass measurements can be taken over time to observe how cells grow, however the apparent mass seen by empty sensors needs to be monitored as well. Over time the sensors exhibit a negative drift in resonant frequency of approximately 100-200 Hz/day. This drift is compensated for by simultaneously measuring empty neighboring sensors. Correcting for field drift effects in the apparent mass measurement involves estimating the equivalent mass change from field drift as measured by the empty sensors and subtracting from the cell mass measured from loaded sensors.

The subsequent chapters further explains how we use our sensor to combine these mass measurements with other physical properties of adherent human colon cancer cells, showing that these properties can be simultaneously estimated for single cells. Previous work has shown that there are several technology limitations that inhibit application of microcantilever to measurement and analysis, including insufficient cell capture efficiency, media perfusion for long term monitoring, cell adhesion, cell movement/spreading and cell-sensor modelling. This dissertation aims to address several issues that are introduced when measuring adherent cells using new measurement schemes and protocols to pedestal sensors. Our pedestal sensors are further characterized to explore more parameters in orders to investigate the viscoelastic behavior of individual breast and colon cancer cells. Table T1 below shows a comparison of methods of measurement of cell properties highlighting the uniqueness of our pedestal resonant sensor as a tool to monitor the long-term stiffness (elasticity) of cancer cells.

Method characteristics	**QCM-D**	**Micropipette aspiration**	**Magnetic twisting cytometry**	**Atomic Force Microscopy**	**Suspended microchannel resonator**	**Picoscopic cell balance**	**Pedestal resonant sensor**
Single cells	No. Confluent populations only (Large Confluent Area required (14 mm))	Yes. Cells in suspension only	Yes.	Yes.	Single cells in suspension.	Yes. Single cells but not confluent cell populations.	Yes. Single cells but not confluent cell populations.
Adherent *versus* non-adherent	Adherent cells	Non-adherent cells. Some reports of adherent cells	Adherent cells	Adherent cells	Non-adherent cells reported. Suspended adherent cells reported for single-time-point measurement.	Adherent cells	Adherent cells
Elastic measurement components	Tissue layer only	Membrane (Reports of whole cell estimation)	Cytoskeleton	Whole cell and subcellular components	Membrane	Whole cell	Whole cell
Throughput (cells/min)	N/A	0.10	1	0.10	~240	~1000	1
Measure cell mass *versus* time	Yes.	No.	No.	No.	Yes. By flowing cells back and forth through sensor area.	Yes.	Yes
Measure cell elasticity versus long-time	No.	No.	No.	No.	No.	No.	Yes

Table 2:1: Characteristics of some methods for measurement of properties of cells.

Chapter 3 focuses on the characterization of viscosity and elasticity of live and fixed adherent colon cancer cells. We observed the viscoelastic effect of the cells on the resonant frequency and amplitude of the sensor by exploring potential regions of solutions through fitting experimentally observed amplitude and frequency data from our cell population to a representative Kevin-Voigt cell- sensor model. This, in turn, led to an estimation of viscoelastic values through a maximum likelihood probabilistic technique.

An extension of this work is shown in Chapter 4; further focusing on combining the frequency and amplitude of our resonant sensor with an extra observable (vibration induced phase shift) due to the cell height oscillation and differences in refractive index of the cell and media. The chapter

demonstrates the use of this technique to calculate each cell's loss tangent – a relative viscoelastic descriptor of the cell. This descriptor is then used to obtain a decoupled viscoelastic value for each cell. This work elucidates the heterogeneity of individual cells in a population as opposed to previous chapter in this work.

Chapter 5 presents a continuous time – varying simultaneous mass and stiffness measurement of adherent cells. This entails the addition of a fluorescence cell cycle reporter as a biomarker to identify the different stages of the cell cycle and better elucidate the mechanisms of stiffness and mass change more accurately and thoroughly through analysis. Rho factors are also used as control to investigate the sensitivity of these cells to drug-induced stiffness changes while tracking the entire cell cycle.

Chapter 6 concludes with a summary of the dissertation and a discussion of potential future research directions. There are still many improvements that can be made to this sensor and system, including more detailed fluid and solid mechanics models to more accurately determine nano-scaled membraned fluctuations. Another area considered is the additional use of the resonant sensor for drug studies, such as the effect chemotherapeutics on stiffness and mass growth rate. Finally, since it has been shown that a change in contact area drastically changes the mass reading there is there is an opportunity to study cell adhesion and how it is affected by the cell cycle.

2.6 References

1. Xu, W., Sulchek, T., Mezencev, R., Wang, L., McDonald, J., and Kim, B. Cell Stiffness Is a Biomarker of the Metastatic Potential of Ovarian Cancer Cells. *PLoS ONE* 7–10 (2012).
2. Park, K, Millet, L.J., Namjung, K, Huan Li, Xiaozhong, J., Popescu, G, Aluru, N.R, Hsi, K.J. and Bashir, R. Measurement of adherent cell mass and growth. *P Natl Acad Sci Usa* 107, 20691–20696 (2010).
3. Fung, Y. C. Biomechanics: Mechanical Properties of Living Tissues. Springer-Verlag, New York City, NY (1981)
4. Mitchison, J. M. Growth during the cell cycle. *International Review Cytology*, 226:165-258 (2003)
5. Chicurel, M.E., Chen, C.S., Ingber, D.E. Cellular control lies in the balance of forces. *Current Opinion in Cell Biology*, 10(2):232-239 (1998)
6. Cross S. E., Gimzewski J. K. Jin Y. and Rao S. J. Nanomechanical analysis of cells from cancer patients. *Nature Nanotechnology*, 2(12):780-783 (2007)
7. Discher, D. E. Tissue Cells Feel and Respond to the Stiffness of Their Substrate. *Science* 310, 1139–1143 (2005).
8. Tilghman, R.W, Cowan, C.R, Koryakina, Y., Gioeli, D., Slack-Davis, J.K., Parsons, J.T., Mih, J.D., Tschumperlin, D.J, and Blackman, B. R. Matrix rigidity regulates cancer cell growth and cellular phenotype. *PLoS One*, 5(9) (2010)
9. Schmid-Schonbein G. W., Sung, K. L., Tozeren H., Skalak, R., and Chien, S.Passive mechanical properties of human leukocytes. *Biophysical Journal*, 36(1):243-256 (1981)
10. Evans E. and Kukan B. Passive material behavior of granulocytes based on large deformation and recovery after deformation tests. *Blood*, 64(5):1028-1035 (1984)
11. Evans E. and Yeung A. Apparent viscosity and cortical tension of blood granulocytes determined by micropipette aspiration. *Biophysical Journal*, 56(1):151-160 (1989)
12. Sato, M., Theret, D. P., Wheeler, L. T., Ohshima, N., & Nerem, R. M. Application of the micropipette technique to the measurement of cultured porcine aortic endothelial cell viscoelastic properties. *Journal of Biomechanical Engineering*, 112(3):263 (1990)
13. Ward, K. A., Li, W., Zimmer S., and Davis, T. Viscoelastic properties of transformed cells: role in tumor cell progression and metastasis formation. *Biorheology*, 28(3-4):301, (1991)
14. Sato, M., Ohshima, N., and Nerem, R. M. Viscoelastic properties of cultured porcine aortic endothelial cells exposed to shear stress. *Journal of Biomechanics*, 29(4):461-467, (1996)
15. Tsai, M. A., Frank R. S, and Waugh, R. E. Passive mechanical behavior of human neutrophils: power-law uid. *Biophysical* Journal, 65(5):2078-2088 (1993)
16. Trickey, W. R., Lee, G. M, and Guilak, F. Viscoelastic properties of chondrocytes from normal and osteoarthritic human cartilage. *Journal of Orthopaedic Research*, 18(6):891-898, (2000)
17. Trickey, W. R., Vail, T. P. and Guilak, F. The role of the cytoskeleton in the viscoelastic properties of human articular chondrocytes. *Journal of Orthopaedic Research*, 22(1):131-139 (2006)
18. Thoumine, O. and Ott, A. Comparison of the mechanical properties of normal and transformed fibroblasts. *Biorheology*, 34(4):309-326, (1997)

19. Thoumine O., Cardoso O. and Meister, J.J. Changes in the mechanical properties of fibroblasts during spreading: a micromanipulation study. *European Biophysics Journal*, 28(3):222-234, (1999)
20. Henon, S., Lenormand, G., Richert, A. and Gallet, F. A new determination of the shear modulus of the human erythrocyte membrane using optical tweezers. *Biophysical Journal*, 76(2):1145-1151, (1999)
21. Svoboda, K., Schmidt, C. F., Branton, D., and. Block, S. M. Conformation and elasticity of the isolated red blood cell membrane skeleton. *Biophysical journal*, 63(3):784{793, (1992)
22. Wang, N., Butler, J. P. and lngber, D. E. Mechanotransduction across the cell surface and through the cytoskeleton. *Science*, 260:21, (1993)
23. Kuznetsova, T. G. Starodubtseva, M. N. Yegorenkov, N. I. Chizhik, S. A. and Zhdanov R. I. Atomic force microscopy probing of cell elasticity. *Micron*, 38(8):824-833 (2007)
24. Kurland, N. E. Drira, Z., and Yadavalli, V. K. Measurement of nanomechanical properties of biomolecules using atomic force microscopy. *Micron*, 43(2):116{128, 2012.
25. Kloxin, A. M. Kloxin, C. J. Bowman, C. N. and Anseth. K. S. Mechanical properties of cellularly responsive hydrogels and their experimental determination. *Advanced*
26. *Materials*, 22(31):3484-3494, (2010)
27. Bryan, A. K., Goranov, A., Amon, A. and Manalis, S. R. Measurement of mass, density, and volume during the cell cycle of yeast. *Proc Natl Acad Sci USA* 107, 999–1004 (2010).
28. Dohn, S. Sandberg, R. Svendsen, W. and Boisen. A. Enhanced functionality of cantilever-based mass sensors using higher modes. *Applied Physics Letters*, 86(23):233501, (2005)
29. Park K. and Bashir, R. MEMS-based resonant sensor with uniform mass sensitivity.*15th International Conference on Solid-State Sensors, Actuators and Microsystems.2010*
30. Corbin, E. A., Kong, F., Lim, C. T., King, W. P. & Bashir, R. Biophysical properties of human breast cancer cells measured using silicon MEMS resonators and atomic force microscopy. *Lab Chip* 15, 839–847 (2015).
31. Corbin, E. A., Millet, L. J., Pikul, J. H., Johnson, C. L., Georgiadis, J. G., King, W. P. and Bashir, R. Micromechanical properties of hydrogels measured with MEMS resonant sensors. *Biomed Microdevices* 15, 311–319 (2013).
32. Corbin, E. A., Millet, L. J., Keller, K. R., King, W. P. and Bashir, R. Measuring physical properties of neuronal and glial cells with resonant microsensors. *Anal. Chem.* 86, 4864–4872 (2014).
33. Corbin, E. A., Dorvel, B. R., Millet, L. J., King, W. P. and Bashir, R. Micro-patterning of mammalian cells on suspended MEMS resonant sensors for long-term growth measurements. *Lab Chip* 14, 1401–1404 (2014).
34. Martínez-Martín D., Fläschner G., Gaub B., Martin S., Newton R., Beerli C., Mercer J., Gerber C. and Müller, D.J, Inertial picobalance reveals fast mass fluctuations in mammalian cells, *Nature* 550, 500–505 (2017).
35. Byun S., Son S., Amodei D., Cermak N., Shaw J., Kang, J.H, Hecht. V.C.,Winslow, M.M., Jacks T., Mallick P., & Manalis, R. Characterizing deformability and surface friction of cancer cells, *P Natl Acad Sci Usa* 110 (19) 7580-7585 (2013)
36. Gryte D. M., Ward M. D., and Hu.W. S., Real time measurement of anchorage-dependent cell adhesion using a quartz crystal microbalance. *Biotechnol*. 105–108 (1993)

Chapter 3 : Amplitude and Frequency-Based Interferometric Measurements of the Viscoelasticity of Single Adherent Cells Using MEMS Resonant Sensors

As mentioned in previous chapters, many recent studies on the viscoelasticity of individual cells link mechanics with cellular function and health. Here, we introduce a novel measurement of the viscoelastic properties of individual human colon cancer cells (HT-29) using silicon pedestal microelectromechanical systems (MEMS) resonant sensors. We demonstrate that the viscoelastic properties of single adherent cells can be extracted by measuring a difference in vibrational amplitude of our resonant sensor platform. The magnitude of vibration of the pedestal sensor is measured using a Laser Doppler Vibrometer (LDV). A change in amplitude of the sensor, compared to the driving amplitude (amplitude ratio), is influenced by the mechanical properties of the adhered cells. It was observed that the amplitude ratio of fixed cells was greater than the live cells. By combining the amplitude shift with the resonant frequency shift measure, we determined the elastic modulus and viscosity values of 100 Pa and 0.0031 Pa-s, respectively. This method of using the change in amplitude in consonance with a change in frequency of resonant MEMS devices enabled the determination of a refined solution space and helped to improve measuring the stiffness of individual cells as seen in the next chapter. The results presented in this chapter are based on our published work *in Applied Physics Letters*[20], in collaboration with Dr. E.A. Corbin.

3.1 Introduction

Understanding and defining the mechanical properties of cells and tissue as a biomarker has become a nexus of next generation disease diagnostics. Recently, the development of more precise, reliable, and versatile measurement techniques – such as atomic force microscopy (AFM)[1-3], magnetic twisting cytometry[4], micropipette aspiration[5-7], optomechanical measures[8], and quartz crystal microbalance (QCM)[9] – have provided a greater understanding of how the physical

properties of a cell affect its behavior in disease. Viscoelastic properties have been linked to diseases such as cancer, where cancer cells are less stiff than their normal counterparts. These mechanical properties of cancer cells could be useful biomarkers[5] for evaluating cycle progression, cellular physiology, and metabolism that underpin the characteristics of cancer. However, there are many limitations to the current state of the art measurements (see Supplemental Information[10]). Micropipette aspiration uses a flow-through configuration that allows for high throughput, but limits the types of cells for investigation to cells in suspension. Although QCM and AFM can study adherent cells, their samples sizes are limited based on electrode dimensions or data analysis complicated by intricate tip geometry, respectively.

In this chapter, we report on a vibration-based measurement technique used to characterize the viscoelasticity of individual adherent colon cancer (HT-29) cells. We have quantified differences between live and fixed cells using microelectromechanical (MEMS) resonant sensors and the viscoelastic effect on the resonant frequency of the sensor. We demonstrate the use of these resonant sensors to investigate the viscoelasticity of single adherent cells by instead exploring the vibration amplitude effects. Analytical modeling shows that loading the sensor with a viscoelastic material, as opposed to an infinitely stiff point mass, results in a decreased vibration amplitude at resonance. Experimentally we compare live and fixed cells, where fixed cells are known to have a higher stiffness exhibit less of an amplitude effect. Combining the frequency shift reported previously[11], and the amplitude change reported here, we can more concretely determine the viscoelastic properties of the cell.

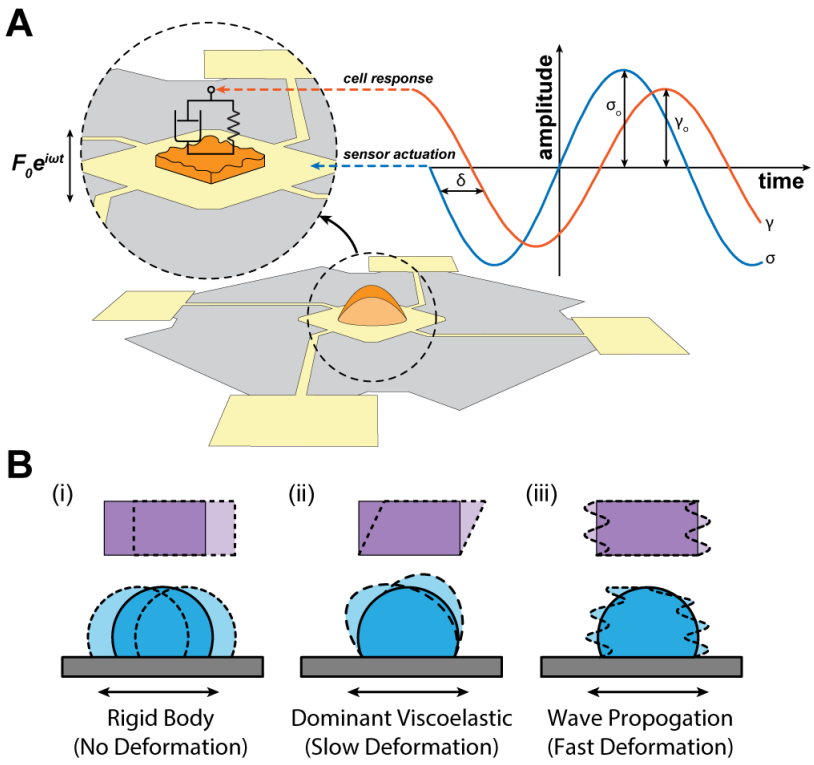

Fig 3:1Experimental overview. (A) Schematic of the vibration of a cell as a Kelvin-Voigt viscoelastic solid on the sensor describing the excitation (Fe^{iwt}) and cell amplitude response. Stress (σ_o) and induced strain (Υ_o) related to the applied force and cell response respectively. (B) Schematic diagram showing the possible scenarios of dominant forces that operate in the regime of vibration: (i) Cell is a rigid body and only translates; (ii) Cell slowly deforms because the wavelength of cell deformation, λ_d, is less than the wavelength of elastic wave propagation, λ_p; (iii) Elastic wave force dominates motion and only propagates fast across cell: $\lambda_d > \lambda_p$.

To observe significant changes in vibrational amplitude of the pedestal, we must consider the dominant forces governing the vibration of the sensor and the cell to ensure that these experimental conditions are appropriate to capture viscoelastic effects. Figure 3.1B shows three case scenarios in which cell deformation (or displacement) is compared to a shear elastic wave propagation. The cases are as follows: *(i) rigid body*, no deformation; *(ii) dominantly viscoelastic*, $\lambda_p < \lambda_d$, the elastic wave propagates slower than the cell deforms; and *(iii) elastic wave propagation*, $\lambda_p > \lambda_d$, the elastic wave propagates faster than the cell deforms. We compare the wavelength scale of the cell deformation, λ_d, to the wavelength scale of the shear elastic wave propagation, λ_p. Consideration of a shear force acting on the sensor is sufficient for a tractable cell deformation

analysis. Also, the elastic wave speed propagated is approximately equal to the longitudinal wave speed since it can be assumed that the sensor material is incompressible at the length scale of vibration. We can conclude that the dominant forces in our system are such to produce observable viscoelastic effects.

3.2 Materials and Methods

3.2.1 MEMS Resonant Mass Sensors

The MEMS resonant sensor structure used in this work comprises a 60 × 60 μm^2 platform suspended by four beam springs that are arrayed in a 9 × 9 format of 81 sensors. This MEMS resonant platform sensor that has been designed to eliminate spatially dependence and non-uniform resonant frequency in a first resonance mode, and thus ensures uniform measurement sensitivity. The device, which operates in the first mode, is placed in a static magnetic field and a small amount of current is applied to induce a Lorentz force actuation and a Laser Doppler Vibrometer (LDV) monitors the resulting velocity of the vibrating platform. In this work, we also capture the vibration amplitude response after finding the device resonance.

3.2.2 Frequency Shift and Amplitude Ratio Measurement

Our measurement scheme consists of measuring the amplitude of the sensor three times: empty, then loaded with a live cell, then after the same cell is fixed. A series of resonant measurements enables monitoring the amplitude ratio change. The measurement consists of two calibrations of the device prior to the final measurement. The first is to determine the spring constant and this measurement is performed in air where the sensor has no additional mass (~160 kHz). The surface of the sensors were functionalized with collagen (0.1 $\mu g \cdot mL^{-1}$ in PBS) for 1hr. The second measure is to provide a reference for the cell loaded measurement and is performed in the cell medium (~60 kHz) with no additional mass. The cells were then seeded onto the sensor platforms and the cell

were left in the chamber for 2 hours to allow for adherence to the sensor and for temperature stabilization. We then carry out a frequency shift operation by comparing the frequencies of unloaded sensors and cell-loaded sensors as discussed in Chapter 2. Subsequently, we capture the vibration amplitude response after finding the device resonance. The viscoelastic amplitude measurements are determined by using the ratio of amplitudes at the resonant frequency of the empty sensor and the sensor loaded with a cell.

Viscoelastic amplitude measurements can be taken while cells grow; however, the amplitude ratio of empty sensors needs to be monitored as well. Over time the sensors exhibit a negative drift in resonant frequency and in amplitude. We compensate for this drift by simultaneously measuring empty neighboring sensors throughout the observation period. Correcting for drift effects in the amplitude measurement involves estimating the amplitude as measured by equivalent empty sensors and subtracting from the amplitude measured from loaded sensors.

Material viscosity is dependent on vibration frequency such that at higher driving frequencies the cell will exhibit greater viscous behavior. In our system we use the shift in resonant frequency from cell mass and viscoelasticity to extract material properties, assuming these properties to be constant near the frequencies used. We assume that the influence of resonant frequency shift on viscosity is negligible as the shift is very small relative to nominal driving frequency (< 1%), which translates to a change in viscosity of < 0.1%.

3.2.3 Biological Cell Culture

To investigate the amplitude effects experimentally, human colon adenocarcinoma cells (HT-29) were cultured on the resonant sensors functionalized with collagen similar to earlier studies[11].

Briefly, HT-29 cells were grown at 37 °C in Dulbecco's Modified Eagles Medium (DMEM) supplemented with sodium pyruvate, 10% fetal bovine serum (FBS) and 1% penicillin streptomycin. Cells were seeded onto the sensor area at a density of ~300 cell/mm^2 within a 6 mm diameter PDMS culture chamber. After measuring the amplitude of the resonant peak with a live cell attached to the sensor, the cells were then fixed with 4% paraformaldehyde for 30 min, which has been shown to increase stiffness with minimal volumetric decrease[12,13].

3.2.4 Mechanical Model Dynamics

For this chapter, we consider the ratio of the amplitude of a cell-filled sensor to that of the empty (unloaded) sensor. The unloaded sensor is modeled as a one degree of freedom (1-DOF) system, while the loaded sensor is considered in two contrasting scenarios: with the cell being a point mass or a viscoelastic solid (figure 3.3A). As in previous works, we model the viscoelastic cell as a Kelvin-Voigt solid[14] and the entire system of the viscoelastic solid adhered to the sensor is modeled as a two degree of freedom (2-DOF) spring-mass-damper dynamic system. The 2DOF model of the resonant sensor system with attached Kelvin-Voigt solid can be described by the following equations of motion:

$$\begin{bmatrix} m_1 & 0 \\ 0 & m_2 \end{bmatrix} \begin{Bmatrix} \ddot{x}_1 \\ \ddot{x}_2 \end{Bmatrix} + \begin{bmatrix} c_1 + c_2 & -c_2 \\ -c_2 & c_2 \end{bmatrix} \begin{Bmatrix} \dot{x}_1 \\ \dot{x}_2 \end{Bmatrix} + \begin{bmatrix} k_1 + k_2 & -k_2 \\ -k_2 & k_2 \end{bmatrix} \begin{Bmatrix} x_1 \\ x_2 \end{Bmatrix} = \begin{Bmatrix} F_0 \\ 0 \end{Bmatrix} e^{i\omega t} \qquad (3.1)$$

For each sensor, the spring constant k_1 and resonant frequency ω_1 are measured, and together are used to calculate the mass of the sensor, $m_1 = k_1/\omega_1^2$. The coefficient of viscous damping for each sensor, c_1 is estimated to be approximately 9.5 x 10^{-6} N·s·m^{-1}.

3.2.5 Viscoelastic State Determination

The estimation of viscoelasticity was done by assessing the speed of propagation of the Elastic Wave shown in equation 3.2.

$$s \approx \sqrt{G/\rho}, \tag{3.2}$$

where s is the speed of propagation, G is the Shear Modulus, and ρ is the density. Assuming a Shear Modulus of 10^4 Pa (in media) and density of 10^3 kg/m^3 for cells in media, we can approximate the speed of propagation to be, $s \approx \sqrt{10^4/10^3}$, 3.1 m/s.

Next, we calculate the displacement of the sensor at resonance since the highest sensor displacement (oscillation) occurs there. From LDV operation, the displacement of the sensor can be determined from equation S3.

$$X_0 \approx \frac{V}{2\pi f}, \tag{3.3}$$

where X_0 is the displacement, f is the frequency of vibration (Hz), and V is the velocity of oscillation. From characterization of our sensors, the resonant frequency of the sensor in fluid is 40 kHz. The amplitude of vibration measured from our lock-in amplifier is 4 V. Finally, the velocity of vibration is determined from experimental parameters 0.02 m/s. Therefore, the displacement of the sensor would be 0.08 μm. It would then be possible to determine the time of wave propagation using equation 4.4.

$$t_p = \frac{X_0}{s}, \tag{3.4}$$

where the time of wave propagation would be 0.0258 μs. Finally, we can compare the time of wave propagation, t_p, and the time of deformation at resonance, t_d (25 μs). Thus, since we can determine that wavelength, λ is proportional to time, t and $t_p << t_d$, therefore, $\lambda_p < \lambda_d$, which indicates that our sensor operation is operating in case (ii) – dominant force of vibration is viscoelastic.

3.2.6 System Linearization and Sensitivity Analysis

In order to check that our measurement lies in a linear regime of vibration, we observed several input (drive voltage) values to output our amplitude ratio (system gain) values to obtain a highly

linear relationship. Figure 3.2 (Left) shows the input-output relationship confirming that the sensor vibrates within a linear regime as described by the R^2 value of the linear regression model. Consequently, 200 amplitude measurements were taken to characterize the sensitivity and observed that a sensitivity of 1% of mean measurement taken. Again, this is shown on the Figure 3.2 (Right)

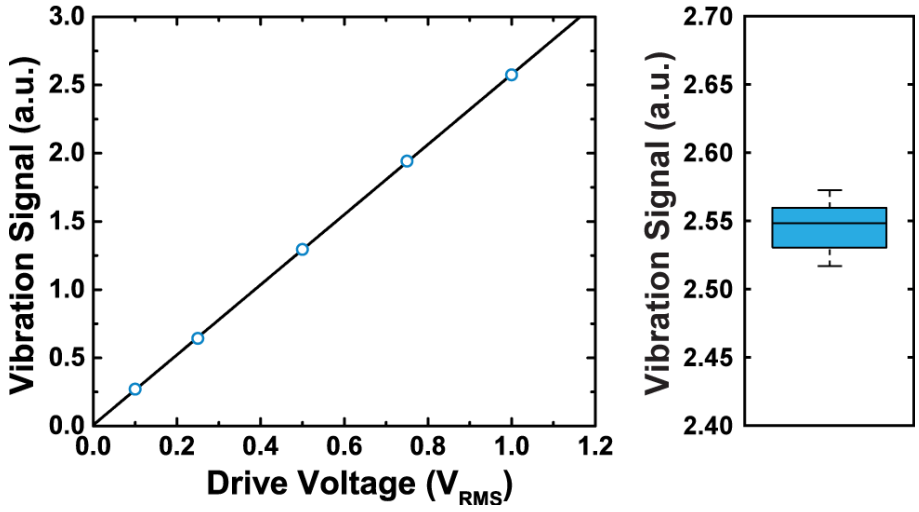

Fig 3:2 Linearity and Sensitivity Characterization of sensor and system showing input-output relationship.

3.3 Results and Discussion

Figure 3.1A shows a schematic of a single cell vibrating on the sensor where we compare the driving amplitude of the sensor to the amplitude response of the sensor loaded with a cell. In this case the cell is presented as a Kelvin-Voigt viscoelastic solid, where the material behavior is considered as that of a spring and damper in parallel. To elucidate the effect of the viscoelasticity of the cell on the amplitude, the ratio of the apparent amplitude (2-DOF) to the applied amplitude (1-DOF) was calculated over a wide range of elastic moduli and viscosities of cells (figure 3.3B). The shape of the model clearly shows that the viscoelastic parameters affect the amplitude ratio, with areas of very strong effects, similar to the frequency response previously investigated[11,15,16]. We illustrate this effect in figure 3.3C by simulating the response across the frequency spectrum

for both low and high viscoelastic mass loaded sensors. The inset of figure 3.3C more clearly portrays the drop in amplitude with changing viscoelastic parameters as compared with an empty sensor, where the amplitude decrease of the low viscoelastic case is much larger with respect to the reference, than the high viscoelastic case.

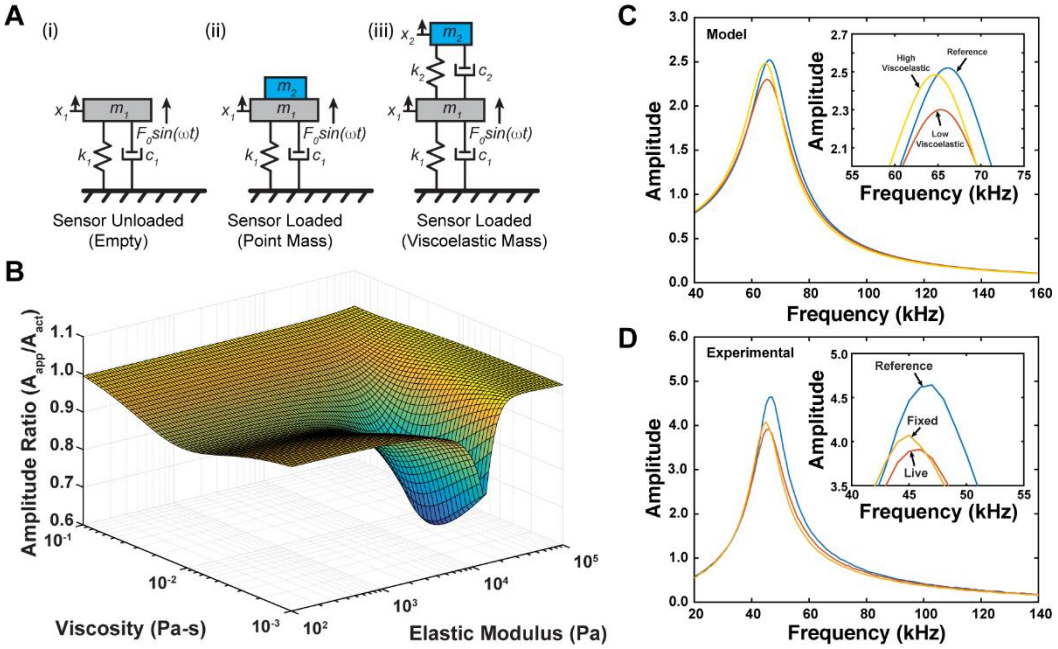

Fig 3:3(A) Schematics of a Kelvin-Voigt viscoelastic solid model system (i) a 1DOF representing the model of an unloaded sensor (ii) a 2-DOF dynamical sensor-cell model demonstrating a conventional mass-spring-damper system and (iii) an improved mass-spring-damper 2-DOF system used to obtain the vibrational amplitude and frequency from experimental data. (B) A three-dimensional surface plot depicting how cell viscoelasticity (elastic modulus and viscosity) affect amplitude ratio (amplitude ratio is apparent amplitude divided by actual amplitude). (C-D) Frequency spectra of the viscoelastic response of a (C) model viscoelastic solid and (D) HT-29 cell; Insets: highlights the shift in amplitude.

Figure 3.4A shows the amplitude ratio comparison between both live and fixed values of all cells investigated in this study (n = 16). There is a consistent increase in the amplitude ratio of the fixed cell compared to the live cell. Again, the amplitude ratio for both live and fixed cells is defined as the amplitude of a cell-loaded sensor (live or fixed) to the amplitude of a reference (empty) sensor. We further illustrate the amplitude differences for each cell by plotting the live amplitude ratio against the fixed amplitude ratio (figure 3.4B) and comparing to a slope of unity (dotted line). The

inset of figure 3.4B shows a histogram of the difference of the live and fixed ratios for each cell and a normal distribution fit (dotted line) to the data, compared to a normal distribution centered at zero. A paired t-test confirmed the significance of the observed differences before and after fixation (p-value < 0.0001). Paraformaldehyde is known to increase the stiffness of a cell and, through measurements with AFM, fixed cells exhibit greater viscous behavior[15]. Our experimental findings of increased amplitude with fixation agree with this known increase in cell viscoelasticity.

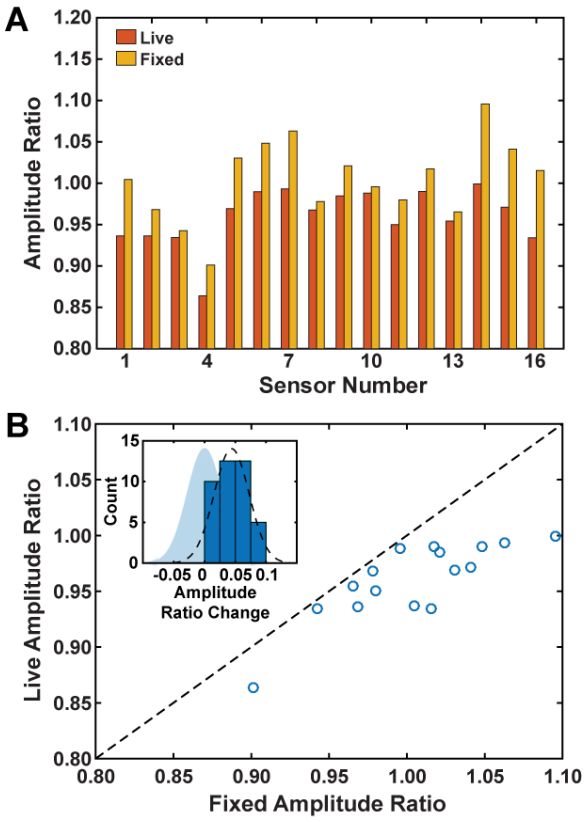

Fig 3:4 Experimental results: (A) Bar chart showing an amplitude ratio comparison between both live and fixed values of the same cells (B) A dotted line of unity slope comparing the plot of live amplitude against fixed amplitude ratios shows a significant difference between the ratio before and after fixation. The inset shows a histogram of the difference of the live and fixed ratios for each cell. A normal distribution (dotted line) is fitted to this data and compared to a standard normal distribution.

An additional and complementary viscoelastic effect on the device resonance behavior is the shifting of resonant frequency due to the cell oscillating out of phase with the sensor platform[11,15-17]. The frequency response with respect to viscoelastic parameters produces a similar yet distinct analytical model shape over a range of elastic moduli and viscosities compared to the amplitude response. Both amplitude and frequency models contain many solutions to any given measurement, and strategies need to be devised to restrict these solution spaces. In the past, we achieved this by using a range of hydrogel concentrations and assuming a model relationship[16], or relied on a population measurement with several different cell sizes[15]. Both approaches require many measurements to approach a solution. However, combining both amplitude and frequency measurements narrows the solutions for individual cells based on the overlapping regions from each measurement.

Figure 3.5 shows the entire solution space regarding possible viscoelastic properties of cells that could lead to the observed data. To create these plots, we took the measured amplitude and frequency data, calculated the mean and standard deviation, and created probability maps for each expected point based on a normal distribution. The resulting solution sets for both the amplitude space and frequency spaces are presented in figures 3.5A and 3.5B, respectively. The amplitude solutions exist in two distinct regions – one that encompasses low viscoelastic properties and one that includes much stiffer and more viscous materials. Similar behavior occurs from the frequency shift model, but the possible solutions only exist in a single, low viscoelastic region. We multiplied the two probabilities to determine the common solution space in figure 3.5C. Through the use of both measurements we deduce that the viscoelasticity of the cells resides within this area, which agrees well with previous results[18]. The maximum probability of this solution states that the elasticity and viscosity values are 100 Pa and 0.0031 Pa-s, respectively, at the frequency of

measurement.

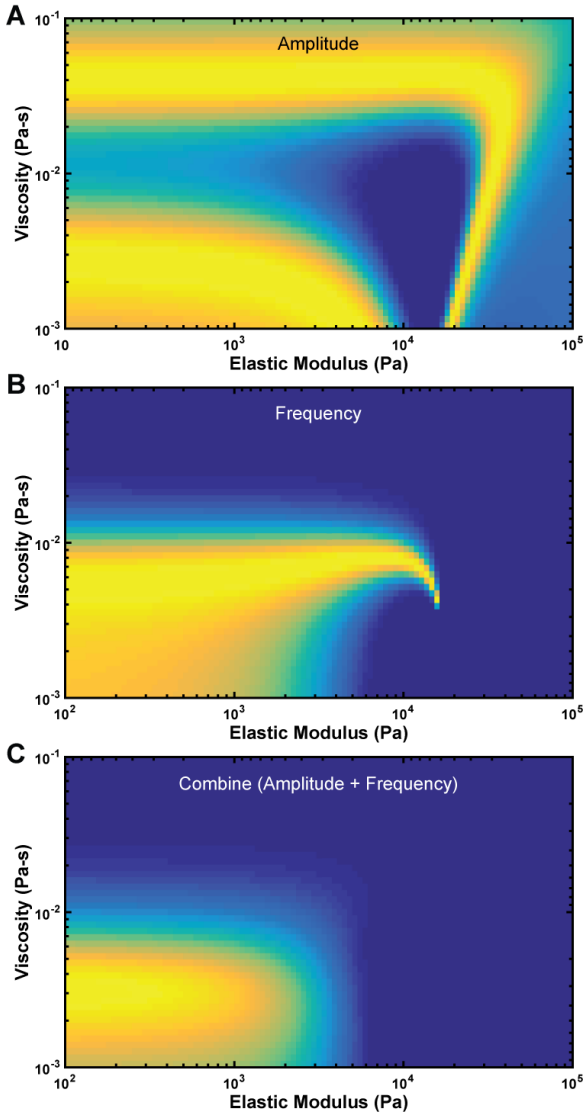

Fig 3:5 Potential real solution space (yellow) of viscoelasticity of cells obtained from a normal distribution of observed data (A) two distinct regions (yellow) of amplitude solution space (B) frequency-shift solution space. (C) Resulting overlapping region of amplitude and frequency-shift solution spaces. The estimated elastic modulus and viscosity from the cell population density is 100 Pa and 0.0031 Pa-s, respectively.

3.4 Conclusion

This work provides a non-destructive method for measuring the viscoelastic properties of cells; however, there are some considerations for future work. Here, we utilized the known size and shape of these cells, in combination with the dark field cross-sectional area of the cell captured

during measurement, to estimate each cell size based on previous work relating dark field area to confocal volume[11]. This estimation could be improved by incorporating advanced optical imaging capabilities into the LDV system to simultaneously determine the volume, amplitude, and frequency data. Also, the nature of the substrate affects how a cell organizes its cytoskeleton, which in turn influences the effective cell stiffness. The viscoelastic property measurements in this work are limited by the base substrate of the sensor material with a thin surface layer of collagen. Future studies capable of manipulating substrate rigidity, such as deposition of micropatterned hydrogels[16,19], could explore the spectrum of cell biomechanics and substrate dependence.

In previous work, we have used the same platform to make measurements of cell mechanics in a similar fashion[15]. However, in those works, we only took advantage of the resonant frequency shift that occurs from material viscoelasticity, while in this current work we explored the vibration amplitude dependence on viscoelasticity. This approach is advantageous because it better decouples the material mass from the viscoelastic properties. In this respect, the use of the two independent and complementary measurements can generate more accurate estimates of cell properties from the resonant sensors. In future chapters (4-5) we incorporate all of these measurements into cell growth experiments with the resonant sensors for real-time measurement of mass and stiffness over time.

3.5 References

1) Kuznetsova, T. G., Starodubtseva, M. N., Yegorenkov, N. I., Chizhik, S. A. & Zhdanov, R. I. Atomic force microscopy probing of cell elasticity. *Micron* 38, 824–833 (2007).
2) Cross, S. E., Jin, Y.-S., Rao, J. & Gimzewski, J. K. Nanomechanical analysis of cells from cancer patients. *Nature Nano* 2, 780–783 (2007).
3) Plodinec, M. *et al.* The nanomechanical signature of breast cancer. *Nature Nano* 7, 757–765 (2012).
4) Wang, N., Butler, J. P. & Ingber, D. E. Mechanotransduction across the cell surface and through the cytoskeleton. *Science* 260, 1124–1127 (1993).
5) Hochmuth, R. M. Micropipette aspiration of living cells. *J Biomech* 33, 15–22 (2000).
6) Sato, M., Ohshima, N. & Nerem, R. M. Viscoelastic properties of cultured porcine aortic endothelial cells exposed to shear stress. *J Biomech* 29, 461–467 (1996).
7) E Evans, A. Y. Apparent viscosity and cortical tension of blood granulocytes determined by micropipet aspiration. *Biophys J* 56, 151–160 (1989).
8) Park, K., Mehrnezhad, A., Corbin, E. A. & Bashir, R. Optomechanical measurement of the stiffness of single adherent cells. *Lab Chip* 15, 3460–3464 (2015).
9) Li, J., Thielemann, C., Reuning, U. & Johannsmann, D. Monitoring of integrin-mediated adhesion of human ovarian cancer cells to model protein surfaces by quartz crystal resonators: evaluation in the impedance analysis mode. *Biosens Bioelectron* 20, 1333–1340 (2005).
10) Corbin, E. A., Park, K. & King, W. P. Room-temperature temperature sensitivity and resolution of doped-silicon microcantilevers. 94, 243503 (2009).
11) Park, K. *et al.* Measurement of adherent cell mass and growth. *P Natl Acad Sci Usa* 107, 20691–20696 (2010).
12) Braet, F., Rotsch, C., Wisse, E. & Radmacher, M. Comparison of fixed and living liver endothelial cells by atomic force microscopy. *Appl Phys A-Mater* 66, S575–S578 (1998).
13) Hutter, J. *et al.* Atomic force microscopy investigation of the dependence of cellular elastic moduli on glutaraldehyde fixation. *J Microsc-Oxford* 219, 61–68 (2005).
14) Fung, Y.-C. *Biomechanics: Mechanical Properties of Living Tissues*. (Springer-Verlag, 1981).
15) Corbin, E. A., Kong, F., Lim, C. T., King, W. P. & Bashir, R. Biophysical properties of human breast cancer cells measured using silicon MEMS resonators and atomic force microscopy. *Lab Chip* 15, 839–847 (2015).
16) Corbin, E. A. *et al.* Micromechanical properties of hydrogels measured with MEMS resonant sensors. *Biomed Microdevices* 15, 311–319 (2013).
17) Corbin, E. A., Millet, L. J., Keller, K. R., King, W. P. & Bashir, R. Measuring physical properties of neuronal and glial cells with resonant microsensors. *Anal. Chem.* 86, 4864–4872 (2014).
18) Abdolahad, M., Mohajerzadeh, S., Janmaleki, M., Taghinejad, H. & Taghinejad, M. Evaluation of the shear force of single cancer cells by vertically aligned carbon nanotubes suitable for metastasis diagnosis. *Integr. Biol.* 5, 535–8 (2013).
19) Corbin, E. A., Dorvel, B. R., Millet, L. J., King, W. P. & Bashir, R. Micro-patterning of mammalian cells on suspended MEMS resonant sensors for long-term growth measurements. *Lab Chip* 14, 1401–1404 (2014).
20) Corbin, E.A., Adeniba, O.O., Ewoldt, R.H., & Bashir, R. Appl Phys Lett 108, (2016).

Chapter 4 : Optomechanical Microrheology of Single Adherent Cancer Cells

It has been established that there is a close relationship between the mechanical properties of cells and their physiological function. Non-invasive measurements of the physical properties of cells, especially of adherent cells, are challenging to perform. Through a non-contact optical interferometric technique, we measure and combine the phase, amplitude, and frequency of vibrating silicon pedestal micromechanical (MEMS) resonant sensors to quantify the 'loss tangent' of individual adherent human colon cancer cells (HT-29). The loss tangent, a dimensionless ratio of viscoelastic energy loss and energy storage – a measure of the viscoelasticity of soft materials, obtained through an optical path length (OPL) model, was found to be 1.88 ± 0.08 for live cells and 4.32 ± 0.13 for fixed cells; revealing significant changes ($p < 0.001$) in mechanical properties associated with estimated nanoscale cell membrane fluctuations of 2.87 ± 0.1 nm for live cells and 3.86 ± 0.2 nm for fixed cells. By combining these values with a corresponding two-degree-of-freedom (2-DOF) Kelvin-Voigt model, we extract the elastic stiffness and viscous loss associated with each individual cell rather than estimations from a population. The technique is unique as it decouples the heterogeneity of individual cells in our population and further refines the viscoelastic solution space. The results presented in this chapter are based on our published work in *APL Bioengineering*[34].

4.1 Introduction

The mechanical response of soft materials is generally reported as the frequency-dependent viscoelastic behavior determined using rheological techniques. However, performing rheology on living cells is particularly challenging due to invasiveness of applied forces and choosing appropriate time-dependent loading conditions to probe viscous material properties[1]. Recently, it

has been shown that mechanical properties of cells are directly correlated with biological processes, such as in cancer[2-4] and blood diseases[5,6]. For example, normal cells are known to be stiffer than their cancerous counterparts. In practice, these mechanical biomarkers have the potential to contribute to early detection and diagnostic techniques.

In the past few years, there has been a variety of experimental techniques and models to measure and describe the rheological behavior of cells and tissue under different physiological conditions. These quantitative experimental techniques can be broken into two main categories: passive and active. Passive techniques involve the measurement of thermal fluctuations of embedded particles[7]. Approaches for active microrheology generally involve the application of a local force and the measurement of material response. Some of these prominent techniques for active microrheology measurement include atomic force microscopy[8], cell poking[9], shear flow cytometry[10], microplates[11-13], optical tweezers[14-16], optical stretchers[17,18], magnetic tweezers[19,20], and optomechanical techniques[21]. These techniques probe the behavior of cells at different length scales and timescales and employ different stress-strain magnitude and behaviors.

In this paper, we present a technique for measuring the viscoelastic properties of individual adherent cells using a microresonator sensor. This technique simply combines the simultaneous measurement of resonant frequency shift[22], amplitude change[23], and mechanical driven optical path phase[21] within a cell using a microresonator to more uniquely determine the viscoelastic properties of a single cell without requiring averaging over a population of cells. This overcomes limitations of our previous techniques that depended on additional measurements of average cell height, reference measurements, and other ensemble average cell group measurements. Here, we

measure the loss tangent of adherent colon cancer (HT-29) cells, a descriptor of the relative viscoelastic properties of a cell. Using this technique, we are also able to quantify the nanoscale membrane fluctuations of individual live HT-29 cells and their stiffer fixed counterparts.

4.2 Materials and Methods

4.2.1 Measurement Scheme: Combining Frequency, Amplitude and Phase Shift

As shown in Figure 4.1a, the technique to extract loss tangent of individual cells involves measuring the frequency (f), amplitude (A), and optical phase shift ($\Delta\phi$) in four distinct schemes. First, measuring the response of a dry (unloaded) sensor and unloaded wet sensor (in-media) to determine the baseline resonant frequency and amplitude. Second, a live cell is loaded on the sensor and then the frequency and amplitude shifts are then measured, along with optical path length (OPL) variations between laser paths inside and outside the cell. The laser path length will change due to height oscillations of the cell during vibration, resulting in a phase shift[3,23-25]. Figure 4.1b-c shows SEM images of our MEMS resonant sensor structure that are electromagnetically actuated to produce vertical motion in the first resonance mode. Details of the resonant sensors and experimental setup used in this study are described elsewhere[25]. The viscoelastic effect of HT-29 cells on the resonant frequency and amplitude of the sensor were previously quantified to generate a large space of potential solutions[23].

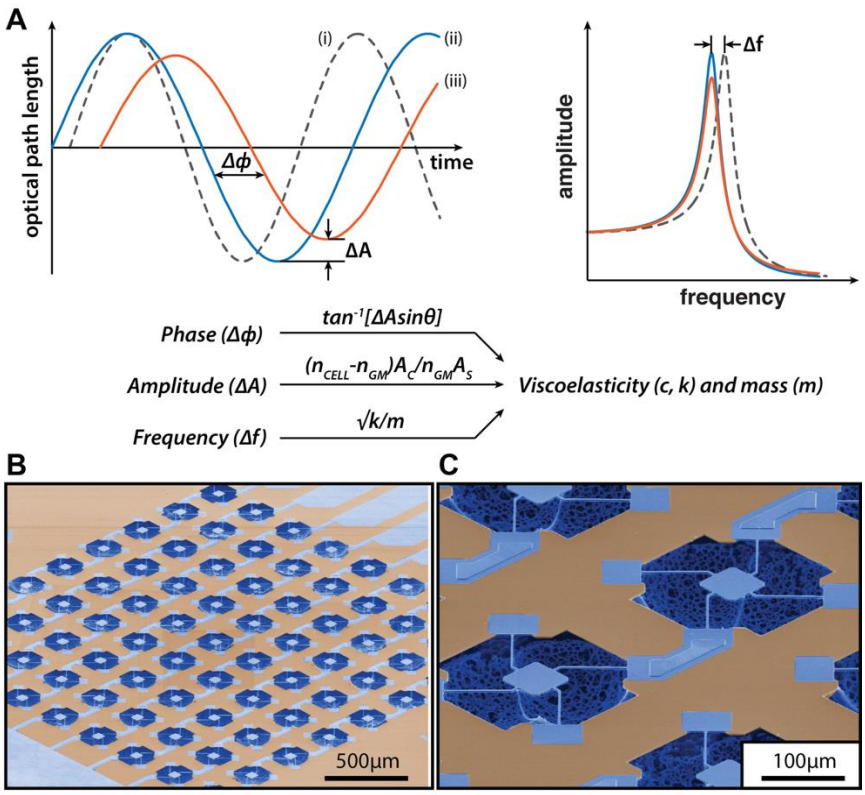

Fig 4:1 Overview of measurement scheme. (a) Top Left: Plot showing the optical path length, OPL(t) as a function of the apparent phase shift and apparent amplitude increase and time: (i) for a dry-unloaded reference sensor (dotted line), (ii) an outside-cell loaded sensor (blue) (and/or an unloaded wet sensor – for frequency measurement) (iii) an inside-cell loaded sensor (red). Phase shift ($\Delta\phi$) varies for loaded sensor outside and inside cell. Top right: Spectra showing frequency shift and amplitude change measurement due to dry unloaded and wet unloaded reference (dotted and blue lines) and loaded sensors (red). Bottom: Summary of how the phase shift ($\Delta\phi$), amplitude ratio, (ΔA), and frequency shift (Δf) relate to the viscoelastic properties and mass of the cell. (b) SEM Image showing 9 x 9 array of pedestal sensors. (c) SEM Image showing a close-view layout of individual 60 x 60 μm^2 sensors.

4.2.2 Optical Path Length (OPL) Model

The current study takes a step further by focusing on combining the complementary optical path phase-shift and membrane fluctuation measurements to improve the stiffness and viscous dissipation solution space. As was previously established, a Laser Doppler Vibrometer (LDV) can measure a time-derivative of the OPL and therefore can determine the membrane oscillation of the cell[21,26]. Figure 4.2a is a schematic overview of the resonant measurement method and represented variables in equations (1-3).

$$\boldsymbol{OPL}(t) = \sum n_i d_i(t) = \mathrm{n_{GM}} * (\mathrm{P}_{sensor}(\mathrm{t}) - h(\mathrm{t})) + \mathrm{n}_{cell} * h(t)$$
$$\approx \mathrm{n_{GM}As} * (1 + \Delta\mathrm{A}) * \sin(\omega\mathrm{t} + \Delta\phi) + \mathrm{const.} \quad (1)$$

$$\Delta A = \left[\frac{(\mathrm{n}_{cell} - \mathrm{n_{GM}})}{\mathrm{n_{GM}}} * \frac{\mathrm{Ac}}{\mathrm{As}}\right] \quad (2)$$

$$\Delta\phi = \arctan\left[\frac{(\mathrm{n}_{cell} - \mathrm{n_{GM}})}{\mathrm{n_{GM}}} * \frac{\mathrm{Ac}}{\mathrm{As}} * sin(\theta)\right] \quad (3)$$

where, n_{cell} represents the refractive index of the cell, n_{GM} represents the refractive index of the media, A_c represents the amplitude of the cell height oscillation with respect to cell initial height also denoted as the cell membrane fluctuation (amplitude), A_s represents the amplitude of the sensor oscillation, θ represents the phase of the cell height oscillation with respect to the sensor, ω represents the oscillating resonant frequency, $\Delta\phi$ is our measured maximum phase shift of the OPL. $P_{sensor}(t)$ and $h(t)$ are the instantaneous sensor position and cell height.

4.2.3 Membrane Fluctuation Determination: Analytical Estimation and Simulation

We can uniquely compute the individual cell membrane fluctuation at resonance, A_c for one cell per sensor, which overcomes the initial bulk estimate limitation. This is calculated via equation (2) by estimating A_s =180pm (from measured velocity and oscillating frequency) for a 35nN excitatory input in media, n_{GM} = 1.35, and n_{cell} = 1.38 and 1.55 for live and fixed cells, respectively[21]. To better understand how the changes in cell membrane fluctuations occur, we modeled our sensor-cell system as a 2-DOF suspended mass model where the cell mass (m_2) is considered a Kelvin-Voigt viscoelastic solid with elastic stiffness (k_2) and viscous coefficient (c_2) connected to the sensor, and the sensor mass (m_1) is connected to the fixed substrate by a second Kelvin-Voigt spring-damper (k_1, c_1). The model assumes an oscillatory force $F(t)$ applied to the sensor mass. Figure 4.2b illustrates the effect of both high and low viscoelastic cell mass (m_2) loaded sensors on the membrane fluctuations by simulating the time-dependent transient and steady state dynamic responses at a representative resonant frequency (ω) of our sensors. In these

simulations, the ratio, $\frac{c_2}{k_2}$ is held constant and the stiffness/dissipation pair (k_2, c_2) is scaled for cases of high and low viscoelasticity. These simulations depend on a few required assumptions that the cell membrane is homogeneous and smooth as well as the average cell-surface oscillation is calculated at the steady state.

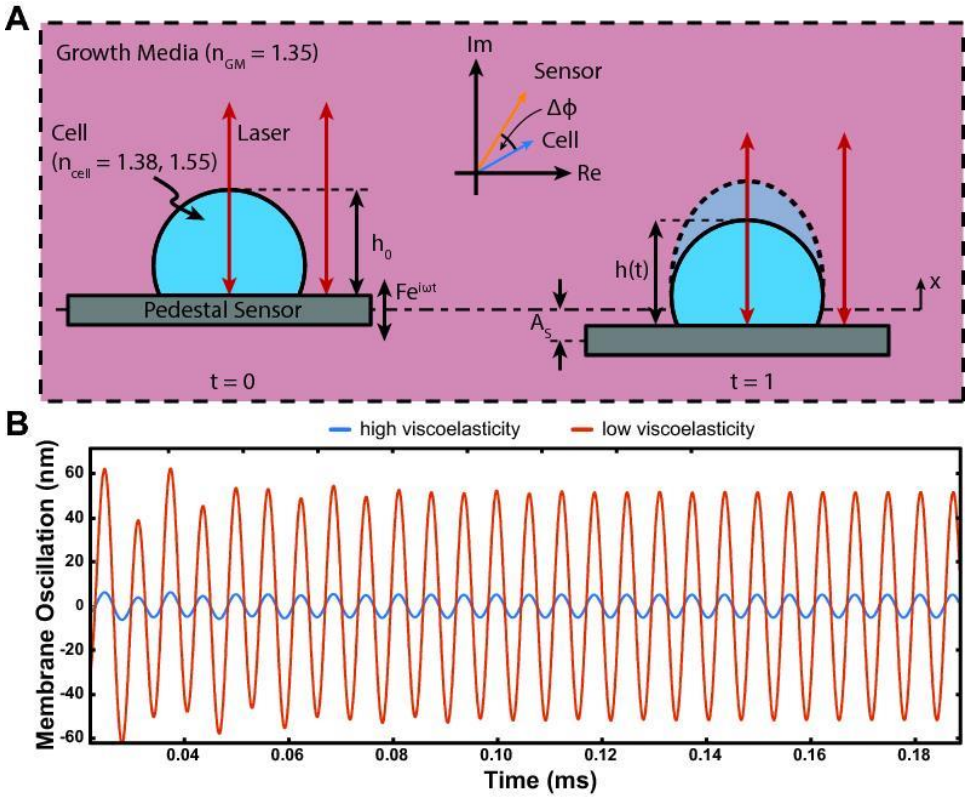

Fig 4:2 (a) Schematic depicting two time steps of the applied stimuli ($Fe^{j\omega t}$). Left: Pedestal sensor supporting cell with static height, h_0 and a refractive index, n_{cell}. Right: Showing the instantaneous cell height oscillation with respect to the sensor, $h(t) = h_0 + A_C\ sin(\omega t + \theta_c)$; A_C denotes the amplitude of the cell height with respect to the static height, h_0 (membrane fluctuation), θ_c denotes the phase difference between cell height oscillation with respect to the applied force and A_s represents the amplitude of the sensor oscillation at resonance frequency, ω. Shift ($\Delta\phi$) indicates the observed optical phase shift between two light paths, one through the cell and the other directly on the sensor (red lines with arrows). (b) Shows a simulation of both transient and steady state membrane fluctuations of a cell with high and low viscoelasticity, i.e. the ratio, $\frac{c_2}{k_2}$ is held constant while the viscoelastic coefficients (c_2 k_2) are scaled for high and low viscoelasticity.

4.2.4 Data Analysis and Cell Culture

We combined interferometric techniques to measure the viscoelasticity of both live and fixed individual HT-29 cells. Cells were cultured and fixed on resonant sensors as described in previous

work[25]. To fully investigate the mechanical response of live cells compared with fixed cells, we started with the data collection of the necessary established methods, including amplitude ratios[23], phase shift[21], and frequency shift[25], to ultimately convey a meaningful rheological translation.

The experimental parameters based on the LDV measurements are related to mechanical quantities as given in equations (2) - (3). Knowing the mechanical amplitude ratio and phase shift between the cell and sensor oscillations and calibrating sensor mass, stiffness, and dissipation allows us to extract cell viscoelastic properties at their probe resonant frequencies.

4.2.5 Estimation of Viscoelastic Coefficients, (k2, c2)

The mechanical phase difference (θ) is related to cell viscoelastic properties that we extract by considering the full 2-DOF suspended mass system. To estimate the viscoelastic coefficients (k_2, c_2), our microresonator is modeled as a 2-DOF Kevin-Voigt model as described in equation (4) in simplified matrix form.

$$\begin{bmatrix} (k_1 + k_2 - m_1\omega^2) + (c_1 + c_2)\omega j & -k_2 - c_2\omega j \\ -k_2 - c_2\omega j & (k_2 - m_2\omega^2) + c_2\omega j \end{bmatrix} \begin{Bmatrix} \boldsymbol{A_s} \\ \boldsymbol{A_c} \end{Bmatrix} e^{j\omega t} = \begin{Bmatrix} F \\ 0 \end{Bmatrix} e^{j\omega t}; \quad (4)$$

Note that the physical quantities of interest are found by taking the imaginary components, e.g. $F(t) = F\sin\omega t = \mathrm{I_m}\{Fe^{j\omega t}\}$; where $\boldsymbol{A_s} = A_s^R + jA_s^I$ and $\boldsymbol{A_c} = A_s^R + jA_c^I$ are the vector amplitudes of the sensor and cell states x_{sensor} and x_{cell} respectively, and $Fe^{j\omega t}$ is the input force. Equation (4) is further decomposed as the instantaneous sensor and cell responses in equation (5).

$$x_{sensor}(t) = |\boldsymbol{A_s}|\sin(\omega t + \theta_s) \quad (5a)$$

$$x_{cell}(t) = |\boldsymbol{A_c}|\sin(\omega t + \theta_c) \quad (5b)$$

where $\theta_s = \tan^{-1}\left\{{(A_s^I)}/{(A_s^R)}\right\}$ and $\theta_c = \tan^{-1}\left\{{(A_c^I)}/{(A_c^R)}\right\}$. Here, θ_s and θ_c denote the phase differences between the sensor and cell height oscillation with respect to the excitatory force, $F(t) = F\sin\omega t$. Our modeled cell-sensor phase difference,

$$\theta = \theta_c - \theta_s \quad (6)$$

and modeled cell-sensor amplitude ratio becomes:

$$\Delta A = \frac{(n_{cell} - n_{GM})}{n_{GM}} \frac{|A_c|}{|A_s|} \quad (7)$$

Observed amplitude ratio (ΔA) and mechanical phase shift (θ) inferred from equation (2) are substituted to simultaneously solve equations (6) and (7) for k_2 and c_2.

4.2.6 Loss Tangent Estimation: Using Area-to-Height

The loss tangent, $tan(\delta)$,[27,28] is a dimensionless parameter that measures the ratio of energy dissipated to energy stored and can be used as a viscoelasticity indicator of our probed cell. It is totally independent of the mass of each cell and is different from our estimated cell-sensor mechanical phase shift (θ), which largely depends on our three parameters, frequency (f), amplitude ratio (ΔA) and optical phase shift ($\Delta\phi$). Furthermore, loss tangent, $tan(\delta) = \frac{c_2\omega}{k_2}$, does not assume any cell geometry. However, the viscoelastic coefficients (k_2, c_2) can be related to the apparent inherent viscoelastic moduli (E, μ) by $k_2 = \frac{EA}{H}$ and $c_2 = \frac{\mu A}{H}$. Ratio $\frac{A}{H}$ denotes the area-to-height information of each cell where the average cell area is 250μm^2 with an estimated cell height of 8μm.

4.3 Results and Discussions

Figure 4.3a depicts an increase in membrane fluctuation amplitude of the live cells relative to fixed cells for individual cells at the resonant frequency of each respective sensor. Qualitatively, this indicates the live cells are more compliant (softer). To quantitatively illustrate this trend, we fit a normal distribution to our membrane fluctuation data and compare as shown in Figure 4.3b. Live values of membrane fluctuations show a narrower distribution with a mean and standard deviation of 2.87 $\pm$ 0.1 nm compared to fixed cells with 3.86 $\pm$ 0.2 nm. A paired t-test value of

($p < 0.001$) further confirmed the statistically high significance of the observed fluctuation decrease after fixation. These experimental findings agree well with previous studies on the increase in cell stiffness and viscosity after fixation[3]. Other cell vibration and membrane fluctuation measurements on red blood cells[29-31] show significantly higher amplitude values; however, this difference in amplitude can be attributed to reasons of integrin-induced tension[32] in adherent cancer cells[31]. In addition, resonant sensors in other methods were more compliant (0.01 – 0.05 N/m) as compared to our resonant sensors (~19.4 N/m), thus supporting larger deflections of the sensor and cell membrane[33].

The amplitude ratio is another key variable in determining the individual cell loss tangent. Figure 4.3 is a plot of observed amplitude ratio (ΔA) of live and fixed cells, where there is an increase in the amplitude ratio for the fixed cells over live cells, matching well with previous studies[23]. A higher amplitude ratio for fixed cells implies that a relative increase in the refractive index (and viscoelasticity) exceeds the relative change in the actual cell-to-sensor amplitude ratio. We can further exemplify the amplitude change for each cell by plotting the live amplitude ratio against the fixed amplitude ratio (Figure 4.3d) and comparing with a slope of unity (dotted line). Figure 4.3e shows a comparative difference between the loss tangent of live and fixed cells at resonance (~32.0 kHz and ~31.8 kHz, respectively), where values above unity indicate a more dissipative, viscous-like state and values below unity indicate elastic-like state shown graphically in figure 4.3f. Our observed data shows that all cells tend toward a more viscous state with a bias for fixed cells being more viscous than live cells. Fixed cells show an increase in the loss tangent over live cells indicating that fixed cells exhibit more energy dissipation (viscous) ($tan(\delta) > 1$) than energy stored (elastic) within the resonant frequency regime. The average loss tangent values for

live and fixed cells are 1.876 ± 0.075 and 4.316 ± 0.126, respectively.

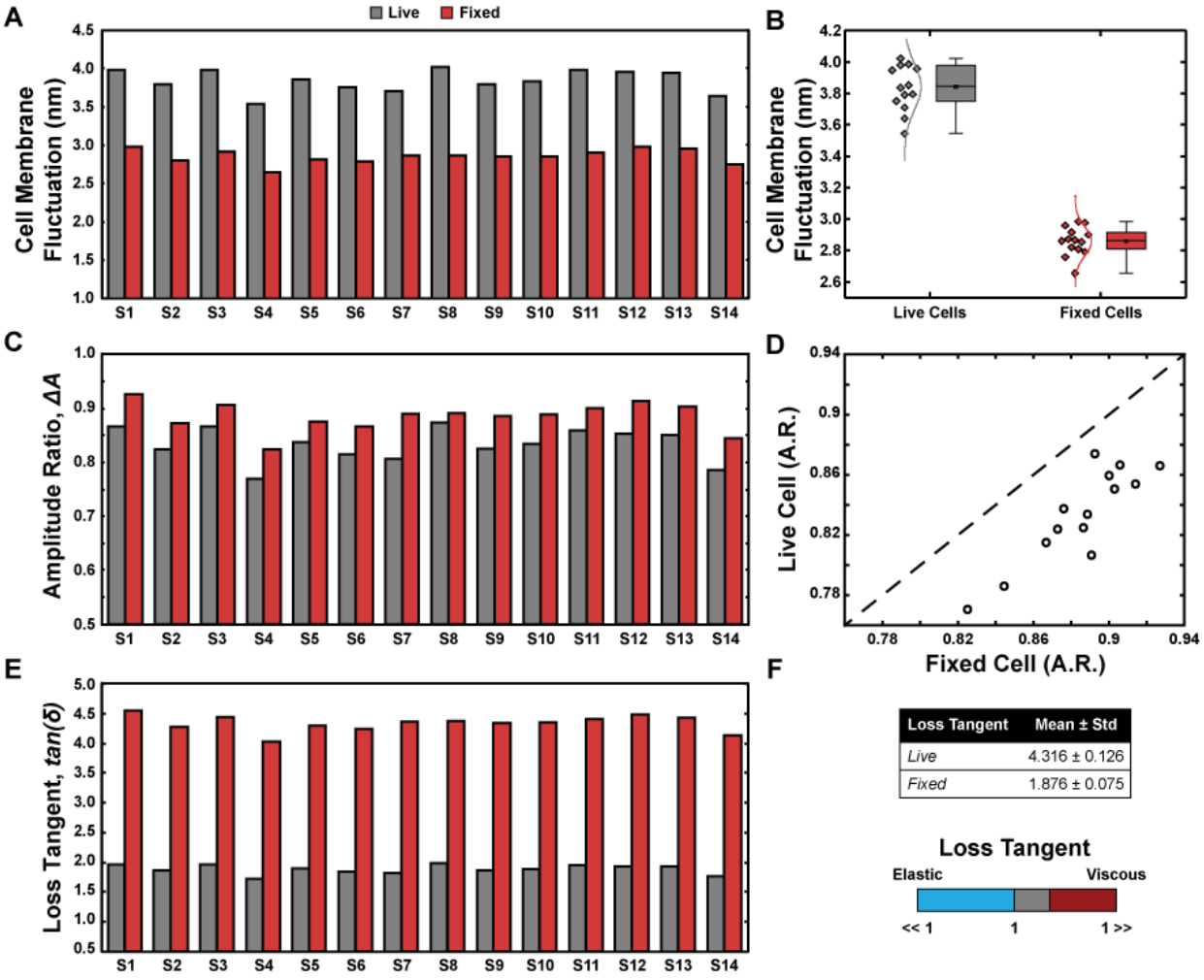

Fig 4:3 (a) Cell Membrane fluctuations (height oscillation), A_c *of 14 live and fixed cells validating 2DOF Kevin-Voigt simulation. (b) Boxplot providing a summary of the spread of membrane fluctuation,* A_c*. (c) Experimental amplitude ratios for live and fixed cells. A higher amplitude ratio implies that a relative increase in the refractive index (and viscoelasticity) exceeds the relative change in the actual cell-sensor amplitude ratio. (d) The dotted line of unity slope comparing the plot of live amplitude against fixed amplitude ratios shows a significant difference between the ratio before and after fixation. (e) Estimated loss tangent,* $an(\delta) = \frac{c_2\omega}{k_2}$*, , a relative viscoelastic descriptor for live and fixed cells at their individual sensor resonant frequencies,* ω*. (f) Scale bar from Elastic to Viscous showing where both live and fixed cells fall on the range of values.*

While a large loss tangent identifies a more viscous (or fluid-like) behavior, it does not automatically mean the stiffness of the cell is low, rather it means that viscosity dominates over elasticity within our regime of vibration. Our derived tensile storage and loss moduli solution pair ($E' = \frac{k_2 H}{A}, E'' = \frac{c_2 H}{A}\omega$) is used to extract the apparent elasticity (E) and viscosity (μ) for

each cell as shown in figure 4.4; where $E' \equiv E$ and $E'' = \mu\omega$

Figure 4.4 compiles the result of our rheological investigation for the 14 different cells. The loss tangent, $tan(\delta)$, does not assume a particular cell – sensor geometry. Thus, it is independent of the sensor material property, and the details of contact mechanics providing a quantitative measure of the overall rheological behavior of the sample. Figure 4.4a (i-ii) shows that there is no correlation between the loss tangent and the apparent mass for (i) live and (ii) fixed cells (R^2 = 0.232 and 0.083, respectively) to further demonstrate that cell viscosity (c_2) also affects the dynamics of the system, in addition to cell elastic stiffness (k_2). For consistency, we measured the fixed cell mass values (frequency shift) and compared with the same cells before fixation.

The computed apparent elasticity (storage modulus) and viscosity is shown in Figures 4.4b-c. Live cells showed lower elasticity of 259 $\pm$ 44 Pa, whereas fixed cells showed higher elasticity of 712 $\pm$ 40 Pa. The apparent viscosity values showed a similar trend to elasticity with low viscosity values for live cells at 2.4 $\pm$ 0.3 mPa.s and high viscosity values for fixed cells at 15.4 $\pm$ 0.4 mPa.s. These viscosity estimates which describe the energy loss comprise the inherent viscosity of cells and surrounding solvent and can be broken apart further for different media conditions. The errors bars in Figures 4.4b-c are incurred through optical imaging (area-height ratio estimation), frequency, and loss tangent uncertainties propagation. These findings are consistent with previous studies showing an increase in cell stiffness and viscosity after fixation[3].

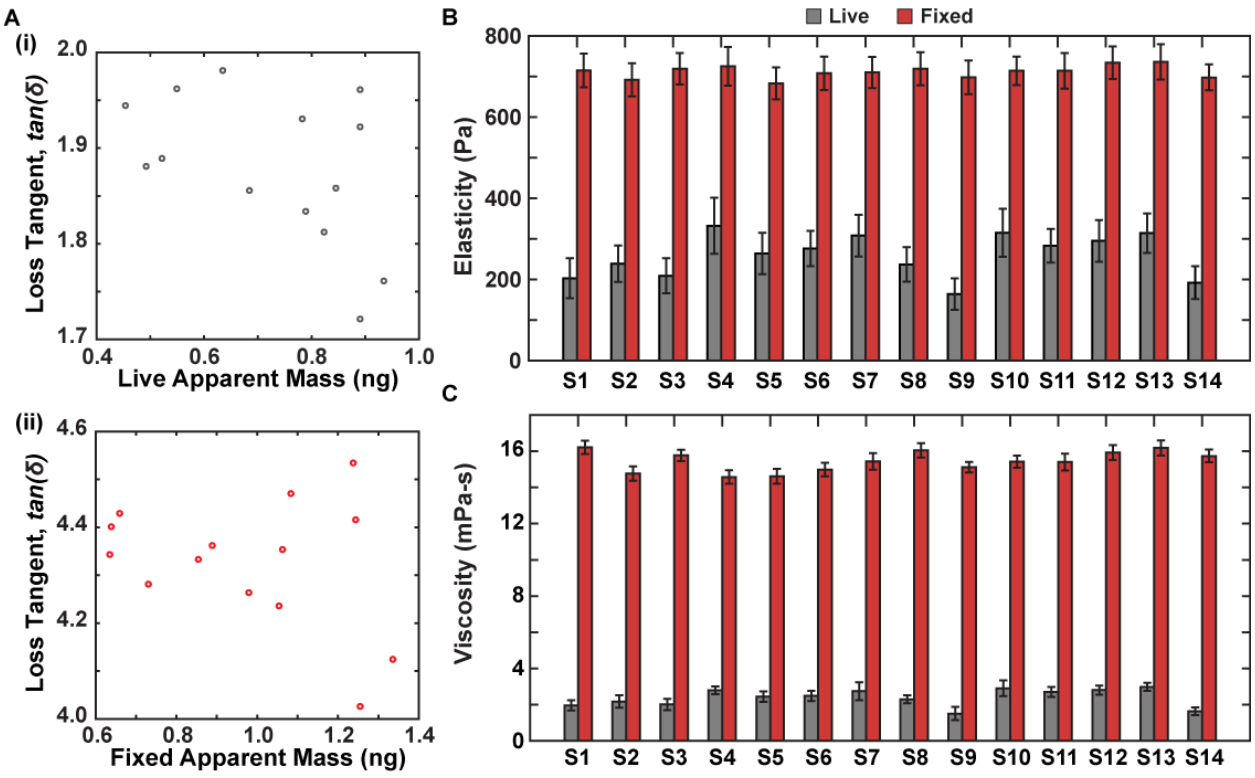

Fig 4:4 (a) (i-ii) Plots depicting the lack of correlation between the loss tangent $(tan(\delta) = \frac{c_2\omega}{k_2})$ *and the apparent mass of both live and fixed cells further proving that apart from the cell elastic stiffness* (k_2) *and the viscous effects* (c_2) *set the dynamics of the system. (b) Elasticity of both live and fixed cells determined independently from mass. (c) Viscosity of both live and fixed cells determined independently from mass.*

4.4 Conclusion

In this study, we derived an expression for loss tangent measurement of each cell by using a MEMS resonant sensor to capture three parameters; frequency shift, amplitude shift, and phase shift; allowing us to determine the viscoelastic moduli and therefore quantify the ratio of energy dissipation upon deformation of each probed cell. We found that fixed cells show a substantially larger loss tangent than their live counterparts, revealing that fixed cells are more dissipative and elastic at our resonant frequency. By constraining our governing equations with an additional optical phase shift we are able to obtain a tighter moduli solution space. Our technique can open opportunities to allow for continuous real-time measurements of changes in mass, stiffness, and viscoelasticity over the growth period of single cells; allowing them to serve as a diagnostic tool

to identify phenotypes by their mechanical signature and response to mechanical stimulation.

4.5 References

1) Verdier, C., Etienne, J., Duperray, A. & Preziosi, L. Review: Rheological properties of biological materials. *Comptes Rendus Physique* 10, 790–811 (2009).
2) Cross, S. E., Jin, Y.-S., Rao, J. & Gimzewski, J. K. Nanomechanical analysis of cells from cancer patients. *Nature Nano* 2, 780–783 (2007).
3) Corbin, E. A., Kong, F., Lim, C. T., King, W. P. & Bashir, R. Biophysical properties of human breast cancer cells measured using silicon MEMS resonators and atomic force microscopy. *Lab Chip* 15, 839–847 (2015).
4) Krisenko, M. O., Cartagena, A., Raman, A. & Geahlen, R. L. Nanomechanical property maps of breast cancer cells as determined by multiharmonic atomic force microscopy reveal Syk-dependent changes in microtubule stability mediated by MAP1B. *Biochemistry* 54, 60–68 (2015).
5) Lim, C., Zhou, E. & Quek, S. Mechanical models for living cells - A review. *J Biomech* 39, 195–216 (2006).
6) Bannister, L. & Mitchell, G. The ins, outs and roundabouts of malaria. *Trends Parasitol.* 19, 209–213 (2003).
7) Gittes, F., Schnurr, B., Olmsted, P. D., MacKintosh, F. C. & Schmidt, C. F. Microscopic Viscoelasticity: Shear Moduli of Soft Materials Determined from Thermal Fluctuations. *Phys. Rev. Lett.* 79, 3286–3289 (1997).
8) Barbee, K. A., Davies, P. F. & Lal, R. Shear stress-induced reorganization of the surface topography of living endothelial cells imaged by atomic force microscopy. *Circ. Res.* 74, 163–171 (1994).
9) Petersen, N. O., McConnaughey, W. B. & Elson, E. L. Dependence of locally measured cellular deformability on position on the cell, temperature, and cytochalasin B. *P Natl Acad Sci Usa* 79, 5327–5331 (1982).
10) Dewey, C. F., Bussolari, S. R., Gimbrone, M. A. & Davies, P. F. The dynamic response of vascular endothelial cells to fluid shear stress. *J Biomech Eng* 103, 177–185 (1981).
11) Rotsch, C., Braet, F., Wisse, E. & Radmacher, M. AFM imaging and elasticity measurements on living rat liver macrophages. *Cell Biol. Int.* 21, 685–696 (1997).
12) Sato, M., Nagayama, K., Kataoka, N., Sasaki, M. & Hane, K. Local mechanical properties measured by atomic force microscopy for cultured bovine endothelial cells exposed to shear stress. *J Biomech* 33, 127–135 (2000).
13) Alcaraz, J. *et al.* Microrheology of Human Lung Epithelial Cells Measured by Atomic Force Microscopy. *Biophys J* 84, 2071–2079 (2003).
14) Thoumine, O. & Ott, A. Time scale dependent viscoelastic and contractile regimes in fibroblasts probed by microplate manipulation. *Journal of Cell Science* 110 (Pt 17), 2109–2116 (1997).
15) Caille, N., Thoumine, O., Tardy, Y. & Meister, J.-J. Contribution of the nucleus to the mechanical properties of endothelial cells. *J Biomech* 35, 177–187 (2002).
16) Desprat, N., Richert, A., Simeon, J. & Asnacios, A. Creep Function of a Single Living Cell. *Biophys J* 88, 2224–2233 (2005).
17) Laurent, V. M. *et al.* Assessment of Mechanical Properties of Adherent Living Cells by Bead Micromanipulation: Comparison of Magnetic Twisting Cytometry vs Optical Tweezers. *J Biomech Eng* 124, 408–14 (2002).
18) Balland, M., Richert, A. & Gallet, F. The dissipative contribution of myosin II in the

cytoskeleton dynamics of myoblasts. *Eur. Biophys. J.* 34, 255–261 (2005).
19) Yanai, M., Butler, J. P., Suzuki, T., Sasaki, H. & Higuchi, H. Regional rheological differences in locomoting neutrophils. *American Journal of Physiology - Cell Physiology* 287, C603–11 (2004).
20) Guck, J. *et al.* The optical stretcher: a novel laser tool to micromanipulate cells. *Biophys J* 81, 767–784 (2001).
21) Park, K., Mehrnezhad, A., Corbin, E. A. & Bashir, R. Optomechanical measurement of the stiffness of single adherent cells. *Lab Chip* 15, 3460–3464 (2015).
22) Corbin, E. A. *et al.* Micromechanical properties of hydrogels measured with MEMS resonant sensors. *Biomed Microdevices* 15, 311–319 (2013).
23) Corbin, E. A., Adeniba, O. O., Physics, R. E. A.2016. Dynamic mechanical measurement of the viscoelasticity of single adherent cells. *aip.scitation.org* doi:10.1063/1.4942364
24) Corbin, E. A., Adeniba, O. O., Cangellaris, O. V., King, W. P. & Bashir, R. Evidence of differential mass change rates between human breast cancer cell lines in culture. *Biomed Microdevices* 19, 10 (2017).
25) Park, K. *et al.* Measurement of adherent cell mass and growth. *P Natl Acad Sci Usa* 107, 20691–20696 (2010).
26) Mehrnezhad, A. & Park, K. Multifrequency Optomechanical Stiffness Measurement of Single Adherent Cells on a Solid Substrate with High Throughput. *Anal. Chem.* 89, 10841–10849 (2017).
27) Ferry, J. D. *Viscoelastic properties of polymers*. (John Wiley & Sons, 1980).
28) Fung, Y.-C. *Biomechanics: Mechanical Properties of Living Tissues*. (Springer-Verlag, 1981).
29) Park, Y. *et al.* Measurement of red blood cell mechanics during morphological changes. *P Natl Acad Sci Usa* 107, 6731–6736 (2010).
30) Evans, J., Gratzer, W., Mohandas, N., Parker, K. & Sleep, J. Fluctuations of the Red Blood Cell Membrane: Relation to Mechanical Properties and Lack of ATP Dependence. *Biophys J* 94, 4134–4144 (2008).
31) Monzel, C. & Sengupta, K. Measuring shape fluctuations in biological membranes. *J Phys D Appl Phys* 49, 243002–22 (2016).
32) Löffek, S., Franzke, C.-W. & Helfrich, I. Tension in Cancer. *Int J Mol Sci* 17, (2016).
33) Kim, S.-O., Kim, J., Okajima, T. & Cho, N.-J. Mechanical properties of paraformaldehyde-treated individual cells investigated by atomic force microscopy and scanning ion conductance microscopy. *Nano Converg* 4, 5 (2017).
34) Adeniba, O. O., Corbin, E. A., Ewoldt, R. H., Bashir, R., APL Bioengineering, 2**,** 16 (2018).

Chapter 5 : Simultaneous Time – Varying Viscoelasticity, Mass and Cell Cycle Monitoring of Single Adherent Cancer Cells

Biophysical properties like stiffness and mass of cancer cells are useful biomarkers to evaluate their relative metastatic potential. Evaluation of these parameters versus cell cycle has not been reported and can provide further insights into cell cycle progression and the uncontrolled proliferation of cancer. Using our pedestal microelectromechanical systems (MEMS) resonant sensors, we have developed a non-contact interferometric measurement technique that simultaneously tracks the dynamic changes in the viscoelastic moduli and mass of adherent colon (HT-29) and breast cancer (MCF-7) cells from the interphase through mitosis and then to the cytokinesis stages of their growth cycle. We show that by combining three optomechanical parameters into an optical path length (OPL) equation and a two-degree-of-freedom model, we measure can simultaneously extract the viscoelasticity and mass as a function of the nano-scaled membrane fluctuation of each cell in a population. The technique is unique as it highlights the unique mechanical signatures at each stage of an individual cells across its cycle. Our measurements suggest that probed cells consistently indicate sharp viscoelastic and mass fluctuations around mitosis.

5.1 Introduction

The cytoskeleton is an interconnected filamentous network that is responsible for organizing cellular content, interfacing with the external environment, and coordinating forces for movement and shape. Recent work has shown that both internal and external forces act through the cytoskeleton to influence the mechanical properties and behavior of cells as they progress across their growth cycle (interphase and mitosis). [10,23]. This cytoskeletal structure have also been shown

to have important roles in arranging and maintaining the integrity of intracellular compartments. The polymerization and depolymerization of actin filaments and microtubules generate directed forces that drive changes in cell shape and, together with molecular motors that move along the actin filaments and microtubules, guide the organization of cellular components. More specifically, cytoskeletal muscle proteins of the cell — actin and myosin II — are usually credited for the force behind all cell movements and shape changes. However, recent work suggests that phosphorylation of moesin, an actin-binding protein, is sufficient to cause rounding of cells and efficient mitotic spindle assembly at the onset of cell division[19,26]. These studies suggest a new paradigm for a non-motor protein causing cell-shape change. It was therefore inferred that cell rounding caused by moesin phosphorylation is necessary for stabilizing and aligning the metaphase spindle.

Cellular viscoelasticity has been shown to be significantly affected by disease. It is commonly known that cancer cells are softer than their normal counterpart[1,2]. Recent work in the cardiovascular sciences has shown the direct effects of viscoelasticity and force output using drug-induced systems[3,4]. Other biomarkers like cell mass is believed to be an important physiologic parameter that if dysregulated could give rise to disease[5]. Considering cell mass is determined not only by the cytoskeleton but by the contents within such as water and proteins, tracking changes in cell mass and viscoelasticity may provide key insights for understanding the changes in cellular structure, response, and function. Some relevant work[16] reveal linear dependence of cell mass on its average growth rate further suggesting internal size-independent homeostasis through gene-dosage regulation or amount of DNA that can initiate the transcription process[27]. Researchers have made significant strides in understanding the underlying physiology of a cellular system by capturing real time monitoring of these biophysical properties in downstream functional

consequences[5,15,16,20].

As our MEMS resonant sensors can allow measurement of stiffness and mass over time, we can also observe the changes in growth at various checkpoints in a cell cycle. Our sensor has features that are unique as compared to other methods such as quartz crystal microbalance (QCM)[6], atomic force microscopy (AFM)[1,7,8], micropipette aspiration[9–11], suspended microchannel resonator (SMR)[12,13]. Most of these are limited by the inability to estimate time-varying elasticity and viscosity moduli alongside mass measurements of a whole cell over time[14]. Our work presents the first (or novel) investigation of a time-varying simultaneous estimation of viscoelasticity and mass for individual adherent cells.

5.2 Results

5.2.1 Non-destructive mapping of cell viscoelasticity

In this work, we can repeatedly measure the viscoelastic moduli and mass changes corresponding to cell growth, proliferation, decoupling and reattachment of single HT-29 and MCF-7 cells. We used a MEMS resonant sensor consisting of a 60 × 60 μm^2 platform suspended by four beam springs that are arrayed in a 9 × 9 format of 81 sensors (fig. 5:1a). The sensors operate with the aid of electromagnetic stimulation generating Lorentz force actuation and producing an out-of-plane motion in the first resonance mode. Similar to previous studies[2,14–17], the velocity of the sensor vibration is monitored and measured by a laser Doppler vibrometer (LDV) in conjunction with a lock-in amplifier to capture our sensor responses. Our system observables, the frequency ($\boldsymbol{f}$), amplitude ($\boldsymbol{A}$), and optical phase shift ($\Delta\boldsymbol{\phi}$) are collected from the LDV measurements to extract the mass and viscoelastic values for individual cells versus time. More particularly, the measurements were carried out in three schemes. First, the responses of an

unloaded vibrating sensor (without media) was measured to determine the spring constant. Secondly, we measured the responses of an unloaded wet sensor (in-media) to determine a reference resonant frequency and amplitude for subsequent comparative analysis. Thirdly, the sensor is loaded with a live cell and then the frequency and amplitude shifts are collected; while the laser is simultaneously being passed through the cell to measure the OPL variations between laser paths inside and outside the cell. The laser path length changes due to height oscillations of the cell during vibration, resulting in a phase shift (fig. 5:1b-c)[2,14–16]. The OPL changes observed correlates directly to the material and structural properties of the cell. These measurements are performed over time to capture the growth progression of each cell from an initial adherence stage through spreading, division (retraction) and reattachment (fig. 5:1d). Details of the resonant sensors and experimental setup used in this study are described elsewhere[16]. The viscoelastic effect of HT-29 cells on the resonant frequency and amplitude of the sensor were previously quantified to generate a large space of potential viscoelastic moduli solutions[14]. By incorporating the OPL shift as an additional variable, we can examine the morphological and phenotypical heterogeneity of each cell in a population on a cell-by-cell basis.

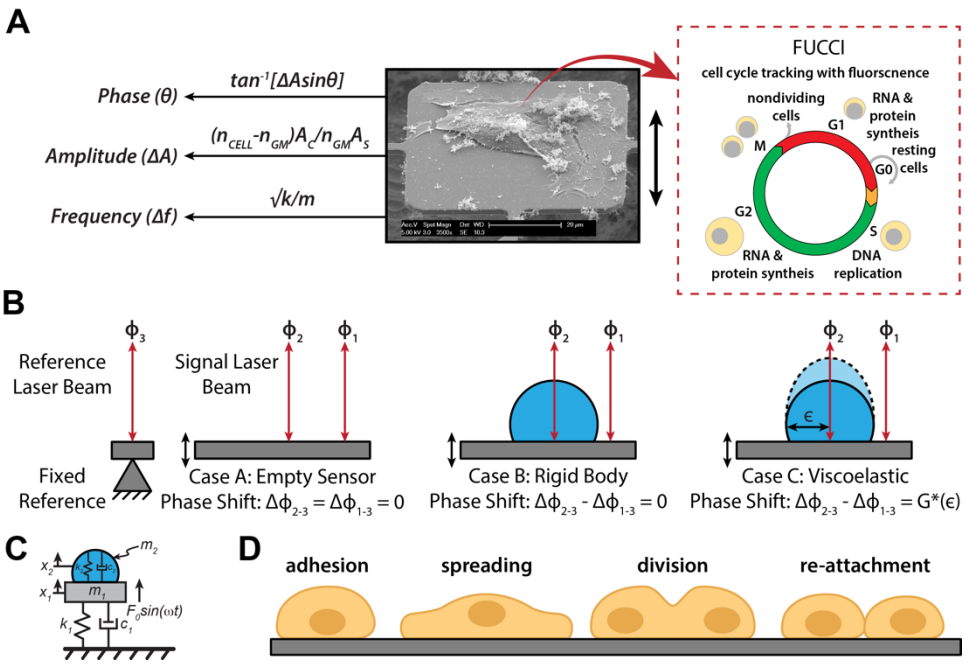

Fig 5:1 Overview of measurement scheme. (A) Summary of the vibration induced phase shift ($\Delta\phi$), amplitude ratio, (ΔA), and frequency shift (Δf) relate to the viscoelastic properties and mass of the cell. These parameters are extracted during the vibration of a cell-loaded sensor while the cell cycle stage progression is being observed through phases G1 – S – G2 – M. (B) Cross-sectional figures elucidating the vibration induced phase shift, $\Delta\phi$ of a targeting signal beam, ϕ_1 and ϕ_2 on an empty sensor; inside and outside a rigid cell; and inside and outside of a viscoelastic cell; compared to a reference beam, ϕ_3. G(ϵ) represents the cell dynamic moduli (viscoelastic moduli) as a function of lateral position, ϵ, which tracks the cell heights oscillation. (C) 2-DOF model. (D) Cell physiological transition from initial adhesion through cell rounding/division to reattachment to a patterned surface.*

5.2.2 Mechanical viscoelastic properties change as cells grow

Investigating temporal events across the cell-cycle requires single cell analysis within the larger population. The cell cycle is a highly regulated process linked with environmental properties and morphological changes (fig. 5:2a). Prior to cell division (fig. 5:2b-c, markers i/ii), the baseline viscoelastic values of these cells agrees with our previous viscoelastic average values of ~152 ± 30 Pa and ~1.1 ± 0.3 mPa-s for HT-29 cells as well as ~260 ± 80 Pa and ~1.4 ± 0.8 mPa-s for MCF-7 cells[18] (summarized in table 5:1). At the onset of mitosis (marker iii) - a cell undergoes changes to its architecture (morphology) for mitosis; where a cell partially detaches from the substrate and becomes round in shape, which is necessary for subsequent mitotic events (i.e.

spindle morphogenesis)[19]. This process of cell rounding involves rearrangement of the actin cytoskeleton, de-adhesion, and an increase in cortical rigidity (fig. 5:1d). If we consider the dynamics around cell division (mitosis, marker iv, untreated), we observe a sharp decrease in stiffness during mitosis, which at first pass suggests a decrease in inertial coupling (fig.5:2 and fig 5:3a). However, upon entry into mitosis the cortical actin stiffens and the cell becomes round to facilitate division, thereby causing a reduced cell height oscillation leading to an increase in our stiffness value vibration This occurrence of this peak elasticity value suggests that the cell cortical stiffening effects outweighs any potential effect that a cell detachment could possibly cause before mitosis.

The increase in cortical rigidity is directly observed across both cell types as a sharp (1.1 -1.6 fold) increase in the viscoelastic values while this agrees very well with previous studies[19,20,21].. Table 1 and 2 depict this elasticity value difference between the average interphase (markers i-iii) values versus value at the onset of mitosis, during mitosis and after mitosis (marker iii-iv) for both cell lines. It has been shown that moesin, a protein activated upon entry into mitosis controls cortical rigidity, cell rounding and spindle morphogenesis. At the point of division during mitosis, a sharp decrease in apparent cell mass is observed (marker iv). This sudden decrease in apparent mass during mitosis is caused by the cell partially detaching from the platform, temporarily decreasing its contact area; leading to a reduction of the inertial loading of the cell and causing a probable higher strain rate and viscosity. Subsequently, there is a corresponding decrease in cell elasticity due to this detachment. After exiting mitosis (marker v), the post-mitosis viscoelastic values are restored to baseline values equivalent to pre-mitosis. Prior studies suggest there exists tensional homeostasis through contractions to counterbalance forces along the stress fibers that help cell attachment and re-attachment to surfaces[22,23].

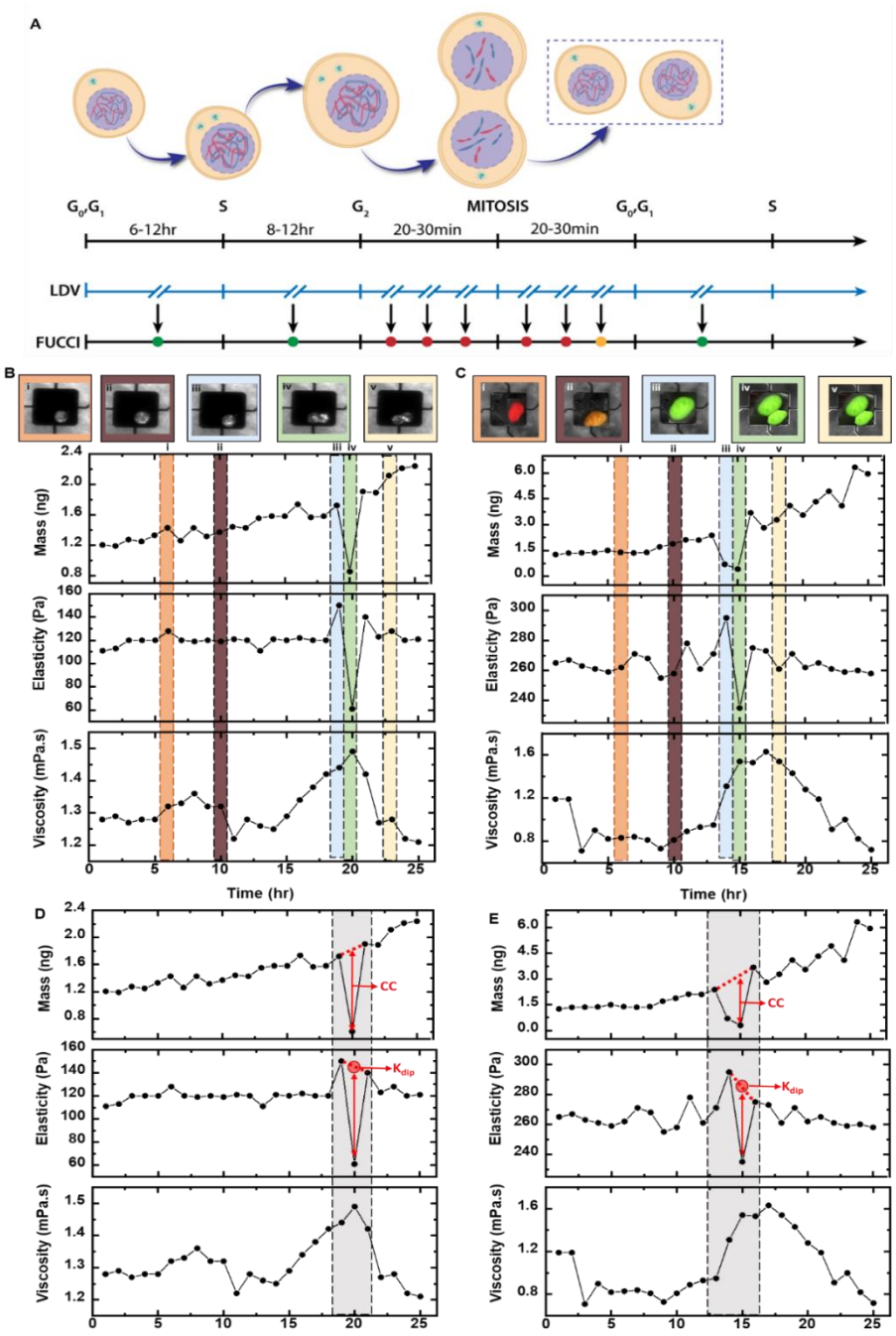

Fig 5:2 (A) Experimental timeline highlighting the transition of cell optomechanical measurement on sensors with respect to the LDV position while carrying out fluorescence imaging. (B) Cell mass, elasticity and viscosity versus time (hrs) (i) For single cell growth analysis of HT-29 cells, the mass and stiffness data was analyzed prior to- (i, ii, iii) and after a mitotic event (iv, v). Division is shown with the individual cells and daughter cells. (C) For a MCF-7 cell, the mass and stiffness data was analyzed prior to- (i, ii, iii) and after each mitotic event (iv, v). Division is shown with the individual and daughter cells. These parameters are extracted during the vibration of a cell-loaded sensor while the cell cycle stage progression is being observed through phases G1 (Red) – S(Orange) – G2 (Green)– M(Green) using FUCCI cell cycle reporter. (D)&(E): Showing coupling coefficients CC and intermediate mitotic stiffness Kdip

5.2.3 Drug-induced increase of actin polymerization, increases viscoelastic properties as cell grow.

The cell cycle and mitosis are highly regulated processes that involve a dynamic modulation of the cytoskeletal mechanical structure. Rho GTPases are a key regulator necessary to maintain the dynamics of cell shape during not only the cell cycle progression but also at the onset of mitosis. To further investigate the structural changes within the cell and the influence on viscoelasticity, we quantified changes in mass and viscoelastic properties of both cell types over the cell cycle when the cytoskeletal structural components were specifically manipulated using a Rho activator. Treatment with a Rho activator, a direct agent that stimulates actin polymerization, increased the viscoelastic moduli as compared to the untreated samples over the time course (fig. 5:3). Stimulating actin polymerization through Rho-mediation causes an increase in the inertial coupling (i.e. an increase in stiffness) of the cells with the sensor and reduction in growth rate of the cell. This is consistent with prior studies[18,21] which have revealed that compared to their non-treated counterparts, Rho-activator-mediated cancer cells are stiffer; and this cell stiffness is dependent on actin polymerization and the activation of stress fibers; potentially increasing the spring and damper-like behaviors of constituent actin fibers. These studies showed through fluorescent staining that the cell spread differently and wider due to the activation of these stress fibers[21].

Consequently, we observe the final average values to be order of magnitude of 2.5 fold increase (for apparent mass measurements) and ~3 fold increase (for viscosity and elasticity measurements). Further explaining the effect of an increased tension as a result of stress fiber development. We, therefore infer that since there in more tension in the stress fibers and a higher focal adhesion, it results in a reduced membrane fluctuation (structural deformation) and hence a higher apparent mass reading due to an increased cell-sensor coupling..

When the HT-29 cell line is treated with a Rho activator, we observe that the growth rate

is slowed down. Fig 3a shows the apparent mass trend of a Rho-mediated HT29 cell whose values are shifted backwards by ~ 6 hours before aligning with its unmodified counterpart. Whereas, we observed that the MCF-7 rho-mediated cell does not show any signs of division possibly due to the fact that rho is introduced in a the G_1 or S checkpoint phase; the cell gets stuck and there by affecting division and activating apoptosis after a prolonged arrest.

The mass and elasticity values at this division points were interpolated to obtain CC and K_{dip}; coupling coefficient and mitotic elasticity (summarized on Table 5:3) are suggestive of a measure of decoupling (partial detachment) of a cell from the surface during division.

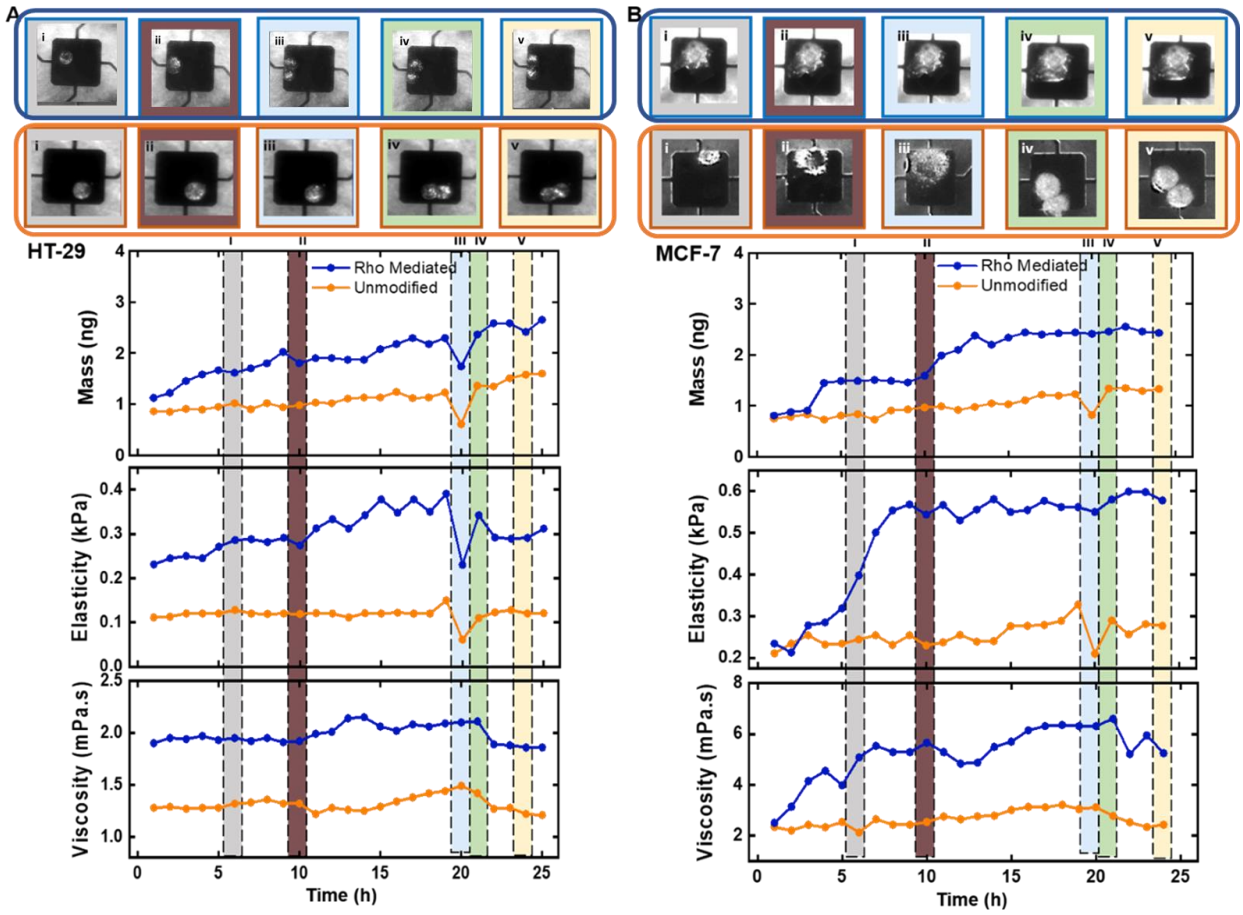

Fig 5:3 RhoA significantly increases elasticity and viscosity. (A) Time-Varying Mass, Elasticitiy and Viscosity measurement of RhoActivator – mediated HT-29 cells and unmodified HT-29 cells measured by our MEMS resonator. Plot show a significant increase in cell viscoelastic moduli of modified HT-29 cells due to phosphorylation of actin. (B) Comparison between plot showing a significant increase in cell viscoelastic moduli of modified MCF-7 cells due to phosphorylation of actin fibres. Dashed lines are used to trace the mass and viscoelastic values per cell cycle stage. Here MCF-7 remains in the G2 checkpoint phase before apoptosis.

5.2.4 Local stiffness shifts within cell over mitosis.

As stated above, there are temporal changes to the viscoelastic properties of cells around mitosis. To investigate the short-term viscoelastic response spatially across the cell, our resonant sensors are used as a vibrating substrate to initiate a vibration induced phase shift (VIPS). While the platform of our mass sensor is oscillating at a fixed frequency, the phase of the substrate's velocity is measured by the LDV and the lock-in-amplifier on a grid-by-grid basis outside and across the

cell (fig. 5:4**)**. A cell vertically vibrating on a substrate experiences a structural deformation due to oscillation of its height, and the degree of the height oscillation is inversely proportional to the cell stiffness. At the onset to mitosis (fig. 5:4a), an average value of ~ 0.35 ± 0.11° confirms that there is an increased stiffening since this value is inversely proportional to stiffness (elasticity). During mitosis (fig. 5:4b), an average apparent phase shift of ~ 0.8 ± 0.23° indicating the reduction in coupling of a cell to a sensor and a higher cell height oscillation. Post-mitosis (fig. 5:4c), the cell-sensor interaction changes as the daughter cells reattaches, which translates to a restored average phase shift value of ~0.5 ± 0.15°[17,24]. This technique helps in elucidating the heterogeneity of each cell's profile and further validates the characteristic transitioning of a cell across its growth cycle.

5.3 Discussion

The replication of intracellular materials and balance of contractile forces is a highly regulated process during cell growth. For example, it is proposed that tensional homeostasis occurs in cell cycle in order to regulate contractile forces along its stress fiber[22,23]. While the precise mechanisms of tensional homeostasis remain arguably unclear, it is likely that stiffness (viscoelasticity) is differentially regulated by many factors, including: cell contact (adherent vs. suspended cells), diffusive and surface bound signaling cues, genetic and epigenetic programs operating in the range of cells (quiescent or dividing) in the various tissues. With our resonant sensor, we are able to show long-term trends of live non-apoptotic mitotic HT-29 and MCF-7 cells; which are agreeable with other established methods and hypothesis.

Further work would explore the mechanical signatures that characterize morphological behaviors especially during division of these cells as observed in figs. 5:2-3 via an exploration of coupling coefficients, CC and mitotic stiffness, K_{dip}. Meanwhile, we observe a significantly

increased value of CC for MCF 7 cells; perhaps suggesting a higher cell-sensor inertial coupling for MCF 7 cells due to a higher stiffness value and a correspondingly reduced membrane fluctuation. K_{dip} for both cells lines expectedly correspond to averaged elasticity values of cells during division. Multiple viscoelastic moduli at check points in our cell cycle are also consistent with expected phenomena[19,24]. Our observed optomechanical parameters, the vibration induced phase shift – VIPS ($\Delta\phi$), amplitude ratio (ΔA), and frequency shift (Δf) are reported with theoretical analysis to provide information on viscoelastic properties in tandem with established mass trends observed from earlier work[24]. These parameters are extracted from the vibration of a cell-loaded sensor while the cell cycle stage progression and growth is being observed through phases G_1 – S – G_2 – M (fig.5: 2). We have further incorporated a FUCCI cell cycle reporter to optically monitor these cells across each stage to correlate the stiffness and growth profile more precisely. These long-term measurement techniques used for cell growth measurement can potentially be integrated into a multi-modal mechanical characterization of single cells.

Consequently, it is also clearly shown that the cell with lower mechanical stiffness exhibits larger VIPS (fig. 5:4) demonstrating the potential of non-invasive mechanical phenotyping of adherent cells. Another interesting addition was the ability to modulate cell stiffness by treating them with Rho activators to help in creating a control for our measurement in fig. 5:2. The protocol further proved that our measurement is sensitive enough to detect changes in stiffness values.

With an enhanced throughput, and additional capabilities with fluorescent imaging, we believe that our measurement system can make a significant contribution to understanding various cellular processes, such as cell growth, apoptosis, cell differentiation, and cell proliferation.

Here we evaluate single cell viscoelastic properties of two different cell types with drug-induced cytoskeletal changes to investigate how filamentous actin contributes to cell

viscoelasticity. Using a pedestal microelectromechanical systems (MEMS) resonant sensors, we develop a long-term measurement technique that simultaneously estimates the time-varying viscoelastic properties and mass of adherent colon (HT-29) and breast cancer (MCF-7) cells by combining three optomechanical parameters using the optical path length (OPL) equation and a two-degree-of-freedom model (2-DOF). These measurements, which include the vibrational amplitude and resonant frequency of our electromagnetically actuated pedestal sensor, were combined with a vibration induced phase shift (VIPS) to elucidate the underlying events across the cell-cycle. Our results clearly show a trend that agrees well with an expected cortical stiffening (and rounding) at each mitotic entrance. Viscoelasticity of HT-29 and MCF-7 cells were also modulated through drugs (RhoGTPase Activators) to investigate the sensitivity of our system.

5.4 Methods

Cell-Media Refractive Index Difference and Optical Path Length (OPL) Model

To explicitly decouple the viscoelastic moduli of individual cells from a sample population, the membrane fluctuation (height oscillation) is combined with a mechanically-induced and optically-measured phase-shift of each cell using an optical path difference model. The LDV measures the time-derivative of the OPL and is used to determine the membrane oscillation of the cell[17,24,25]. Figure 5:1C is a schematic overview of the optical path of the laser in conjunction with difference in refractive index of each surrounding layer (air, media, cell) of its travel length. The phase shift induced during vibration is largely a function of each cell height oscillation when presented as a soft material as opposed to a rigid body. In other words, no significant phase shift is experienced when the sensor is empty, or our probed sample is not within a linear regime of compressibility (non-deformable).

The equation for the optical path length model is represented in equation (1) and resonant measurement parameters (amplitude ratio and mechanical phase difference) from this are shown in equations (2) and (3).

$$\boldsymbol{OPL}(t) = \sum n_i d_i(t) = \mathrm{n_{GM}} * (H_{sensor}(\mathrm{t}) - h(\mathrm{t})) + \mathrm{n}_{cell} * h(t) \approx \mathrm{n_{GM}As}* (1 + \Delta \mathrm{A}) *\sin(\omega \mathrm{t} + \Delta\phi) + \mathrm{const.} \quad (1)$$

$$\Delta A = \left[\frac{(\mathrm{n}_{cell} - \mathrm{n_{GM}})}{\mathrm{n_{GM}}} * \frac{\mathrm{Ac}}{\mathrm{As}}\right] \quad (2)$$

$$\Delta\phi = \arctan\left[\frac{(\mathrm{n}_{cell} - \mathrm{n_{GM}})}{\mathrm{n_{GM}}} * \frac{\mathrm{Ac}}{\mathrm{As}} * sin(\theta)\right] \quad (3)$$

where vertical heights include $H_{sensor}(t)\ and\ h(t)$ representing the instantaneous sensor position and cell height. n_{cell} and n_{GM} represent refractive index of the cell and surrounding media respectively. A_c represents the amplitude of the cell height oscillation with respect to cell initial height also denoted as the cell membrane fluctuation (amplitude), A_s represents the amplitude of the sensor oscillation, θ represents the phase of the cell height oscillation with respect to the sensor, ω represents the oscillating resonant frequency, $\Delta\phi$ is our measured maximum phase shift of the OPL. At every time point of each long-term experiment, we compute the individual cell membrane fluctuation (cell height oscillation) at resonance, A_c, via equation (2) by estimating $A_s \approx 0.29$ nm (from measured velocity and oscillatory frequency) for a 35 nN excitatory input in media, $n_{GM} = 1.35$, and $n_{cell} = 1.38$ for live cells[17].

Cell-Sensor Modelling and Assumptions

As in previous studies[2,14–17,24], our sensor-cell configuration is modelled as a 2-DOF suspended mass model where the cell is represented by a Kelvin-Voigt viscoelastic solid with a mass (m_2), elastic stiffness (k_2), and viscous coefficient (c_2) connected to the sensor. The sensor mass (m_1) is also connected to the fixed substrate by a second Kelvin-Voigt spring-damper (k_1, c_1).

The model as shown in figure 5:1D assumes an oscillatory force $F(t)$ applied to the sensor mass.

The cell-sensor interactions used in this work depends on a few required assumptions that the cell membrane is homogeneous, smooth and the average cell-surface (membrane) oscillation is calculated at its steady state. Also, the total mass of the cell, m_2 is assumed to be concentrated at the center of the cell. The displacement (and the input force) of the cell is also assumed to be applied at the center of the cell mass. Consequently, the center of the cell is in phase with the membrane of the cell; implying that $A_c = A_s$ (see chapter 4). We model the 2-DOF system behavior as described fully in the chapter 4

Cell Culture, Measurement Calibration and Drift Characterization

As shown in equations (1 – 3), we combined interferometric techniques to measure the viscoelasticity of HT-29 and MCF-7. Briefly, these cells were grown at 37 °C in Dulbecco's Modified Eagles Medium supplemented with sodium pyruvate, 10% fetal bovine serum and 1% penicillin streptomycin. The cells were seeded onto the sensor area at a density of ~300 cell/mm^2 within a 6 mm diameter PDMS culture chamber. Cells were cultured on resonant sensors functionalized with collagen. A separate cell sample cells was treated with 2 μg/mL of Rho Activator II (Cytoskeleton, Inc.) and incubated for 4 hours before and during our mechanical measurements. We, also collected instantaneous amplitude ratio[14], phase shift[17], and frequency shift[16] measurements, calibrated the sensor mass, and characterize long-term drifts to estimate the viscoelasticity of each live cell and fully understand the underlying mechanics of each cell as they progress across their various growth stages from interphase through mitosis.

FUCCI Cell Cycle Marker

In order to capture the transitions through the cell cycle, we used the fluorescence ubiquitination cell cycle indicator (FUCCI), a genetically encoded, two-color (red and green)

indicator that allows us to follow cell division within our cell population. During the G1/S transition, a dynamic color change occurs, from red-through-yellow-to-green, representing the progression through cell cycle and division as shown in Figure 5:1B (right). A 20 μL dilution mix of the BacMam reagents (geminin-GFP and Cdt1-RFP) was added to 50,000 adherent cells targeting 40 particles per cell. The reagent is a baculovirus, an insect virus that does not replicate in mammalian cells. After gentle rotation, we incubated the cells overnight (≥16 hrs) at 37 °C and then fluorescence imaging was carried out to measure the cell cycle transition.

Imaging of Cultured Cells (Olympus BX 51)

Cells were grown on our sensors and stably transduced with BacMam reagents. They were then subjected to long-term, time-lapse imaging using a computer-assisted fluorescence microscope (Olympus, BX 51, cellsens software) equipped with an objective lens (20X Olympus Plan Achromat Objective, 0.4 NA, 1.2 mm WD), a halogen lamp (excitation source), and a CCD camera. For fluorescence imaging, the halogen lamp was used with two filter cubes FITC and TRITC. The FITC filter with an excitation maximum wavelength of 490nm and emission maximum wavelength of 525nm was used to observe the fluorescence of Premo geminin-GFP. The TRITC filter with an excitation maximum wavelength of 557nm and emission maximum wavelength of 576nm was used to observe the fluorescence of Premo Cdt1-RFP.

Figure 5:2A describes the transition between the Olympus BX51 fluorescence microscope and LDV stage as each cell progresses across its cycle. The cells were collected intermittently from the LDV stage to the microscope for imaging at different time windows of the growth stage. For instance, since it takes 6-12 hours to transition from stage G_0 /G_1 to the S growth phase. The MCF-7 cells were quickly imaged on our upright fluorescence microscope within the smallest detectable measurement time frames of ~5-10 mins before resuming the cell mass/stiffness measurements.

The same procedure was carried out through phases G_0 /G_1 – S to G_2 – M transitions.

Estimation of Instantaneous Cell Viscoelastic Coefficients, (k_2, c_2) and Moduli (E, μ)

The mechanical phase difference (θ) is related to cell viscoelastic properties that we extract by considering the full 2-DOF suspended mass system. To estimate the viscoelastic coefficients (k_2, c_2), our microresonator is modeled as a 2-DOF Kevin-Voigt model as described in equation (4) in simplified matrix form.

$$\begin{bmatrix} (k_1 + k_2 - m_1\omega^2) + (c_1 + c_2)\omega j & -k_2 - c_2\omega j \\ -k_2 - c_2\omega j & (k_2 - m_2\omega^2) + c_2\omega j \end{bmatrix} \begin{Bmatrix} \boldsymbol{A_s} \\ \boldsymbol{A_c} \end{Bmatrix} e^{j\omega t} = \begin{Bmatrix} F \\ 0 \end{Bmatrix} e^{j\omega t}; \quad (4)$$

Note that the physical quantities of interest are found by taking the imaginary components, e.g. $F(t) = F\sin\omega t = \mathrm{I_m}\{Fe^{j\omega t}\}$; where $\boldsymbol{A_s} = A_s^R + jA_s^I$ and $\boldsymbol{A_c} = A_s^R + jA_c^I$ are the vector amplitudes of the sensor and cell states x_{sensor} and x_{cell} respectively, and $Fe^{j\omega t}$ is the input force. Equation (4) is further decomposed as the instantaneous sensor and cell responses in equation (5).

$$x_{sensor}(t) = |\boldsymbol{A_s}|\ \sin(\omega t + \theta_s) \quad (5a)$$

$$x_{cell}(t) = |\boldsymbol{A_c}|\ \sin(\omega t + \theta_c) \quad (5b)$$

where $\theta_s = \tan^{-1}\left\{{(A_s^I)}/{(A_s^R)}\right\}$ and $\theta_c = \tan^{-1}\left\{{(A_c^I)}/{(A_c^R)}\right\}$. Here, θ_s and θ_c denote the phase differences between the sensor and cell height oscillation with respect to the excitatory force, $F(t) = F\sin\omega t$. Our modeled cell-sensor phase difference,

$$\theta = \theta_c - \theta_s \quad (6)$$

and modeled cell-sensor amplitude ratio becomes:

$$\Delta\mathrm{A} = \frac{(\mathrm{n}_{cell} - \mathrm{n_{GM}})}{\mathrm{n_{GM}}}\ \frac{|\boldsymbol{A_c}|}{|\boldsymbol{A_s}|} \quad (7)$$

Observed amplitude ratio (ΔA) and mechanical phase shift (θ) inferred from equation (2) are substituted to simultaneously solve equations (6) and (7) for k_2 and c_2. Our recent work[24] shows further details of these calculations.

The viscoelastic coefficients ($k_2,\ c_2$) can be related to the apparent inherent viscoelastic moduli (E, μ) by $k_2 = \frac{EA}{H}$ and $c_2 = \frac{\mu A}{H}$. Ratio $\frac{A}{H}$ denotes the area-to-height information of each cell where the average cell area is ~250μm^2 with an estimated cell height of ~8μm and fitted accordingly in previous work[16].

Coupling Coefficient: 'CC' and Mitotic Elasticity, K_{dip}

Due to finite viscoelasticity (stiffness), we observe a reduction in the coupling of a cell's inertial loading with the sensor during mitosis; hence, the dip in mass and elasticity values in figure 5:2B-C. To compensate for these apparent losses in values during mitotic division, we interpolated the mass values, before and after the dip (through averaging) to calculate the coupling coefficient, 'CC', an absolute difference between the interpolated mass values and apparent mass value. Likewise, we interpolated the cell elasticity values during division to obtain an elasticity value of K_{dip}

Interplay between the Corrected Mass & Stiffness values

Prior studies[2,14–16], demonstrate that our 2-DOF model represented by equation (4) shows that the measured apparent mass in figure 5:2B-C, is a function of the cell viscoelastic moduli. Thus, all measured mass values in the remainder of this work were corrected by a range of values (~1.2-1.8) to account for the finite stiffness of the cell at every time instant; this only changes with slight variations in the cell's viscoelasticity (stiffness) and morphology. Particularly, figure 5:2D-E highlights how k_{dip}, which denotes an apparent elasticity value estimated during mitosis is a huge deviation from the average elasticity values, E – shown at other time instants.

Vibration Induced Phase Shift (VIPS)

The measurement VIPS points are shown and scaled as shown in the color bar and total

number of the measurement points is over ~120 for each measurement. The VIPS profile in Fig.5: 4 between the measurement points is calculated with linear interpolation. This technique helps in elucidating the homogeneity of each cell's profile and further validates the characteristic transitioning of a cell across its growth cycle.

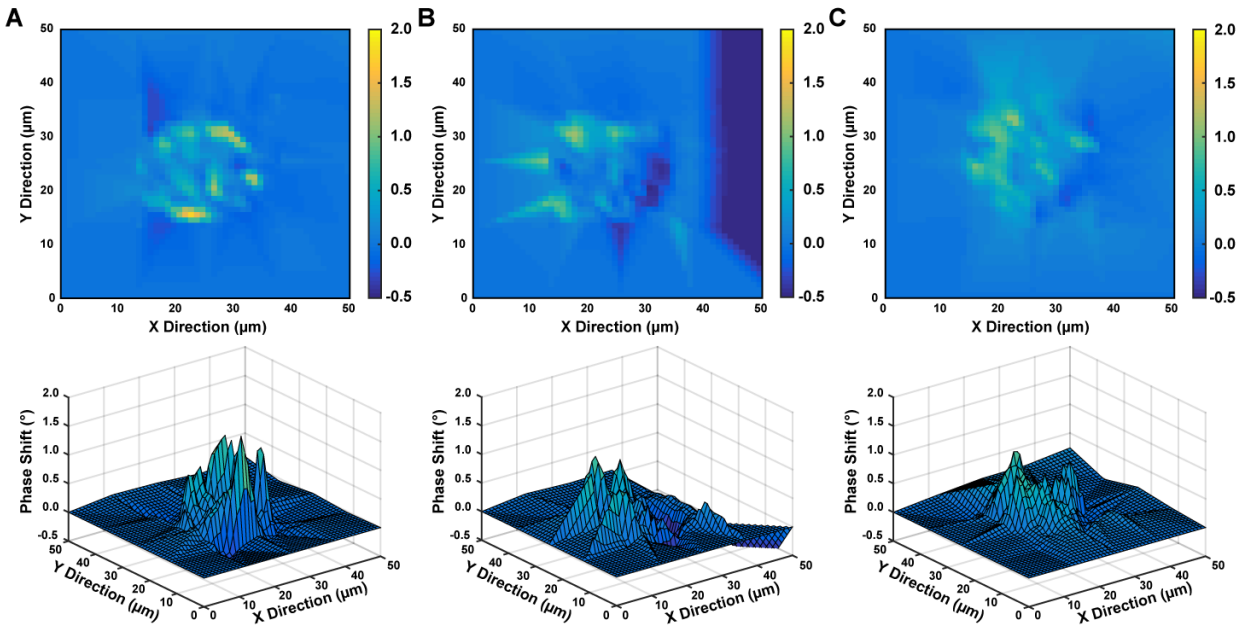

Fig 5:4. Map of Vibration Induced Phase Shift indicating stiffness of a HT-29 cell at different growth stages (before (I), during (II) and after mitosis(III)). The cell's height oscillation degree is inversely proportional to the stiffness (elasticity) across and around the cell's profile: I: A VIPS average value of 0.35° depicts stiffening before mitosis II: VIPS average of ~0.8° shows a reduction in stiffening during detachment of cell from our sensor platform. III: With a VIPS average value of ~0.5° depicts restoration of cell stiffness to its baseline.

Cell lines/ (Avg. Elasticity Values (Pa) from previous studies)	**HT 29 (~152 ± 30.0)**	**MCF 7 (~260 ± 80.0)**
i	120 ± 40.5	270 ± 80.1
ii	129 ± 41.4	280 ± 85.6
iii	150 ± 59.1	315 ± 49.0
Iv*(MassDip)	40 ± 15.2	210 ± 18.4
v	119 ± 35.0	240 ± 25.1

Table 5:1 Summary of elasticity on Figures 4 for HT-29 cells and MCF-7 cells in comparison to average values from previous studies.

Cell lines/ (Avg. Viscosity (mPa-s) from previous studies)	HT 29 (~1.1 ± .3)	MCF 7 (~1.4 ± .8)
i	1.3 ± 0.2	1.2 ± 0.4
ii	1.33 ± 0.9	0.9 ± 0.4
iii	1.44 ± 0.7	1.6 ± 0.5
Iv*(MassDip)	1.50 ± 0.8	1.61 ± 0.4
v	1.21 ± 0.39	0.9 ± 0.5

Table 5:2 Summary of viscosity on Figures 4 for HT-29 cells and MCF-7 cells in comparison to average values from previous studies.

	HT 29 (n = 9)	MCF 7 (n=5)
Coupling Coefficient: 'CC'	0.21 ± 0.1	0.38 ± 0.3
Elasticity during mitosis: K_{dip}	147 ± 23.0	307 ± 25.1

Table 5:3. Summary of Coupling Coefficient, CC and Elasticity during mitosis, Kdip for all collected HT 29 and MCF 7 cells.

5.5 References

1. Cross, S. E., Jin, Y.-C., Rao, J. & Gimzewski, J. K. Nanomechanical analysis of cells from cancer patients. *Nat. Nanotechnol.* **2**, 780–783 (2007).
2. Corbin, E. A., Kong, F., Lim, T. & King, P. Biophysical properties of human breast cancer cells measured using silicon MEMS resonators and atomic force microscopy. *Lab Chip* (2014). doi:10.1039/C4LC01179A
3. Chen, C. Y. *et al.* Suppression of detyrosinated microtubules improves cardiomyocyte function in human heart failure. *Nat. Med.* **24**, 1225–1233 (2018).
4. Robison, P. *et al.* Detyrosinated microtubules buckle and bear load in contracting cardiomyocytes. *Science (80-.).* **352**, (2016).
5. Martínez-Martín, D. *et al.* Inertial picobalance reveals fast mass fluctuations in mammalian cells. *Nature* **550**, 500–505 (2017).
6. Li, J., Thielemann, C., Reuning, U. & Johannsmann, D. Monitoring of integrin-mediated adhesion of human ovarian cancer cells to model protein surfaces by quartz crystal resonators: Evaluation in the impedance analysis mode. *Biosens. Bioelectron.* **20**, 1333–1340 (2005).
7. Kuznetsova, T. G., Starodubtseva, M. N., Yegorenkov, N. I., Chizhik, S. A. & Zhdanov, R. I. Atomic force microscopy probing of cell elasticity. *Micron* **38**, 824–833 (2007).
8. Plodinec, M. *et al.* The nanomechanical signature of breast cancer. *Nat. Nanotechnol.* **7**, 757–765 (2012).
9. Hochmuth, R. M. Micropipette aspiration of living cells. *J. Biomech.* **33**, 15–22 (2000).
10. Sato, M., Ohshima, N. & Nerem, R. M. Viscoelastic properties of cultured porcine aortic endothelial cells exposed to shear stress. *J. Biomech.* **29**, 461–467 (1996).
11. Evans, E. & Yeung, A. Apparent viscosity and cortical tension of blood granulocytes determined by micropipet aspiration. *Biophys. J.* **56**, 151–160 (1989).
12. Bryan, A. K., Goranov, A., Amon, A. & Manalis, S. R. Measurement of mass, density, and volume during the cell cycle of yeast. *Proc. Natl. Acad. Sci.* **107**, 999–1004 (2010).
13. Byun, S. *et al.* Characterizing deformability and surface friction of cancer cells. *Proc. Natl. Acad. Sci.* **110**, 7580–7585 (2013).
14. Corbin, E. A., Adeniba, O. O., Ewoldt, R. H. & Bashir, R. Dynamic mechanical measurement of the viscoelasticity of single adherent cells. *Appl. Phys. Lett.* **108**, (2016).
15. Corbin, E. A., Adeniba, O. O., Cangellaris, O. V., King, W. P. & Bashir, R. Evidence of differential mass change rates between human breast cancer cell lines in culture. *Biomed. Microdevices* **19**, 1–7 (2017).
16. Park, K. *et al.* Measurement of adherent cell mass and growth. *Proc. Natl. Acad. Sci.* **107**, 20691–20696 (2010).
17. Park, K., Mehrnezhad, A., Corbin, E. A. & Bashir, R. Optomechanical measurement of the stiffness of single adherent cells. *Lab Chip* (2015). doi:10.1039/C5LC00444F
18. Bordeleau, F., Lapierre, M. E., Sheng, Y. & Marceau, N. Keratin 8/18 regulation of cell stiffness-extracellular matrix interplay through modulation of rho-mediated actin cytoskeleton dynamics. *PLoS One* **7**, 1–10 (2012).
19. Kunda, P., Pelling, A. E., Liu, T. & Baum, B. Moesin Controls Cortical Rigidity, Cell Rounding, and Spindle Morphogenesis during Mitosis. *Curr. Biol.* **18**, 91–101 (2008).
20. Matzke, R., Jacobson, K. & Radmacher, M. Direct, high-resolution measurement of furrow stiffening during division of adherent cells. *Nat. Cell Biol.* **3**, 607–610 (2001).

21. Sharma, S., Santiskulvong, C., Rao, J., Gimzewski, J. K. & Dorigo, O. The role of Rho GTPase in cell stiffness and cisplatin resistance in ovarian cancer cells. *Integr. Biol. (United Kingdom)* **6**, 611–617 (2014).
22. Wozniak, M. A., Trier, S. M., Keely, P. J., Ponik, S. M. & Eliceiri, K. W. RhoA is down-regulated at cell-cell contacts via p190RhoGAP-B in response to tensional homeostasis. *Mol. Biol. Cell* **24**, 1688–1699 (2013).
23. Webster, K. D., Ng, W. P. & Fletcher, D. A. Tensional homeostasis in single fibroblasts. *Biophys. J.* **107**, 146–155 (2014).
24. Adeniba, O. O., Corbin, E. A., Ewoldt, R. H. & Bashir, R. Optomechanical microrheology of single adherent cancer cells. *APL Bioeng.* **2**, 016108 (2018).
25. Mehrnezhad, A. & Park, K. Multifrequency Optomechanical Stiffness Measurement of Single Adherent Cells on a Solid Substrate with High Throughput. *Anal. Chem.* **89**, 10841–10849 (2017).
26. Carreno, S., Kouranti, I., Glusman, E.S.,Fuller, M.T., Echard, A., and Payre, F. (2008). Moesin and its activating kinase Slik are required for cortical stability and microtubule organization of mitotic cells. J. Cell Biol.180, 739–746
27. Mitchison JM Single cell studies of the cell cycle and some models. Theor Biol Med Model **2**:4–8. (2005)

Chapter 6 : Summary and Future Work

6.1 Dissertation Summary

Development of more precise, versatile and reliable micromechanical systems (MEMS) has begun to bridge the gap between biology and engineering and has contributed to the study of the physical properties of individual cells and other biological targets [1–4]. The work in this dissertation focused on a previously introduced MEMS resonant sensor for measuring the mass at the single cell level[5]. Here, we expanded the use of this technology to also measure stiffness and elasticity of the cells at the same time. This dissertation addressed several issues hindering the progress of MEMS resonant pedestal sensors in the measurement of cellular viscoelasticity and mass.

The research advanced the state of the art in the following ways:

1) using our MEMS resonant pedestal sensors to demonstrate that viscoelastic properties of single adherent cells can be extracted measuring a difference in vibrational amplitude of our resonant sensor platform. This method is used in consonance with a change in frequency of the resonant MEMS devices to determine a refined solution space and helped to further improve measuring the stiffness of individual cells.

2) incorporation of an extra parameters, vibration induced phase shift (VIPS), of a target laser incident on the cell in conjunction with a representative two-degree-of-freedom Kevin – Voigt model allows us to constrain our governing equations and obtain a tighter moduli solution space.

3) extending this work to allow for a long-term simultaneous stiffness and mass measurement of individual adherent cells

4) using a FUCCI cell cycle reporter to monitor the changes in the biophysical properties of normal and cancerous cells across their various cell cycles.

We first use the principle of amplitude ratios of our MEMS resonant sensor to compare the behavior of fixed and live human colon cancer cells. The fixed (stiffer) cells were also used to investigate the effects of material properties on the mass measurement with resonant sensors. Due to the nature of our measurement technique, which uses resonant sensor resonant frequency to estimate mass, the apparent mass reading is influenced by the viscoelastic behavior of soft objects. This effect was previously described by a two-degree-of-freedom system, which was inverted to extract material properties from mass measurements. We were then able to use an optical path length model to extract the nanoscale membrane fluctuation of each individual cell to elucidate the homogeneity of each cell in a sample population. The elasticity (stiffness) and viscosity extracted from these measurements agreed well with independent measurements from atomic force microscopy, and we verified the accuracy of the model in predicting the system behavior. Further extension of this work was carried out to allow for the time-varying measurement of viscoelasticity with mass. The addition of a FUCCI cell-cycle reporter capability allows for continuous monitoring of human colon and breast cancer cells at different stages of their growth cycle.

To our knowledge, this is the first report of time-varying monitoring growth cycle of individual adherent cells while measuring the viscoelasticity and mass using our MEMS resonant sensors. Based on preliminary findings, normal cells have a higher viscoelastic value than cancerous cells which is supported by the stiffening of fixed cells through the polymerization of microtubules [22]. The two-degree-of-freedom system were examined for sensitivity and accuracy of each cell type to investigate the smallest detectable viscoelastic moduli value. The investigation indicated that our measured viscoelastic values for fixed and live cells are consistent with previous work [23].

6.2 Directions for Future Research

The design, implementation, and characterization of the technological developments described in this work ultimately led to the first comparison of normal and cancerous adherent cell growth rates on the single cell level. While more information can be gleaned from these measurements through an increased number of samples, many avenues for further investigations remain. The following sections describe potential future directions for coordinating growth over the cell cycle, using the microfluidic system for studying drug delivery, and further investigation to the biophysical changes occurring during the stiffness and growth measurement.

6.2.1 Improved Mathematical Modeling

Living cells behave both as an elastic solid and as a viscous fluid, and so are considered viscoelastic. Such materials, including biological molecules and cells, cannot be fit using classical models of either elasticity or viscosity. In our work, we have used a standard Kevin-Voigt two-degree-of-freedom system to describe our cell sensor model. This model, for example, is plagued in itself in that it does not help in decoupling a cell's nucleus from its membrane. Meanwhile, in chapter 4 and 5, we used estimations from our cell membrane fluctuations in determining the viscoelastic moduli and apparent mass. We can improve on the accuracy of this estimations through creating an extra lumped material that represents the nucleus vibrating separately from the cell's membrane. Other suggestions entail using a bottom-top approach is assembling a library of sub-cellular components. For example, F-actin, a major component of cell cytoskeleton comprising different filament elasticity, exhibits viscoelasticity as a semi-flexible polymer with linear and nonlinear responses to external forces can be modelled separately and then other sub-components are then collated in one system of individual sub-components.

6.2.2 Effect of Chemotherapeutics on Stiffness and Mass

The ability to study stiffness and mass changes throughout the cell cycle improves the ability to study cancer and the bases of metastatic potential. It also allows for the study of how cellular growth rate responds to various external stimuli, including growth factors and anti-cancer chemotherapeutics. Being able to monitor changes to growth rate during specific cell cycle stages will allow for tailoring of therapies for a wide range of applications. These studies should be greatly aided by already-existing on-chip microfluidic system. We will be able to continuously deliver the fluid solution of interest to the cells on the sensor while monitoring in real time. This way the dosage can be controlled through solution concentration and total volume and can be adjusted as necessary. Beyond cancer, applications in tissue engineering and regenerative medicine may benefit greatly from this technology as the influence of growth factors can be investigated.

6.2.3 Adhesion Sensor

Cells can interact and respond to environmental signals, such as cell adhesion like cell-to-ECM[8]. Many biological processes and cellular activities are influenced by these environmental signals. Some of the biological processes include the regulation of cell growth and differentiation. The development of an adhesion sensor can help defining events in many diseases, including cancer. Our sensor can currently sense changes in adhesion, as seen by when a cell divides, where the cell partially detaches and changes its overall contact area.

It is known that the higher the degree of metastatic potential a cell has the lower adhesion characteristics. There is much interest in understanding the triggers between cell adhesion with behavioral patterns [9–15]. Unlike current techniques for characterizing cell adhesion, which are often destructive and require manipulations [16–20], the objective would be to improve the existing sensor and develop an adhesion sensor for label-free and non-invasive technology. Working along the

same line as drug studies, the platform itself will allow for drug screening of molecules to intervene with the cell adhesion process.

6.2.4 Further fluorescent Labeling for Individual Cell Analysis

The results presented in Chapter 5 demonstrate the ability of MEMS resonant sensors to identify and quantify differences in the stiffness and growth rate of normal and cancerous cells. Our system incorporates a FUCCI cell cycle sensor which visualizing the stage of cell growth across a cycle. However, the data in this work highlights the need for improvements in the system to better allow a more granular report of the mitosis stages (prophase, metaphase, anaphase and telophase) over an entire cell cycle. This is necessary to visualize what exact stages of mitosis is division or reattachment occurring. For instance, we might expect normal cells to exhibit different growth rates between the different cycle stages, while the disruption of cycle checkpoints in cancer may result in a more uniform growth rate over the entire cycle.

Fluorescent indicators for simultaneous reporting all four cell cycle phases will be useful for this. Figure 6.1 further presents this difference in number of stages of cell cycle reported. These biomarkers can be incorporated into the mass measurement and imaged through modification of the existing optical monitoring system. This addition would allow for the growth profile of each individual cell to be related to its specific cell cycle progression. Additionally, group analysis of multiple cells may include binning according to cycle stage, or individual growth curves may be aligned based on a common point in the cycle[7,21]. These analyses may improve cancer studies and better elucidate differences in cellular growth characteristics.

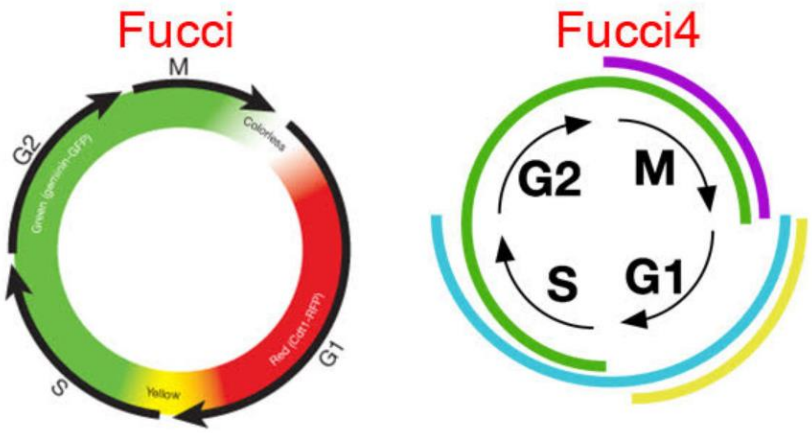

Fig 6:1 Showing the difference between our currently-used fluorescent 3-stage cell cycle reporter and an improved 4-stage cell cycle indicator [24].

6.3 References

1) Bashir, R. BioMEMS: state-of-the-art in detection, opportunities and prospects. *Advanced Drug Delivery Reviews*, 56(11) :1565–1586 (2004).
2) Kim, D., Wong, P. K., Park, K., Levchenko, A., & Sun, Y. Microengineered Platforms for Cell Mechanobiology. *Annual Review of Biomedical Engineering*, 11(1): 203–233 (2009).
3) Lindstro¨m, S., & Andersson-Svahn, H. Overview of single-cell analyses: microdevices and applications. *Lab Chip*, 10(24):3363 (2010).
4) Arlett, J. L., Myers, E. B. & Roukes, M. L. Comparative advantages of mechanical biosensors. *Nature Nanotechnology*, 6(4):203–215 (2011).
5) Park, K., Millet, L. J., Kim, N., Li, H., Jin, X., Popescu, G., Aluru, N. R., Hsia, K. J., & Bashir, R. Measurement of adherent cell mass and growth. *Proc Natl Acad Sci USA*, 107, 20691–20696, (2010).
6) Zambon, A. C. Use of the ki67 promoter to label cell cycle entry in living cells. *Cytometry Part A*, 77(6):564–570, (2010).
7) Ferrezuelo, F., Colomina, N., Palmisano, A., Gari, E., Gallego, C., Csik Csiksz-Nagy, A., & A. Marti. The critical size is set at a single-cell level by growth rate to attain homeostasis and adaptation. *Nature Communications*, 3:1012–11, (2012).
8) Fang, Y. Label-free biosensors for cell biology. *International Journal of Electrochemistry*, *2011*, (2011).
9) Pierres, A., Benoliel, A., Touchard, D., & Bongrand, P. How Cells Tiptoe on Adhesive Surfaces before Sticking. *Biophysical Journal*, 94(10):4114–4122, (2008).
10) Easty, G. C., Easty, D. M., & Ambrose, E. J. Studies of cellular adhesiveness. *Experimental Cell Research*, 19(3):539–548, (1960).
11) Goel, N., Campbell, R. D., Gordon, R., Rosen, R., Martinez, H., & Ycas., M. Self-sorting of isotropic cells. *Journal of Theoretical Biology*, 28(3):423–468, (1970).
12) Lovchik, R. D., Bianco, F., Tonna, N., Ruiz, A., Matteoli, M. & Delamarche, E. Overflow Microfluidic Networks for Open and Closed Cell Cultures on Chip. *Analytical Chemistry*, 82(9):3936–3942, (2010).
13) McCarthy, K. D., & Partlow, L. M. Preparation of pure neuronal and non-neuronal cultures from embryonic chick sympathetic ganglia: a new method based on both differential cell adhesiveness and the formation of homotypic neuronal aggregates. *Brain Research*, 114(3):391–414, (1976).
14) Curtis, A. S. Timing mechanisms in the specific adhesion of cells. *Experimental Cell Research, Suppl* 8:107–122, (1961).
15) Pierres, A., Benoliel, A. M. & Bongrand, P. Cell fitting to adhesive surfaces: a prerequisite to firm attachment and subsequent events. *Journal of European Cells and Materials*, 3:31–45, (2002)**.**
16) Fang. Y. Label-free cell-based assays with optical biosensors in drug discovery. *Assay and Drug Development Technologies*, 4(5):583–595, (2006).
17) Fang. Y. Non-invasive optical biosensor for probing cell signaling. *Sensors*, 7(10):2316–2329, (2007).
18) Fang. Y. Label-free receptor assays. Drug Discovery Today. *Technologies*, 7(1): e5–e11, (2010).
19) Li, J., Thielemann, C., Reuning, U., & Johannsmann, D. Monitoring of integrinmediated

adhesion of human ovarian cancer cells to model protein surfaces by quartz crystal resonators: evaluation in the impedance analysis mode. *Biosensors and Bioelectronics*, 20(7):1333–1340, (2005).
20) Giaever, I. & Keese, C. R. A morphological biosensor for mammalian cells. *Nature*, 366(6455):591–592, (1993).
21) Bajar, B.T. et.al. Fluorescent indicators for simultaneous reporting of all four cell cycle phases. *Nat Methods*,13(12):993-996, (2016)
22) Corbin, E. A., Kong, F., Lim, C. T., King, W. P. & Bashir, R. Biophysical properties of human breast cancer cells measured using silicon MEMS resonators and atomic force microscopy. *Lab Chip* 15, 839–847; (2015).
23) Adeniba, O. O., Corbin, E. A., Ewoldt, R. H., Bashir, R. *APL Bioengineering*, 2, 16 (2018).
24) Premo FUCCI Cell Cycle Sensor *BacMam 2.0* https://www.thermofisher.com/order/catalog/product/P36237